Chemical Modification of Interlayer Surfaces of Layered Silicates and Transformation to Nanostructured Materials

層状ケイ酸塩の層表面化学修飾とナノ構造材料への変換

Thesis Submitted To Waseda University

Nobuyuki Takahashi

Department of Applied Chemistry
Graduate School of Advanced Science and Engineering

February, 2011

The thesis of Nobuyuki Takahashi was reviewed and approved by the following

Dr. Kazuyuki Kuroda

Professor

Waseda University

Thesis advisor

Chair of Committee

Dr. Tetsuya Osaka

Professor

Waseda University

Dr. Yoshiyuki Sugahara

Professor

Waseda University

Dr. Takayuki Homma

Professor

Waseda University

Dr. Eduardo Ruiz-Hitzky

Research Professor

Materials Science Institute of Madrid

PREFACE

Inorganic layered materials possess confined interlayer spaces in nanometer level and lateral size in micrometer level, high surface area, and high accessibility. Layered materials are host materials for intercalation of various guest species. The intercalation compounds have been widely applied for polymer nanocomposites, adsorbents, catalysts, catalyst supports, and cosmetics. The host-guest interactions strongly affect the reactivity and selectivity of intercalation reactions. Especially, electrostatic interactions are relatively strong, and are commonly used. The combinations of ionicity of host-guest species are anion-cation, cation-anion, and neutral-nonion. The selection and control of the layer charge are fundamental study for precise design of layered nanomaterials. However, these conventional methods have been limited in inorganic synthesis. If overall control of layer charges in anion-nonion-cation is achieved, designability of nanostructured layered materials will be expanded significantly.

Layered silicates, whose frameworks are composed of only SiO_4 tetrahedra, should be suitable for various surface modifications. Layered silicates have $SiOH/SiO^-$ groups on the interlayer surfaces and exchangeable interlayer cations. Various guest species have been intercalated via many kinds of reactions such as cation exchange, acid-base reaction, and adsorption by van der Waals force. In addition, covalent modification such as silylation and condensation of $SiOH/SiO^-$ groups has been achieved.

This thesis summarizes the covalent modifications of layered silicates for layer charge control, and their transformations into nanostructured materials. I adopted two ways to achieve them. One is intralayer condensation of anionic SiO^- groups for intercalation of

nonionic surfactants. This method is applied for enlargement of mesopores of 2-D orthorhombic mesoporous silica. The other is capping of SiO^- groups by cationic silylation reagents for a synthesis of anion exchangeable layered hybrids. The layered hybrid is exfoliated into monolayer nanosheets.

This thesis is composed of 7 chapters.

Chapter 1 summarizes the background and objective of this thesis by the overview of conventional studies of layered silicates. Significance of layercharge control by covalent modification is also briefly described.

In chapter 2, a novel method for intercalation of nonionic surfactants into cation exchangeable layered silicates is reported. Layered silicate kanemite with flexible layers was preliminarily reacted with hexadecyltrimethylammonium (C_{16}TMA). C_{16}TMA-kanemite is reacted with an aqueous solution of nonionic surfactants of poly(oxyethylene) alkyl ether (C_nEO_m). A small amount of C_nEO_m was intercalated and C_{16}TMA ions were remained. The product was treated with acid in C_nEO_m solution. The obtained final product includes only C_nEO_m in the interlayer, and has large *d*-spacing (5.5 nm). Therefore, deintercalation of cationic C_{16}TMA and intercalation of C_nEO_m are achieved. Decrease of layer charge by condensation of $SiOH/SiO^-$ groups is important for the intercalation of nonionic C_nEO_m. The C_nEO_m-intercalated kanemite shows a reversible adsorption of *n*-decane and water. This property is advantageous for application of amphiphilic adsorbents.

Chapter 3 describes and discusses the mechanism of the intercalation reaction of C_nEO_m into C_{16}TMA-kanemite. The effect of the density of $SiOH/SiO^-$ groups for intercalation reactions was investigated. The density of $SiOH/SiO^-$ groups of C_{16}TMA-kanemite was varied according to the preparation temperature. With the decrease

of the density of SiOH/SiO^- groups, the intercalated amount of C_nEO_m was increased. On the other hand, 2D-NMR spectrum of C_nEO_m-intercalated kanemite shows that both alkyl chains and oxyethylene chains were interacted with silicate layers. Thus, the hydrophobicity of interlayer surfaces which was obtained by condensation of SiOH/SiO^- groups enhances the intercalation of C_nEO_m.

In chapter 4, the intercalation method of C_nEO_m is applied for the enlargement of pore size of 2-D orthorhombic mesoporous silica. In a previous report, careful acid treatment of C_{16}TMA-kanemite induced the transformation into 2-D orthorhombic mesostructure via bending of silicate layers (KSW-2). However, the pore size control of KSW-2 had not been achieved yet. In this study, $C_{16}EO_{10}$ was added to a solution for the acid treatment due to intercalation of bulky $C_{16}EO_{10}$ into mesopores. The acid treatment in the $C_{16}EO_{10}$ solution induced three simultaneous reactions of (i) intercalation of $C_{16}EO_{10}$, (ii) deintercalation of C_{16}TMA cations, and (iii) mesostructural transformation from lamellar to 2-D orthorhombic phase. Depending on the concentration of $C_{16}EO_{10}$, the d_{11} spacing of the products after the acid treatment varied from 4.0 to 5.4 nm. This method provides a precise control of pore size of KSW-2 type mesoporous silica.

Chapter 5 reports the synthesis of anion-exchangeable layered silicates immobilized with ionic liquids containing cationic imidazolium groups. The confronting arrangement of SiOH/SiO^- groups on layered octosilicate is essential for the bidentate immobilization and high degree of silylation. Two cation exchangeable sites of the SiOH/SiO^- groups on octosilicate were stoichiometrically converted to one anion exchangeable sites of imidazolium groups. Anion exchange capacity (AEC) of the product was 2 meq/g. The affinity of these materials for Cl^-, Br^-, I^-, and NO_3^- was quite different from that of LDH. The layered hybrid is stable at pH 1.0, which is in clear contrast to the

behavior of LDHs. The layered hybrid is applicable as a drug carrier of prodrug in oral administration.

In Chapter 6, exfoliation of anion exchangeable layered hybrid, obtained in chapter 5, is examined in water for preparation of silicate nanosheets. An aqueous suspension of the anion exchangeable layered hybrid was stirred with ultrasonication, and then exfoliated monolayer nanosheets were obtained. This is the first report of exfoliation of layered silicates into monolayer nanosheets. Regardless of the compositions, this is also the first report of full exfoliation of cationic nanosheets in water. The use of water as a solvent is advantageous from the viewpoint of green chemistry. The mechanism of the exfoliation is discussed by comparison with other layered hybrids. High hydration property of imidazolium groups on silicate layers leads to the swelling and further exfoliation into nanosheets. In addition, a transparent and colorless spin-coated film was successfully obtained on a glass substrate from the colloidal aggregates of the nanosheets. The spin-coated film was soaked into an aqueous solution of Orange II which is an anionic dye. Then, an orange-colored transparent film was obtained, suggesting the applicability for host material of functional species.

Chapter 7 summarizes the studies investigated in this thesis and discusses the outlook of covalent modification of layered silicates.

This thesis demonstrates that precise design of $SiOH/SiO^-$ groups makes it possible to control the interlayer environments including layer charges. In addition, I claim that this design of layer charge is valuable for transformation into novel nanostructured materials.

TABLE OF CONTENTS

Chapter 1. Introduction

1. Layered Silicates ····· 1

1.1. Layered materials ····· 1

1.2. Layered silicates ····· 2

1.3. Layered zeolites ····· 3

2. Non-Covalent Modification of Layered Silicates ····· 5

2.1. Intercalation reactions ····· 5

2.2. Transformation into mesoporous silicas ····· 6

2.3. Outlook of non-covalent modification of layered silicates ····· 8

3. Covalent Modification of Layered Silicates ····· 9

4. Silylation Reactions for Structural Design ····· 11

4.1. Silylation reactions of silanol groups of silica ····· 11

4.2. Immobilization of alkyl groups and related groups ····· 12

4.3. Immobilization of alkoxy groups and creating the new frameworks ··· 16

5. Silylation Reactions for Functional Design ····· 19

5.1. Immobilization of amine groups and their utility ····· 19

5.2. Immobilization of thiol groups and their utility ····· 21

5.3. Multi-step immobilization of various groups ····· 23

6. Esterification Reaction ····· 25

6.1. Esterification of silanol groups with alcohols ····· 25

7. Condensation Reaction ····· **28**

7.1. Interlayer condensation ····· 28

7.2. Intralayer condensation ····· 32

8. Pillaring of Layered Silicates by Silylation Reactions ····· **34**

8.1. Pillaring with polymeric silica species ····· 34

8.2. Pillaring with monomeric silylation reagents ····· 36

8.3. Pillaring with phenylene-bridged silylation reagents ····· 38

9. Summary and Significance of This Thesis ····· **41**

10. References ····· **42**

Chapter 2. Intercalation of Poly(oxyethylene) Alkyl Ether into Kanemite

1. Introduction ····· **53**

2. Experimental ····· **56**

3. Results and Discussion ····· **59**

3.1. Intercalation of $C_{16}EO_{10}$ into C_{16}TMA-kanemite ····· 59

3.2. Synthesis and structure of C_nEO_{10}–kanemite ····· 65

3.3. Adsorption of *n*-decane and water ····· 68

3.4. Formation mechanism of $C_{16}EO_{10}$–kanemite ····· 69

4. Conclusion ····· **72**

5. References and Footnotes ····· **73**

Chapter 3. Intercalation Mechanism of Poly(oxyethylene) Alkyl Ether into Kanemite

1. Introduction ····· **77**

2. Experimental ····· **79**

3. Results and Discussion ····· **81**

3.1. Intercalation of $C_{16}EO_{10}$ into C_{16}TMA-kanemite ····· 81

3.2. Intercalation mechanism ····· 83

4. Conclusion ····· **85**

5. References ····· **86**

Chapter 4. Enlargement of Mesopores of 2-D Orthorhombic KSW-2 Type Silica by the Addition of Poly(oxyethylene) Alkyl Ether during the Mesostructural Formation

1. Introduction ····· **87**

2. Experimental ····· **90**

3. Results and Discussion ····· **92**

3.1. Mesostructural control of as-PE-KSW-2 ····· 92

3.2. Pore-expansion of cal-PE-KSW-2 ····· 100

4. Conclusion ····· **105**

5. References ····· **106**

Chapter 5. Anion Exchangeable Layered Silicates Modified with Ionic Liquids on the Interlayer Surface

1. Introduction ····· **109**

2. Experimental ····· **113**

3. Results and Discussion ····· **119**

3.1. Immobilization of ionic liquids onto layered octosilicate ····· 119

3.2. Anion exchange ····· 130

3.3. Sorption and controlled release of prodrug depending on pH····· 135

4. Conclusion ····· 138

5. References and Footnotes····· 140

Chapter 6. Exfoliation of Layered Silicates Immobilized with Imidazolium Groups

1. Introduction ····· 145

2. Experimental ····· 149

3. Results and Discussion····· 152

3.1. Exfoliation of Bim-Oct into nanosheets ····· 152

3.2. Exfoliation mechanism ····· 157

3.3. Spin-coated films of nanosheets ····· 162

4. Conclusion ····· 166

5. References ····· 167

Chapter 7. Conclusion of This Thesis and Future Prospects····· 173

List of Publications ····· 178

Chapter 1

Introduction

1. Layered Silicates

1.1. Layered materials

Inorganic layered materials, which possess frameworks with high aspect ratio and two-dimensionally confined nano-spaces in the interlayers, have been utilized for various applications, such as adsorbents, catalysts/catalyst supports, ion exchangers, and fillers for resins. Many inorganic layered materials (host materials) can accommodate various guest species in the interlayer spaces by using various interactions via intercalation reaction. Surface properties of layered materials, such as their polarity and ionicity, are important for the intercalation. From a view point of ionicity, inorganic layered materials can be classified into three categories as follows; (i) Cation-exchange layered materials, which have negative charge in the layers, such as layered clay minerals, layered metal oxides, and layered silicates, (ii) Anion-exchange layered materials, which have positive charge in the layers, such as layered double hydroxides (LDH), and (iii) Neutral layered materials, such as graphite and layered chalcogenides. There are numerous studies on layered clay

minerals, in particular, organically modified clay minerals by ion exchange with cationic organic substances are extensively studied and many recent excellent literatures are available.[1-11]

1.2. Layered silicates

Crystalline layered silicates,[12-13] whose frameworks are composed of only SiO_4 tetrahedra, possess interlayer exchangeable cations that are often hydrated. Although layered silicates are cation-exchangeable, layered silicates have some differences from layered clay minerals. Layered silicates have interlayer silanol groups. The origin of negatively charged sites is SiO^- groups while that of clay minerals arises from isomorphous substitution of trivalent ions with divalent ions in the layers. In clay minerals, the exact position of substitution sites is very difficult to define except for a few reports of anionic clay LDH.[14] In contrast, the ordering of $SiOH/SiO^-$ groups, namely cation exchangeable sites, of layered silicates can be defined specifically on the basis of their crystal structures.

Natural sodium layered silicates, for example magadiite ($Na_2Si_{14}O_{29}\cdot xH_2O$),[15-17] kenyaite ($Na_2Si_{22}O_{45}\cdot xH_2O$),[15,18] makatite ($Na_2Si_4O_{10}\cdot 5H_2O$,[19-21] and kanemite ($NaHSi_2O_5\cdot 3H_2O$),[22-26] are constantly studied. The crystal structures of makatite and kanemite are determined. The silicate frameworks of both kanemite and makatite are composed of only six-membered rings with Q^3 ($(O^-/HO)Si(OSi)_3$) environmental silica species (Figure 1). The both silicate layers are only single layer of SiO_4 tetrahedra. In the case of kanemite, the ordering of SiO_4 tetrahedra is crank-like along *c* axis (Figure 1a). The silicate layer of makatite has zigzag ordering along *c* axis (Figure 1b). On the other hand, crystal structure of magadiite and kenyaite has not been well known. Especially, magadiite

is one of the most frequently studied layered silicates. Structure analysis and determination of crystal structure of magadiite should be important study in future.

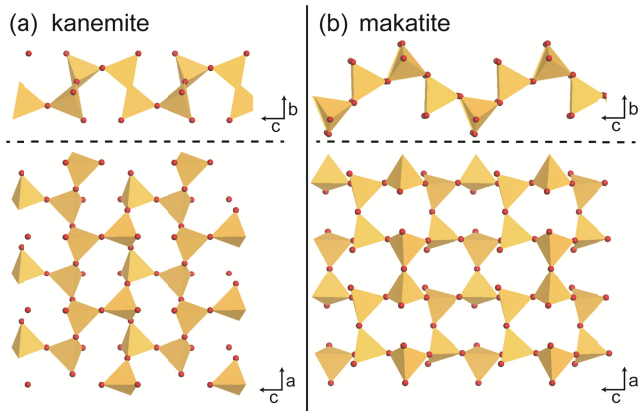

Figure 1. Crystal structures of (a) kanemite and (b) makatite.

Sodium layered silicates have been also obtained by synthesis for example octosilicate ($Na_8[Si_{32}O_{64}(OH)_8]\cdot 32H_2O$ also known as ilerite or RUB-18),[27-34] α-$Na_2Si_2O_5$,[35] β-$Na_2Si_2O_5$,[36] ε-$Na_2Si_2O_5$,[37] and δ-$Na_2Si_2O_5$[38] (precursor of kanemite). In addition, layered silicates including other alkali cations are also well known such as apophyllite,[39] $KHSi_2O_5$,[40] $LiNaSi_2O_5\cdot 2H_2O$ (named as silinaite),[41] $Li_2Si_2O_5$, $K_2Si_2O_5$,[42] $Na_{1.55}K_{0.45}Si_2O_5$,[43] $NaKSi_2Si_2O_5$, $Na_{0.67}K_{1.33}Si_2O_5$,[44-45] $Cs[Si_3O_6(OH)]$, $CsHSi_3O_7$,[46] $Rb[Si_3O_6(OH)]$,[47] and $K_4[H_4Si_8O_{20}H_4]$ (named as K-LDS)[48-49] In usual, frameworks of layered silicates are composed of Q^3 ($(O^-/HO)Si(OSi)_3$) and/or Q^4 ($Si(OSi)_4$) units. Arroyabe *et al.* reported unusual single-layer silicate ($K_2Ca_4Si_8O_{21}$) containing Q^2 ($(O^-/HO)_2Si(OSi)_2$) and Q^3 units.[50]

1.3. Layered zeolites

Interlayer cations are not limited to metal cations. Quaternary ammonium cations, for example, trimethylammonium (TMA) cation, are well known as the structure directing

agents (SDA) of zeolites. Zeolite is composed of SiO_4 tetrahedra which are partly substituted with AlO_4 tetrahedra. Although almost all zeolites contain 3-D connecting porous structures, some zeolites (or their precursors) have layered structures. They can be categorized as layered silicates because of their layer frameworks composed of SiO_4 tetrahedral units and SiOH/ SiO^- groups on the layer surfaces.

The early reports of layered zeolites are EU-19,[51-52] MCM-22,[53] and precursor of FER-type zeolite (PREFER).[54-55] Gies and co-workers synthesized a layered silicate named as RUB-15 possessing a unique framework which is composed of a segment of the sodalite cage.[56] Subsequently, they reported a similar layered silicate (RUB-51).[57] The framework is same as that of RUB-15 but the stacking sequence of the layers is different from that because of the structure of SDA of benzyl trimethylammonium hydroxide. A layered silicate with a unique helical morphology, named as HLS, has been synthesized by using tetramethylammonium hydroxide (TMAOH) and NaOH.[58-59] Furthermore, there are various layered zeolites, such as MCM-47,[60] MCM-69,[61] MCM-65,[62] PLS-1,[63] ERS-12,[64] Nu-6(1),[65-66] and RUB-39.[67]

Jeong and Tsapatsis *et al.* reported layered silicates, denoted as AMH-3, with 3-D microporous layers.[68] Normally silicate layers are used as a sort of "plate", but these studies inspire us that the inside of layers is quite important for embedding porosities and/or functions. In recent years, the Ryoo group has synthesized zeolite nanosheets with single-unit-cell thickness by using carefully designed diquaternary ammonium-type surfactants.[69-70] The down-sizing into nanometer sized layer thickness of zeolite is a breakthrough in zeolite science. Layered silicates can be regarded as an assembly of single-unit-cell nanosheets. Accordingly, layered silicates have a potential to contribute to the design of new silica-based materials with unique and advanced functions. The presence

of reactive SiOH groups on the interlayer surfaces should also widen the possibilities by incorporating various functional groups into the interlayer surfaces.

2. Non-Covalent Modification of Layered Silicates

2.1. Intercalation reactions

Intercalation reactions of layered silicates (and the corresponding layered silicic acids) are driven by hydrogen bonding, cation exchange, dipole-dipole interaction, van der Waals force, and acid-base reaction.[12] These intercalation reactions without covalent bonds are denoted as *non-covalent modifications*.

One of the most studied intercalation reactions of layered silicates is cation exchange. Interlayer cations, such as alkaline metal cations, in layered silicates can be exchanged with various inorganic and organic cations. Iler *et al.*[27] reported the cation exchange reaction of layered silicate with metal cations (Li^+, Na^+, Mg^{2+}, Ni^{2+}, and Cu^{2+}) and hexadecyltrimethylammonium cation. Nowadays, layered silicates are used for softener of water by using the cation exchange property for divalent cations in water.[71-72] In addition, very recently, it has been reported that magadiite exhibits selective adsorption of Zn^{2+} from seawater.[73] Eu^{3+} cation was also intercalated into magadiite.[74] Heat treatment of Eu^{3+}-intercalated magadiite leads Eu^{3+}-rich silicates. The condensation between layers is advantageous for preparing separated Eu^{3+} in solids. Ogawa *et al.* studied the photoluminescence of Eu^{3+} intercalated various layered silicates (kanemite, octosilicate, magadiite, and kenyaite).[75] The luminescence intensity was affected by the layer thickness because of the spatial separation of Eu^{3+} in the direction perpendicular to silicate

sheets on the luminescence self-quenching.

Exchange reaction of interlayer cations with proton is important for the following intercalation processes because alkali metal (mainly sodium) cations hinder other intercalation reactions because of stronger interlayer interactions between the cations and interlayer surfaces. Protonated layered silicates are host materials for alkylamines which are intercalated by acid-base reactions between SiOH and RNH_2.[76-77] Polar organic molecules, such as formamide and dimethylsulfoxide, can also be intercalated into protonated layered silicates.[77-78]

Intercalation of organic cations was studied in the early stage of the study on chemical properties of layered silicates. Lagaly *et al.* investigated the intercalation of alkylamine, quaternary alkylammonium, and alkylpyridinium cations into magadiite.[79] These intercalation compounds have been utilized for intermediates for silylation reactions because of large interlayer space and hydrophobicity of interlayer region.

2.2. Transformation into mesoporous silicas

Hybridization of alkyltrimethylammonium and layered silicates made breakthrough of the unique scientific area of mesoporous silica. Yanagisawa and Kuroda *et al.* reported first achievement of synthesis of mesoporous silica obtained by reaction of kanemite with aqueous solutions of alkyltrimethylammonium in a conference abstract in 1988[80] and a full paper in 1990.[81] Nowadays, mesoporous silicas are industrially manufactured (named as TMPS, TaiyoKagaku Meso Porous Silicas) in Japan, and developed for applications such as adsorbates, fillers, and catalyst supports.

Although silica source is mainly monomeric species in later,[82] mesoporous silicas derived from layered silicates are also studied and indicated unique properties. The

development of mesoporous silica derived from layered silicates is summarized in review by Kimura and Kuroda (Figure 2).[83] 2-D hexagonal mesoporous silica named as FSM-16 was synthesized from kanemite,[84] and related mesoporous silicas were reported.[85-88] Other layered silicates such as α-$Na_2Si_2O_5$ and makatite are also utilized for the synthesis.[86,89] These mesoporous silicas are formed through partial fragmentation of silicate layers.

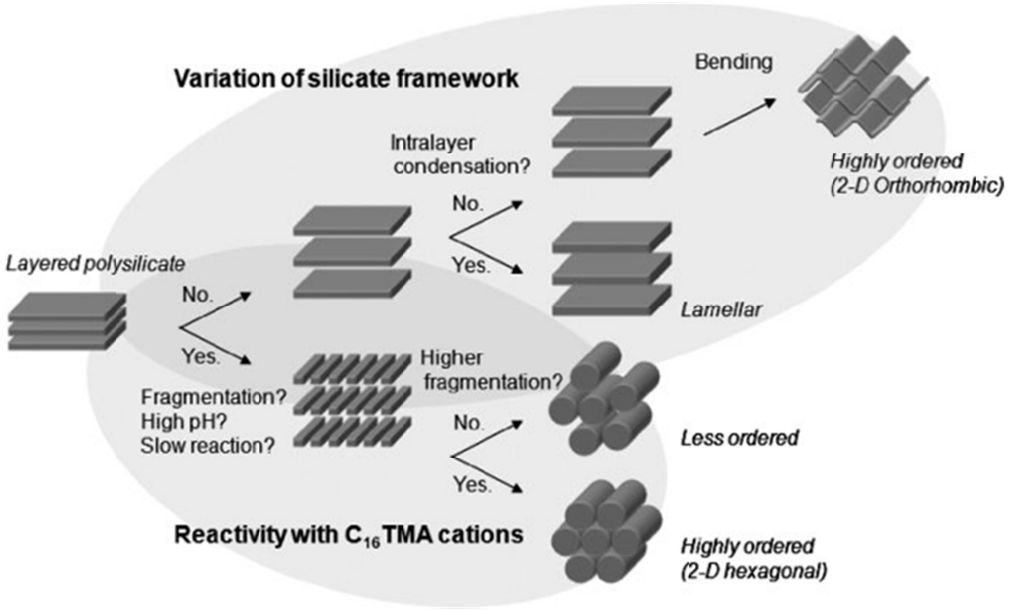

Figure 2. Schematic formation routes of mesostructured C_{16}TMA-silicates derived from layered silicates.[83]

Lamellar hexadecyltrimethylammonium intercalated kanemite (C_{16}TMA-kanemite[90]) was transformed to 2-D orthorhombic structural mesoporous silica named as KSW-2[91] through bending of the silicate layer. Titanium grafted KSW-2 showed a higher catalytic activity than those onto FSM-16 and MCM-41 grafted in the same manner, indicating that the periodicity in the framework influenced the catalytic activity due to the heteroatoms fixed at the silicate surfaces.[92] Although calcination to remove surfactant lead deformation of periodicity in the silicate frameworks of KSW-2,

the crystal structure can be retained by using precise modification of as-synthesized KSW-2 using molecularly designed silylating agents (Figure 3).[93] The crystalline frameworks from layered silicate are necessary for this unique capping process. On the other hand, C_{16}TMA-Octosilicate was transformed to mesoporous silicas via hydrothermal reaction.[94-95] Layered silicates are also used for silica source for zeolites.[96-104]

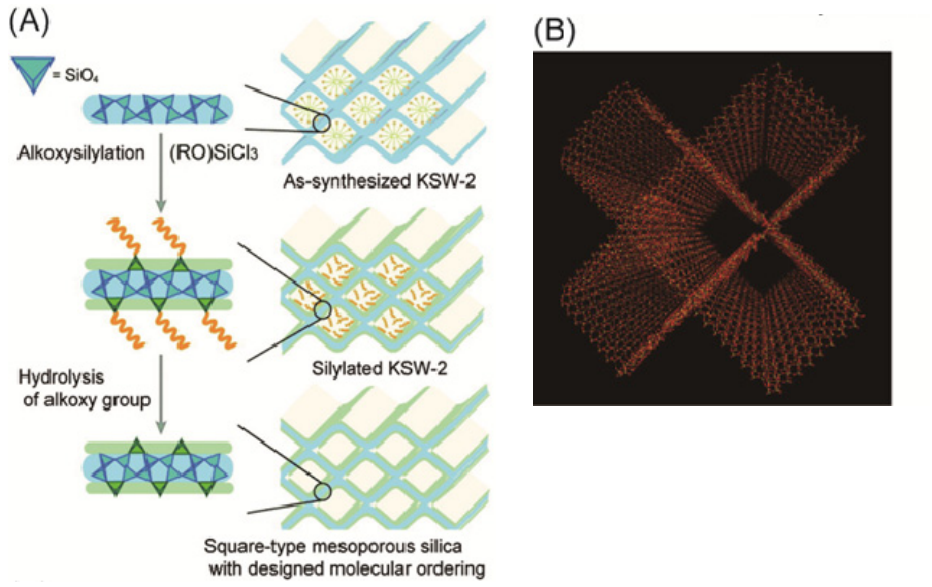

Figure 3. (A) Schematic formation process of KSW-2-based mesoporous silica with molecularly ordered frameworks formed by silylation. (B) Ideal structural model of KSW-2-based mesoporous silica with pore walls reflecting completely the crystal structure of a layered silicate kanemite.[93]

2.3. Outlook of non-covalent modification of layered silicates

Designable regions of stacked layers can be classified into three parts as follows; i) *Interlayer space*, ii) *Intralayer framework* inside layers, and iii) I*nterlayer surface*, the interface between interlayer space and intralayer framework.

Non-covalent modifications are applicable for adsorbents of cations in water, organically modified fillers for nanocomposites, and intermediates for mesoporous silicas. In addition, the variety of guest species is wide because of various interactions. However,

non-covalent modifications can only tune the property of the interlayer space. It is very difficult to immobilize guest species with defined locations and to prevent the release of guest species. In general, the distances of guest species should be controlled precisely for applications, such as single-site heterogeneous catalysts and photofunctional species whose properties are very sensitive to distances. The applicability of non-covalent modifications for these sophisticated purposes is quite limited because of the uncontrollability of the location of guest species.

3. Covalent Modification of Layered Silicates

Layered silicates can be modified covalently (*covalent modifications*), such as condensation, silylation, and esterification of SiOH/SiO^- groups (Figure 4). Layered silicates possess high surface area, and all SiOH/SiO^- groups are located on the surface with well ordering. Therefore, layered silicates can be regarded as a model substance of covalent modification of crystalline inorganic surfaces.

The covalent modifications make it possible to design all the above three regions of layered silicates. Utilizing the crystal structure of the host layered silicates, the density and distance of immobilized functional groups can be deliberately controlled at the angstrom level in two-dimensionally confined spaces. Interlayer surfaces have been modified by silylation or esterification with various functional groups, and the obtained hybrids are applicable for selective adsorbents, supports of nanoparticles, and building units for nanomaterials etc. Building up of crystalline structures of intralayer frameworks has also been achieved by precise alkoxysilylation of octosilicate and condensation of

silanol groups in the same layers. These covalent modifications are bottom-up approach to create new crystalline layers. Interlayer spaces have been transformed to 3D nanoporous structures by both interlayer condensation and pillaring with inorganic robust species. The size of nanopores can be tuned by selecting pillaring reagents, such as monomeric silylation reagents and phenylene-bridged ones, which may be important for specific catalytic reactions.

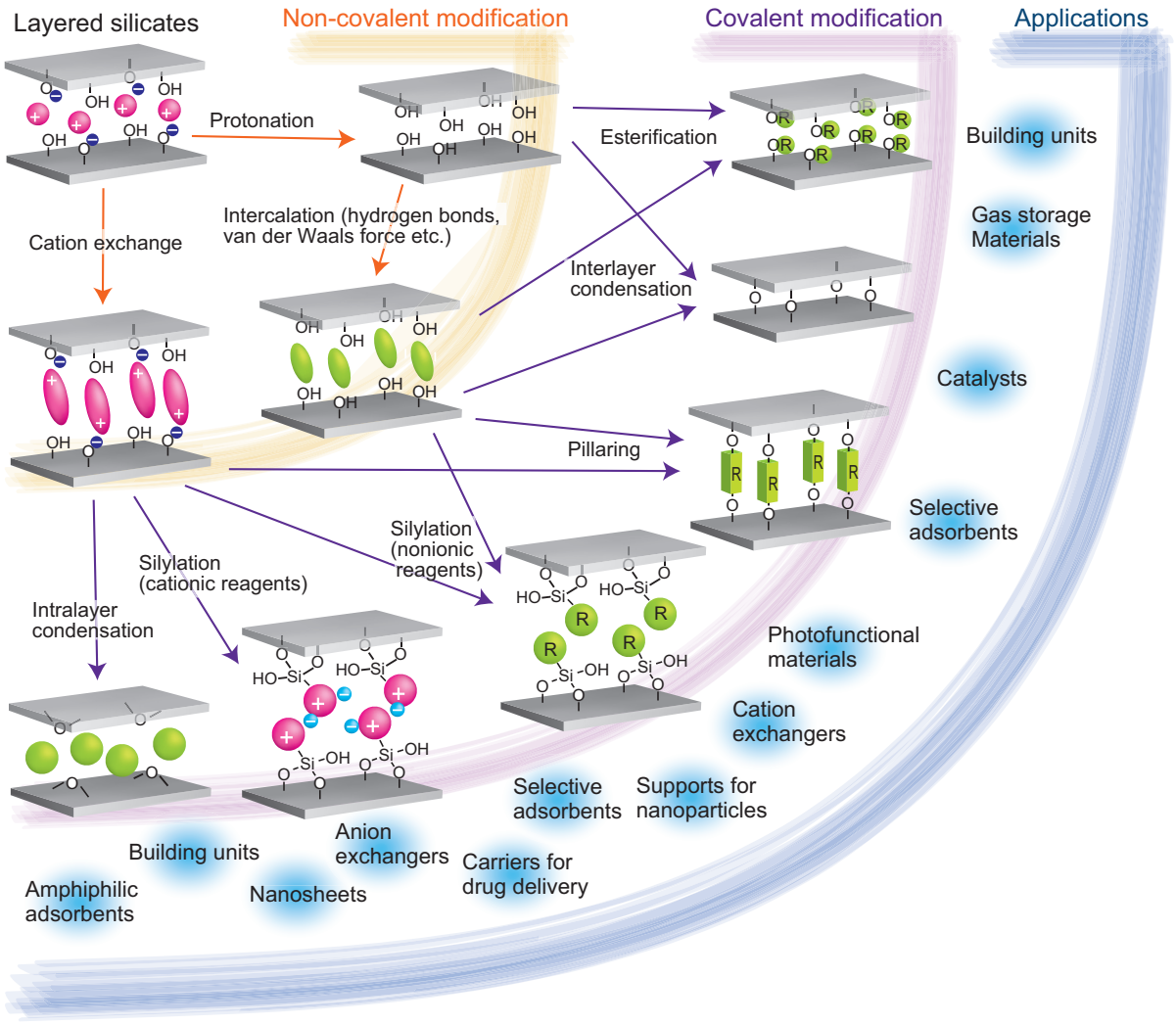

Figure 4. Overview of chemical modification of layered silicates.

4. Silylation Reactions for Structural Design

4.1. Silylation reactions of silanol groups of silica

SiOH groups on silica surfaces can be covalently modified with silylation reagents with chlorosilyl groups or alkoxysilyl groups.[105-106] Organochlorosilanes reacts with silanol groups as follows.

$$\equiv\text{Si-OH} + \text{Cl}_x\text{-SiR}_{3-x} \rightarrow (\equiv\text{Si-O})_x\text{-SiR}_{3-x} + x(\text{HCl})$$

Because of the high reactivity of chlorosilyl groups, this reaction proceeds at room temperature. Silylation reaction is also achieved with organoalkoxysilanes as follows.

$$\equiv\text{Si-OH} + (\text{MeO})_x\text{-SiR}_{3-x} \rightarrow (\equiv\text{Si-O})_x\text{-SiR}_{3-x} + x(\text{ROH})$$

The advantage of using organotrialkoxysilanes is relatively high stability of silylation reagents. However, higher temperature and/or the addition of acid are needed for high degree of silylation.

In general, silylation reagents with three attachable sites (e.g. triethoxysilyl and trichlorosilyl groups) are immobilized onto silica surfaces with from one to three covalent bonds, and the Si atoms become T^1 (R*Si*(OSi)(OR)$_2$), T^2(R*Si*(OSi)$_2$(OR)), and T^3(R*Si*(OSi)$_3$) environments. Silylation reagents with two attachable sites are converted to immobilized silyl groups with mixed environments of D^1 (R$_2$*Si*(OSi)(OR)) and D^2 (R$_2$*Si*(OSi)$_2$). In addition, residual hydrolyzed silanol groups of silylation reagents can be condensed between adjacent reagents, depending on their locations. Although silylation reagents with one attachable site are immobilized to form only M^1(R$_3$*Si*OSi) environment, their silylations with high degree are quite difficult because of steric hindrance.

Consequently, in order to carry out quantitative and regulated silylation of the surfaces of silica, amorphous silica is not so appropriate and the use of crystalline layered

silicates as the scaffolds is quite meaningful and useful, because the immobilization states and distribution of silyl groups can be controlled.

Silanol groups on both interlayer and outer surfaces of layered silicates can be silylated, but the surface areas of outer surfaces are much smaller than those of interlayer surfaces because numerous layers are stacked. In addition, outer surfaces cannot be used as confined space. Thus, the effect of silylation of outer surfaces is smaller than that of interlayer surfaces, except the dispersibility of particles of layered silicates in solvents.

4.2. Immobilization of alkyl groups and related groups

The first study of silylation reaction onto layered silicates was reported by Ruiz-Hitzky and Rojo in 1980.[107] Protonated layered silicates (e.g. magadiite) were treated with polar organic solvents, such as dimethylsulfoxide (DMSO), for the expansion of the interlayer spaces. Hexamethyldisilazane was also used as a reagent. The silylated layered silicates can be regarded as a new family of macromolecular organosilicon compounds and named as *planar silicone*. This discovery indicated that silanol groups of layered silicates can be used as reactive group for this kind of organic reactions. Ruiz-Hitzky, Rojo, and Lagaly studied the mechanism of silylation reaction by using various organosilanes such as (chloromethyl)dimethylchlorosilane, dimethylphenylchlorosilane, triphenylchlorosilane, and hexaethyldisilazane as follows.[108] (i) It is necessary for silylation that hydrogen bonds between interlayer surfaces are attenuated by intercalation of polar organic solvents. (ii) Diffusion of silylation reagents occurs simultaneously with desorption of the polar organic guest molecules.

Dodecyltrimethylammonium (C_{12}TMA) intercalated layered silicates, such as magadiite, kenyaite, and layered octosilicate, can be used for silylation reactions with

trimethylchlorosilane, diphenylmethylchlorosilane, triethylchlorosilane, triisopropylchlorosilane, butyldimethylchlorosilane, octyldimethylchlorosilane, and octadecyldimethylchlorosilane.[109-112] Octyltriethoxysilane was also used for silylation.[113] The disadvantages of using polar organic solvents for intermediates are (i) relatively unstable in air and (ii) the basal spacing could not be enlarged over the unimolecular thickness. The alkyltrimethylammonium intercalated layered silicates are stable and the guest molecules cannot be eliminated by washing with acetone. In addition, the basal spacing of intercalated compounds is larger than 2 nm and adjustable by choosing the length of alkyl chain. Bulky silylation reagents, such as octadecyldimethylchlorosilane, can be immobilized into interlayers.[112] Nowadays, silylation reaction of layered silicates are usually achieved with alkyltrimethylammoniums (such as C_{12}TMA and C_{16}TMA) or alkylamines intercalated intermediates.

Ogawa *et al.* reported that the surface properties of layered silicates can be designed to bind guest species by controlling the degree of silylation as well as the use of organochlorosilanes with different functionalities.[114] Magadiite was silylated with octyltrichlorosilane or octyldimethylchlorosilane. The silylated product with octyltrichlorosilane adsorbed *n*-octanol in the interlayer unlike the product with octyldimethylchlorosilane did not. When the degree of silylation was decreased, both the products adsorbed *n*-octanol. Considering the fact that *n*-decane was not intercalated into both of the products, the interactions between the hydroxyl groups of alcohols and surface SiOH groups on the layer were thought to be important for adsorption. Such a silylation process of layered silicates is effective for the design of interlayer microstructure though immobilized group is simple alkyl groups.

Adsorption properties of alcohols into silylated layered silicates were investigated

in detail by using silylated magadiite with octyltrichlorosilane.[115-116] Larger amounts of alcohols were adsorbed onto the derivatives with lower degree of silylation, indicating a possible control of the interlayer nanospace by varying the amount of grafting alkylsilyl groups.[115] In addition, 1-hexanol was adsorbed preferentially from a 1-hexanol/1-butanol aqueous mixture under limited conditions.[116] This concept of selective adsorbents was applied to molecule-specific adsorbates by using layered titanate. Ide and Ogawa reported that layered titanate immobilized with two different organic functional units (alkyl and phenyl groups) specifically adsorbed 4-nonylphenol (NPh) which is known as a contaminant of water.[117]

Toriya *et al.* reported that immobilization with trimehylchlorosilane onto layered silicate indicated interesting adsorption properties.[118] Trimethylsilylated-kanemite adsorbed benzene rather than water. Perfluoroalkylsilylation, instead of alkylsilylation, of layered silicate is advantageous for the stability and film-forming ability.[119] C_{12}TMA-magadiite reacted with [2-(perfluorohexyl)-ethyl]dimethylchlorosilane showed high thermal stability decomposition at 400 °C which is much higher than octyldimethylsilylated-magadiite (230 °C).

The defined crystal structure of layered silicates is essential for the discussion of structural details of the silylated layered silicates. The crystal structure of kanemite was determined by Vortmann and Gies and co-worker.[26] Silylation of kanemite with mono-, di-, and trichloro(alkyl)silanes was performed by Shimojima *et al*.[120] Kanemite is composed of single layered silicate sheets of six-membered rings. Additional five- and six-membered rings were formed when dichloro- and trichloro-(alkyl)silanes were used. The ^{29}Si MAS NMR spectra of alkyltrichlorosilylated kanemite products showed signals assignable to T^2 (R*Si*(OSi)$_2$(OR)), T^3 (R*Si*(OSi)$_3$), Q^3, and Q^4 environments due to the

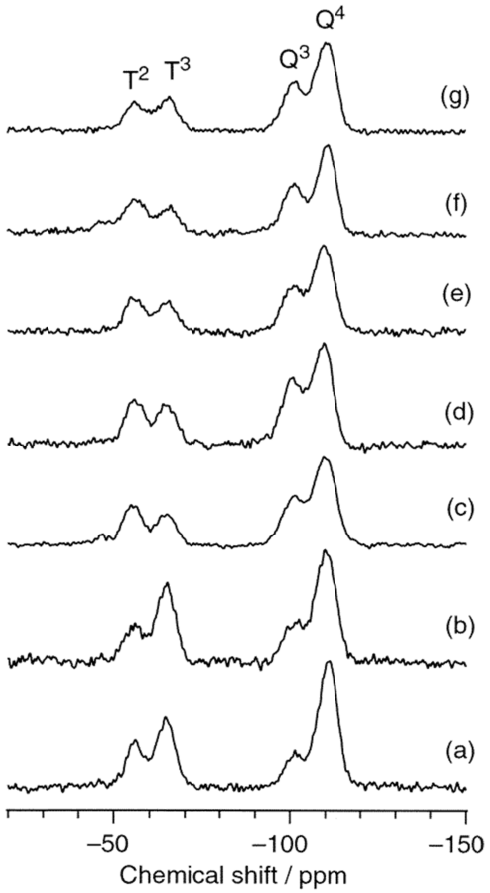

Figure 5. ^{29}Si MAS NMR spectra of alkyltrichlorosilylated kanemite. Alkyl chain length are (a) n = 1, (b) n = 2, (c) n = 4, (d) n = 8, (e) n = 12, (f) n = 16, and (g) n = 18.[120]

attached alkylsilyl groups (Figure 5). The existence of T^3 signals indicates condensation of silylation reagents each other. The degree of silylation was varied from 63 to 73% calculated from $Q^4/(Q^3 + Q^4)$ ratio. Well-ordered (such as only T^2) and full silylation has not been achieved with kanemite. Kanemite has high density (5.6 groups/nm^2) of SiOH/SiO$^-$ groups on the surface because all silicon atoms are Q^3 environment (Figure 1a). The SiOH/SiO$^-$ groups are too close for well-ordered and full silylation.

Immobilization of silylation reagents with alkyl groups provides general features of silylated products because of its simple structures. Such silylation reactions are advantageous for us to compare the similarities and/or differences among the reports on

this topic. The application of the hybrids obtained with alkylsilylation reagents is mainly studied as selective adsorbents. This selectivity depends on the geometrical ordering and/or packing of silylated groups in the two-dimensionally confinement of the interlayer spaces.

4.3. Immobilization of alkoxy groups and creating the new frameworks

As described above, silylation reaction onto the crystalline kanemite surface leads to the immobilization with multiple environments because of the condensation between adjacent reagents.[120] On the other hand, the distance among Si-OH and/or Si-O$^-$ sites of layered octosilicate, which are arranged along one axis, is different from that along the other.[30] The bonding direction on the interlamellar surfaces should be arranged regularly when appropriate silylation reagents are grafted (Figure 6). It should be proposed that layered octosilicate has the most suitable structure for the precise control of silylation.

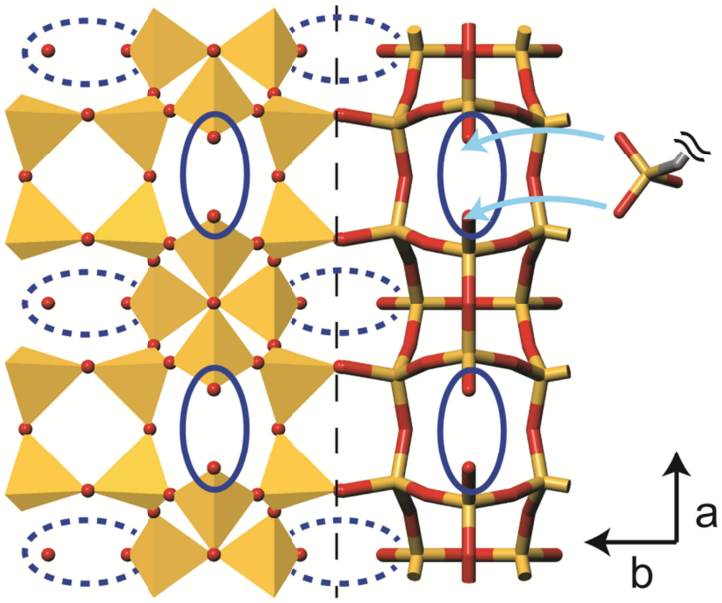

Figure 6. Crystal structure of layered octosilicate. The ellipsoids indicate confronting SiOH/SiO$^-$ groups. The dashed lines mean the groups on the back side of the layer.

A new crystalline silicate structure is created by grafting of dialkoxydichlorosilane on octosilicate (Figure 7).[121] ^{29}Si MAS NMR spectra of the silylated products show the signals due to dialkoxysilyl ($(RO)_2Si(OSi)_2$, R = alkyl) groups with Q^2 units. About 90% of the interlayer surface reactive sites are silylated. The powder XRD profiles, exhibiting a crystalline silicate framework with many peaks at higher angles, are due to the ordering of the framework, which has not been observed for all other silylated derivatives of layered silicates and silicas. The dialkoxysilyl groups are grafted in a controlled manner to form new five-membered rings regularly on the silicate layers. The products are a new type of layered silicates with thicker layers where only Q^4 and Q^2 units are present. In addition, alkoxy groups can be hydrolyzed and formed new SiOH groups. The one layer of SiO_4 tetrahedra was added to pristine octosilicate layers.

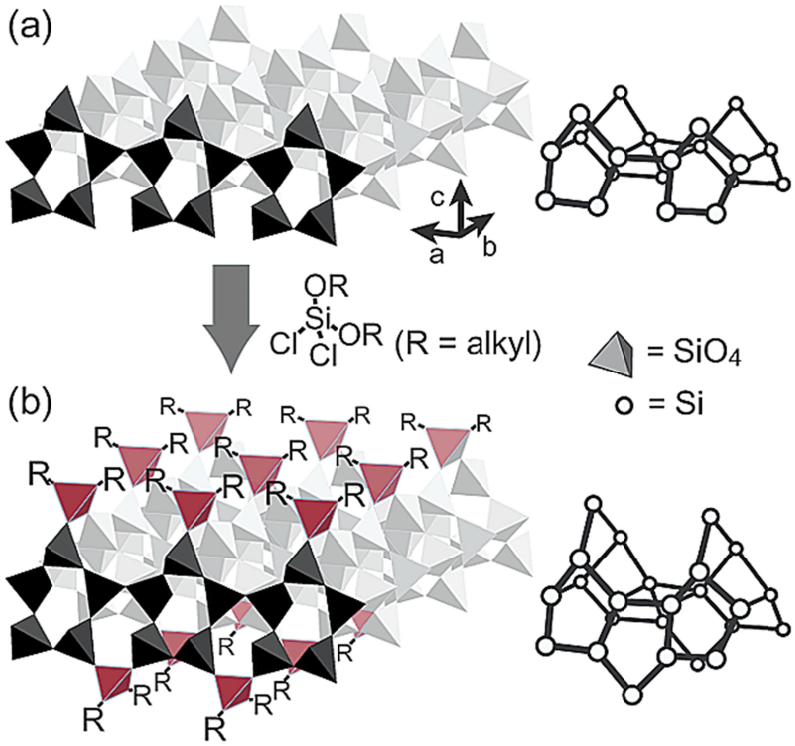

Figure 7. Grafting of dialkoxysilyl groups onto octosilicate. Red tetrahedra indicate the additional silicate framework by silylation with well ordering.[121]

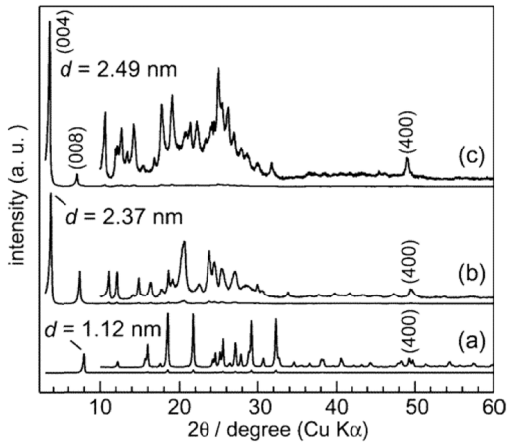

Figure 8. Powder XRD patterns of (a) octosilicate, (b) C_{12}TMA-intercalated octosilicate, and (c) dichlorodioctoxysilylated octosilicate.[121]

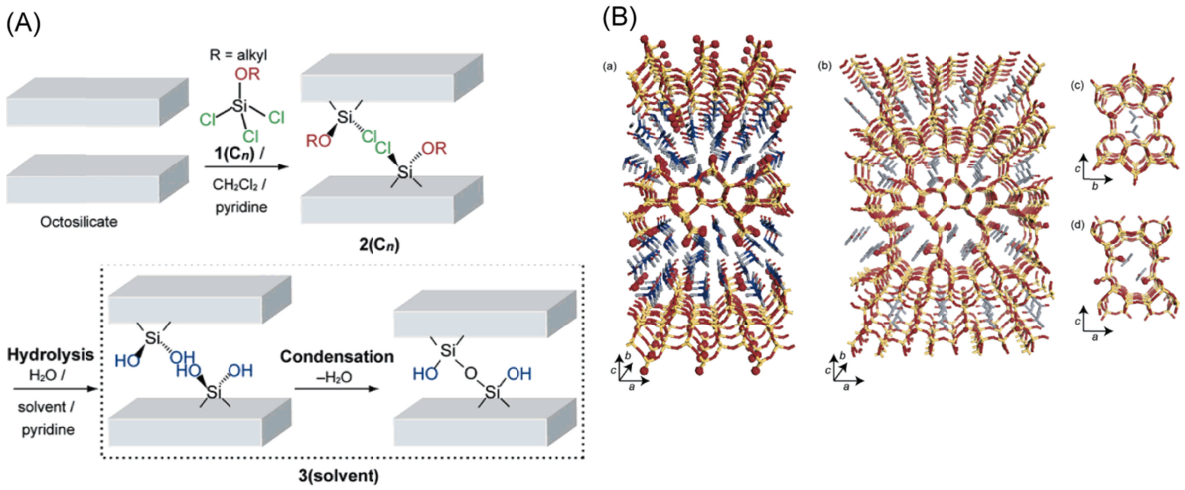

Figure 9. (A) Scheme of silylation of octosilicate by alkoxytrichlorosilane and hydrolysis of the silylated product. (B) Proposed crystal structural simulated model of the products after hydrolyzed by the posttreatment with a water/DMSO (product **1**) or water/acetone (product **2**). Perspective view of (a) product **1** and (b) product **2** along *b* axes. Location of acetone in the cage of product **1**: (c) view along *a* axis and (d) view along *b* axis, respectively.[122]

Subsequently, constructing of silica nanostructure based on the silylation of octosilicate with alkoxytrichlorosilanes and the reaction within the interlayers was achieved (Figure 9).[122] The silylated product has alkoxy and chloride groups, and hydrolysis of these groups by H_2O/DMSO mixture led to the formation of a unique

crystalline layered silicate with geminal silanols. Interestingly, the 2-D layers were subsequently transformed to 3-D networks when acetone was used instead of DMSO during hydrolysis. The acetone molecules are trapped within the 3-D structure (Figure 9B). The formation of these unique 2-D and 3-D silica structures indicates the potential of the silylation reaction for precise design of various silicate structures at the molecular level.

Silylation of alkoxytrichlorosilane was also performed with magadiite and kenyaite.[123] The silylated magadiite was transformed into porous 3-D structure through hydrolysis and condensation of interlayer silanol groups. However, the nanostructure from kenyaite retains the 2-D structure without condensation. This difference is possibly attributed to the original layered silica structures. Thus, not only silylation reagents but also layered silicate with suitable crystal structure should be carefully selected for the precise design of structure of silylated layered silicates.

5. Silylation Reactions for Functional Design

5.1. Immobilization of amine groups and their utility

Aminopropyltriethoxysilane (APTES) is one of the frequently used silylation reagents because of their wide variety of utility. Immobilization of APTES onto the interlayer surfaces of magadiite and kenyaite is reported.[124-125] Leu *et al.* reported that APTES-immobilized kenyaite was used as an intermediate for layered silicate/polyimide nanocomposites.[126] Poly(amic acid) with anhydride end groups was reacted with APTES immobilized kenyaite for covalent immobilization of polyimide onto the layer surfaces. The nanocomposites indicate a maximum increase of 36 °C in the degradation temperature

and a maximum reduction of 54% in moisture absorption.

Zhang *et al.* studied the utility of amine-functionalized magadiite for selective adsorption of metal cations.[127] A silylation reagent including two amine groups (3-(2-aminoethylamino) propyltrimethoxysilane, denoted as AAPTMS) is immobilized onto magadiite. AAPTMS-immobilized magadiite is applicable for selective adsorbents of Cu^{2+}. The two amine groups of silylation reagent are effective as ligand and trap for Cu^{2+} in diluted aqueous solutions. Airoldi group also studied the utility of layered silicates immobilized with various silylation reagents including amino groups for selective adsorbents.[128-132] Silylation reagents with one (APTES), two (AAPTMS), and three (N-3-trimethoxysilylpropyldiethylenetriamine) amino group(s) are immobilized onto kenyaite[128] or layered octosilicate.[130-132] Bis[3-(triethoxysilyl)propyl]tetrasulfide and 3-cyanopropyltriclorosilane are also used for silylation.[128-129] These functionalized layered silicates have an ability to remove divalent cations, such as Co^{2+}, Ni^{2+}, Cu^{2+}, Zn^{2+}, Cd^{2+}, and Hg^{2+} from aqueous solutions.

Ishii *et al.* reported the silylation of *n*-hexylamine intercalated octosilicate with *p*-aminophenyltrimethoxysilane (APhTES).[133] The obtained product contains both *n*-hexylamine and APhTES in the interlayer space (Figure 10). The subsequent ethanol treatment leads to the removal of *n*-hexylamine and immobilization of APhTES. However, these products have no microporosity. The excess APhTES molecules and oligomers are removed by acid treatment. Residual immobilized APhTES bridge the adjacent layers, and produce the microporosity. This rigid phenylene functional group is advantageous for pillaring of interlayer space.

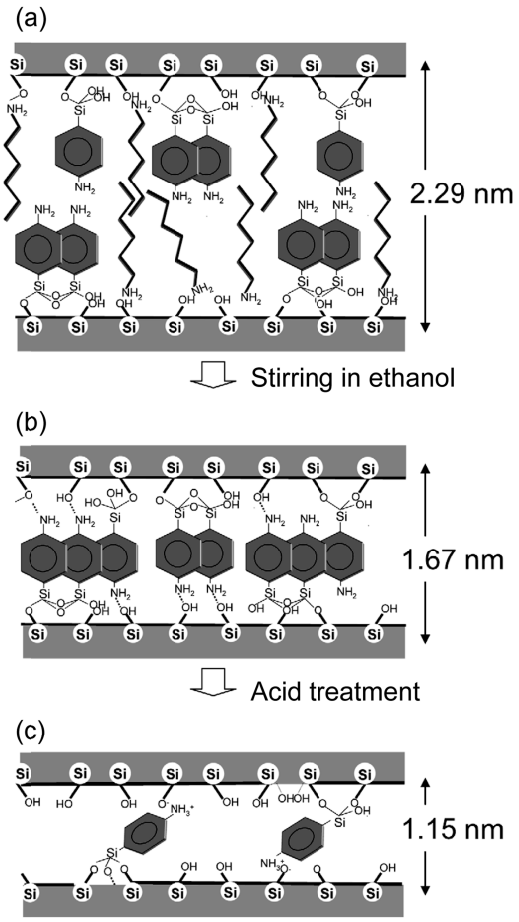

Figure 10. Structural models of (a) APhTES reacted *n*-hexylamine- intercalated H-octosilicate, (b) after stirring in ethanol, and (c) acid treatment.[133]

5.2. Immobilization of thiol groups and their utility

Ogawa, Ide, and co-workers have studied the immobilization of thiol group onto layered silicates.[134-136] Thiol group is usually used for modification on the surfaces of gold. Layered octosilicate is silylated with 3-mercaptopropyltrimethoxysilane (MPTMS), and the hybrid (MPS-Oct) is used for preparation of Au nanoparticles in the interlayer space.[134] Although the height of the interlayer space is 1.1 nm, the lateral size of particles is 4.8 nm on average (Figure 11). Therefore, the morphology of the Au nano particles is thought to be disc-like or polygonal plate-like. The two-dimensional interlayer space directs the formation of platy Au particles. This method is applied for layered titanate.[137]

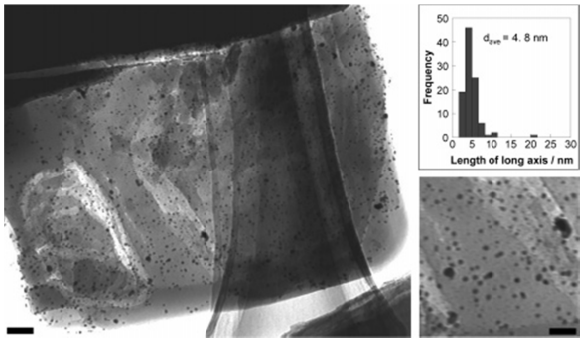

Figure 11. TEM image of Au nanoparticles immobilized on MPS-Oct (scale bar: 50 nm). Inset shows the size distribution of Au nanoparticles and the magnified TEM image (scale bar: 25 nm).[134]

Au nanoparticles are created in the interlayer space of MPTMS-immobilized layered titanate. This nanocomposite is found to catalyze the oxidation of aqueous benzene to phenol by visible light irradiation. In addition, the photocatalytic reaction is substantially accelerated to a higher yield and selectivity of phenol formation when the reaction was conducted in the presence of aqueous phenol.

Thiol groups immobilized on layered octosilicate can be converted to sulfonic acid groups by oxidation with nitric acid.[136] The sulfonated octosilicates swells in water. The distance between the adjacent silicate sheets are varied with the surface coverage of sulfonic acid, and the degree of swelling is controlled by the NaCl concentration in water. The sulfonated octosilicates are well dispersed in water and formed transparent colloidal suspensions. In general, layered silicates composed of only SiO_4 tetrahedra indicate no swelling with water and organic solvents. Silanol groups with high density on the interlayer surfaces hinder the swelling because of hydrogen bond and strong electrostatic interaction between SiO^- and hydrated cations. Therefore, water-swelling of sulfonated octosilicate is an important finding that leads to exfoliation of layered silicates. However, exfoliation of the layer is not properly examined.

From the viewpoint of the functionalities of capping silylation reagents, chloride

or ethoxy (or methoxy) groups are generally used for immobilization. Alkoxysilanes are relatively stable and often used for modification of silica surfaces. However, the reactivity of the alkoxy group is lower than that of chloro group. Reaction of alkoxysilanes onto layered silicates often leads to low degree of silylation and partial condensation of each silylation reagents. Ide and Ogawa developed an efficient way to immobilize alkoxysilanes onto layered silicates with high degree of silylation.[135] C_{12}TMA-intercalated magadiite was dispersed in toluene solution of MPTMS whose amount was equivalent to half of SiOH/SiO^- groups. The mixture was concentrated for 1–2 hours at 90 hPa, 60 °C to evaporate the solvent by using a rotary evaporator. All added MPTMS was immobilized onto magadiite. With conventional reflux method, 85 % of MPTMS was immobilized despite excess amount (28.5 equivalent of SiOH/SiO^- groups) of MPTMS. This solvent evaporation method is very simple and should be applicable for various alkoxysilanes. This method is one of the important methods to obtain high degree of silylation in short time.

MPTMS is widely used for modification of solid supports and self-assembled monolayer (SAM). The thiol groups immobilized onto layered silicates can be regarded as assembled monolayers with high ordering which is hardly obtained by SAM. I prospect that both of the wide variety of applications and the high ordering of MPTMS will provide more intelligent applications than conventional SAMs.

5.3. Multi-step immobilization of various groups

Some silylation reagents, possessing azobenzene[138] for example, are synthesized according to target properties, though various silylation reagents are commercially available. On the other hand, immobilized functional groups on layered silicates are further reacted with other reagents for materials design by using multi step immobilization. In the

case of immobilization of allyldimethylchlorosilane onto magadiite and kenyaite,[139] additional reaction of immobilized groups occurred. During the silylation reaction, HCl (formed from reaction between -SiOH and -SiCl) reacted to allyl group and created new -Si-O-Si$(CH_3)_2$OH groups. Although this is not multi step silylation reaction, it is suggested that immobilized functional group can be used for additional reactions.

γ-Methacryloxypropyltrimethoxysilane is immobilized onto magadiite and used for copolymerization with methylmethacrylate monomers,[140] which provides a unique pathway to prepare nanocomposites with covalent bonding, because normally clay-polymer nanocomposites are prepared by the use of organoammonium exchanged clays with various polymers with non-covalent interactions.

Shindachi *et al.* reported the multi-step immobilization of diarylethene.[141-142] The first step is immobilization of bromo-terminated silylation reagent (4-(bromomethyl)phenylchlorodimethylsilane) onto C_{16}TMA-magadiite. The second step is reaction between immobilized bromo group and trialkylamine terminals on diarylethene through the quaternization of amine groups. Covalently immobilized diarylethene exhibits an improvement of photochromic reversibility if compared with LDHs.

Matsuo *et al.*, reported three-step immobilization of pyrene chromophores. The first step is immobilization of [2-(perfluorohexyl)-ethyl]trichlorosilane onto C_{12}TMA-magadiite.[143] The second is immobilization of APTES to SiOH groups of the silylation reagents and finally the third is reaction between 1-pyrenebutanoic acid succimidyl ester and amine groups of immobilized APTES.

Specht *et al.* achieved two-step immobilization by using hydrosilylation.[144] Apophyllite is reacted with phenylmethylchlorosilane including Si-H group. The Si-H groups of silylated apophyllite are reacted with octane, 3-buten-1-ol, and

but-3-enyl-β-D-glucoside through hydrosilylation reaction.

Although multi step immobilization needs elaborate procedures, immobilized groups can be varied widely. For example, mesoporous silica functionalized with azide groups were used for covalent modification with various groups, such as enzymes,[145] snap-top groups for preadsorbed enzymes in mesopores,[146] and fluorescent molecules,[147] through *click chemistry*.[148] I expect that immobilized groups in layered silicates will also be designed for further reactions with more intelligent covalent modifications and/or more practical applications.

6. Esterification Reaction

6.1. Esterification of silanol groups with alcohols

SiOH groups of layered silicates can be esterified with alcohols. Mercier and Detellier *et al.* investigated the reaction of ethylene glycol onto the interlayer surfaces of H-magadiite.[149] *N*-methylformaide-intercalated magadiite is reacted with ethylene glycol in a reflux condition. Two types of mobility of ethylene glycol in the interlayer region is proved by ^{13}C CP/MAS NMR, suggesting that one is covalently immobilized ethylene glycol onto the surface and the other is intercalated species without covalent bonds.

When H-magadiite is esterified with aliphatic alcohols, the esterification with methanol (or CD_3OD) is confirmed by ^{13}C HD/MAS NMR and ^{2}H NMR.[150] In addition, aliphatic alcohols with various chain length ($C_nH_{2n+1}OH$, n = 2, 4, 5, 6, 8, 9, 14, and 16) are used for esterification. The *d*-values of the esterified H-magadiite are almost constant, suggesting that the alkyl chains are lying parallel to the interlayer surfaces. Butanol-treated

H-magadiite shows a stable dispersibility in toluene although H-magadiite does not. A transparent film was obtained by casting the solution on a glass substrate. Esterification of silanol groups on the surface probably increases the stability of the particles in toluene. Less than 24% of silanol groups of H-magadiite are esterified with various alcohols ($C_nH_{2n+1}OH$, n = 1–16). The low activity of esterification and steric hindrance of the immobilized alcohols should prevent further esterification with high density.

Solvothermal treatment of H-octosilicate with methanol leads highly ordered and highly esterified layered organosilicate.[151] The degree of the esterification reached to 95% by the solvothermal treatment at 120 °C for 200 h. Not only the crystal structure of layers but also layer stacking sequence is investigated precisely, and such a report can be regarded as a sort of standard case for study on interlayer esterification. The *ab* plane of octosilicate is deformed with along both *a* and *b* axes (Figure 12 bottom) because the repulsion of grafted methoxy groups enlarges the six-membered rings and expands the *ab* plane (Figure 12B upper). The crystal system is transformed from tetragonal to monoclinic with increasing the β angle (Figure 12 middle). Therefore, the esterification of silanol groups with high degree strongly influences the overall crystal structure despite covalent modification of only the interlayer surfaces. The crystal structures of covalently modified layered silicates should be carefully analyzed even though only interlayer surfaces are modified.

Esterification reaction is a soft and efficient way for covalent modification of the surfaces of layered silicates. Esterification of layered silicates enables the design of the surface properties such as dispersibility in toluene and transformation of crystal structure. Chemistry of clay minerals shows that Al-OH groups of kaolinite are esterified with alcohols.[152-156] Methoxylated kaolinite can be used for intercalation of bulky molecules

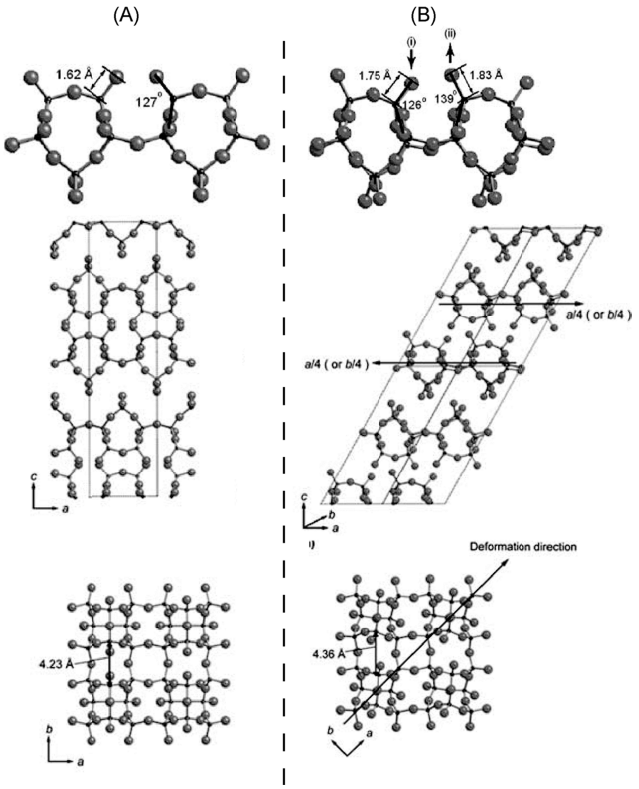

Figure 12. (A) Projection of silicate frameworks ((a) *c* axis and (b) *ab* plane). Left: H-octosilicate based on the crystallographic data. Right: Methoxylated octosilicate; this model was derived from the molecular mechanics calculation. (B) Projections of structures of (a) H-octosilicate based on the crystallographic data and (b) methoxylated octosilicate derived from the calculation. The pair of oxygen atoms on Q^3 silicons in the methoxylated octosilicate (b) are not equivalent to each other, labelled as (i) and (ii).[151]

which cannot be intercalated into pristine kaolinite.[157-160] Consequently, further intercalation reactions of methoxylated layered silicates is also interesting because their surface properties are changed from that of pristine layered silicates via capping of silanol groups. On the other hand, the variation of the alcohols used has been narrow so far. Expansion of the variation of the alcohols should be achieved in order to design layered silicates for various applications. It should also be noted that methoxylated octosilicate can be considered as crystalline polymeric alkoxysilanes, suggesting the applicability for building units of nanostructural materials with crystallinity.

7. Condensation Reaction

7.1. Interlayer condensation

Silanol groups on the interlayer surface of layered silicates can be condensed between layers, and transformed to 3-D structures retaining the crystallinity of the layers. This transformation is called as topotactic conversion. The topotactic conversion via interlayer condensation has received keen interests from the viewpoint of the synthesis of zeolites from layered silicates (layered zeolites).[161]

Schreyeck *et al.* synthesized layered (alumino)silicate by using bulky template.[54-55] Interestingly, calcination of this as-made product leads to FER-type zeolite with the 3-D porous structure. A proposed structure of layered silicate (PREFER) is composed of (100) ferrierite layers which are not interconnected (Figure 13). Millini *et al.* also reported transformation of layered borosilicate of ERB-1 into MWW type zeolite by calcination.[162] However, the crystal structure of these layered silicates was not definitely determined.

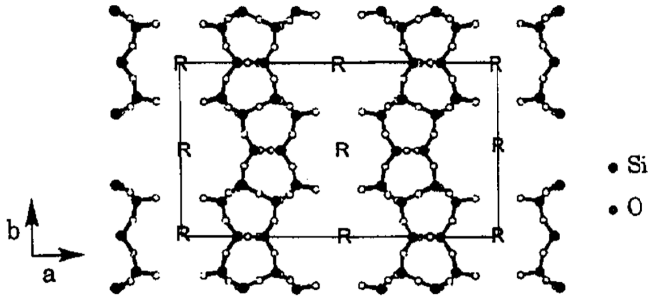

Figure 13. Proposed structure of PREFER.[54]

Ikeda *et al.*, synthesized a new layered zeolite named as PLS-1 (Pentagonal-cylinder Layered Silicate) with shared faces of pentagon cylinders made up of

five-membered rings, or pentasil rings.[63] After calcination of PLS-1, a novel zeolite with a cylindrically double saw edged structure (CDS-1) is obtained as the result of dehydration-condensation between the pentasil layers (Figure 14). The crystal structures of both PLS-1 and CDS-1 were determined, and the topotactic conversion of PLS-1 to CDS-1 via interlayer condensation of silanol groups is clearly demonstrated.

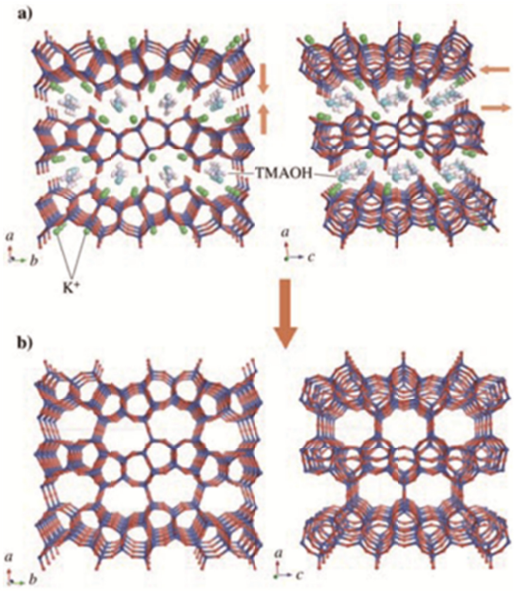

Figure 14. Perspective view of the crystal structure of a) PLS-1 along the [001] (left) and [010] directions (right) as well as b) CDS-1 along the [001] (left) and [010] directions (right). Color coding: blue = Si, red = O, green = K, white = C, cerulean = N, sky blue = OH. CDS-1 consists of silicates layers based on a framework of PLS-1 with 5MRs and forms 8MRs in the [001] and [010] directions.[63]

In the same year, Zanardi *et al*. determined the crystal structure of layered silicate named as Nu-6(1) which can be converted to zeolite (Nu-6(2)) by topotactic conversion.[66] The synthesis of Nu-6(1) and Nu-6(2) was already reported by Whittam in 1983.[65] The structure of layered Nu-6(1) is based on the pentasil layer in EU-19[51-52] and MCM-69.[61] However, the different structure-directing agent (4,4´-bipyridine) used in the synthesis gives rise to a different symmetry and stacking parameter. On the other hand, layered silicate RUB-39[67] is also transformed to a 3-D structure named as RUB-41.[163] PLS-3 and

PLS-4, whose structures are similar to those of PREFER and RUB-36, are converted to FER- and CDO-type zeolites.[103] Boron-incorporated CDS-1 is synthesized from PLS-1 containing boron.[164]

The topotactic conversion via interlayer condensation is achieved with not only layered zeolites but also layered silicates with thinner layers. Topotactic conversion of layered octosilicate into a 3-D structural zeolite (RUB-24) was reported by Marler and Gies *et al*.[165] Interlayer cations of octosilicate are exchanged with alkylammonium cations, and then calcined. The obtained RUB-24 has one-dimentional pore system consisting of straight and non-interconnecting eight-membered rings. Interestingly, the space group of RUB-24 ($I4_1/amd$) is same as that of octosilicate,[30] suggesting the same layer stacking sequence with 4_1 screw axis parallel to *c* axis. Oumi *et al.* reported the topotactic conversion of acetic-acid-intercalated octosilicate (Ac-Oct) into RWR-type zeolite.[166] The d_{004}-value of Ac-Oct is less than that of octosilicate by 0.18 nm, suggesting that the silanol groups on both sides of the layer are located in closer positions.

Afterwards, Ikeda *et al.* investigated the effect of the layer stacking sequence for the topotactic conversion to RWR-zeolite (Figure 15).[167] Original Na-type layered octosilicate and H-octosilicate become amorphous when they are calcined. Calcination of tetramethylammonium-intercalated octosilicate (TMA-Oct) also leads to the formation of an amorphous structure because of inappropriate layer stacking sequence. However, acid-treated TMA-Oct, whose layer stacking sequence is similar to that of octosilicate, is converted to a RWR-type zeolite. Similar phenomenon is reported by using magadiite.[168] Thus, the important factors for topotactic conversion to 3-D zeolite structures are (1) closer contacts between silanol groups and (2) control of stacking layers having silanol groups which should face each other appropriately.

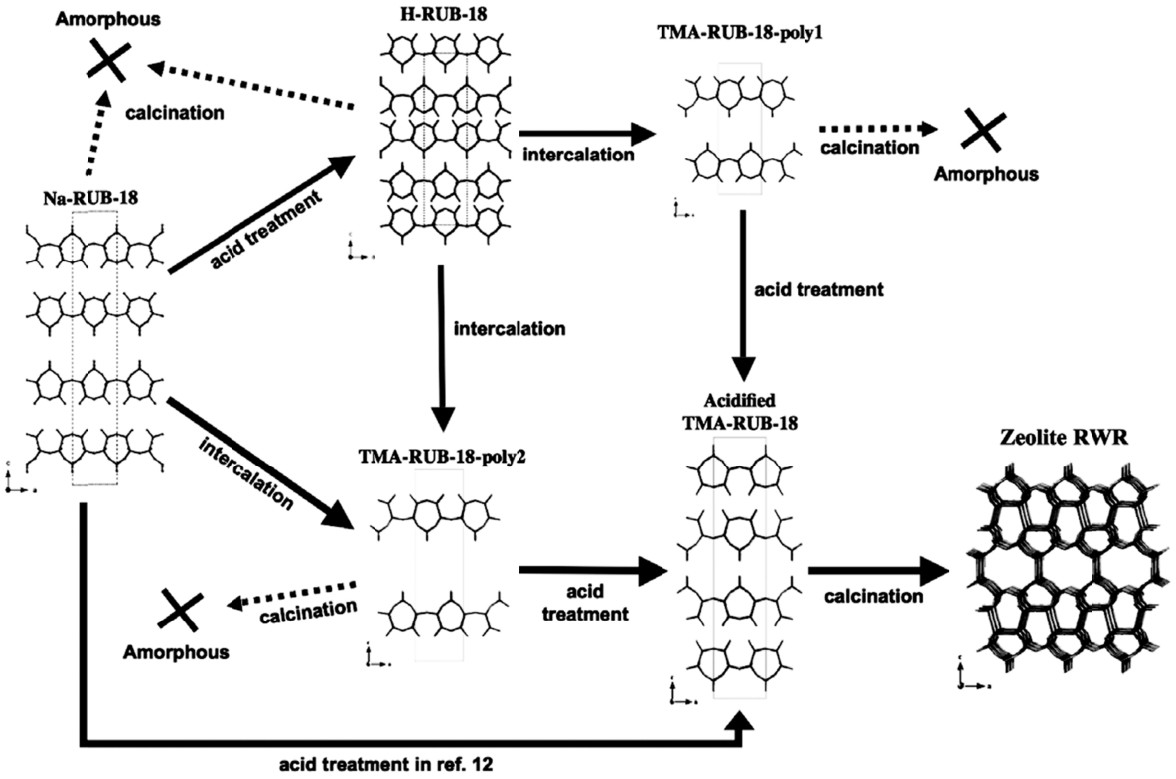

Figure 15. Schematic diagram of the topotactic conversion route from Na-RUB-18 to zeolite RWR. [167]

The crystal structure, in particular undulation of interlayer surface is an important factor for topotactic conversion because the undulation of interlayer surface determines the size and shape of the pores formed by condensation. Gies and co-workers reported the synthesis of a layered silicate RUB-15, whose framework is composed of a segment of the structure of sodalite cage (Figure 16).[56] Moteki and Okubo *et al.* reported the topotactic conversion of RUB-15 into the sodalite structure.[169] HCl-treated RUB-15 is transformed to only an amorphous structure by calcination. However, after acetic acid treatment, RUB-15 was successfully converted into the 3-D structure with sodalite cages. The product with micropores shows H_2 adsorption property. The selection of layered silicates and careful control of the layer stacking sequence are vital for the material design of 3-D structures obtained by topotactic conversion.

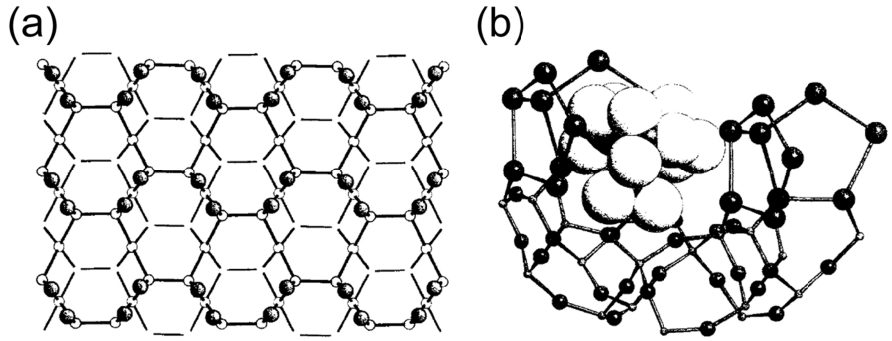

Figure 16. (a) Schematic view of a section of the silicate layer of RUB-15 including the terminal OH groups (Projection along [100]). The Si atoms are located at the nodes of the network; the O atoms are located close to the midpoint between two Si atoms. Shaded spheres are OH groups. (b) The TMA ion embedded inside the hydrated silicate layer. The TMA ion is shown as a space-filling model. Small, medium, and large spheres represent Si, O, and OH and H_2O, respectively.[56]

The topotactic conversion of layered silicates into 3-D zeolitic structures is an effective method for creation of novel zeolite structures. Each layer with zeolitic structure can be regarded as a building unit for bottom-up approach for synthesis of zeolites. The crystal structure of obtained materials reflects the structure of those building units, namely layered silicates. Therefore, the topotactic conversion by using unique structural layered silicates will lead to the formation of zeolites with novel structures through a clearly defined transformation process. Layered silicates with dimples on the interlayer surfaces, such as RUB-15, transform into a 3-D structure with confined space. If layered silicates with unique structures would be obtained, their topotactic conversion will provide novel 3-D structures which have not been obtained by conventional hydrothermal synthesis.

7.2. Intralayer condensation

Condensation of silanol groups of layered silicates is usually dehydration reaction between interlayer confronting silanol groups in adjacent layers (Figure 17a). The distance of neighboring silanol groups on the same plane is usually close each other in many

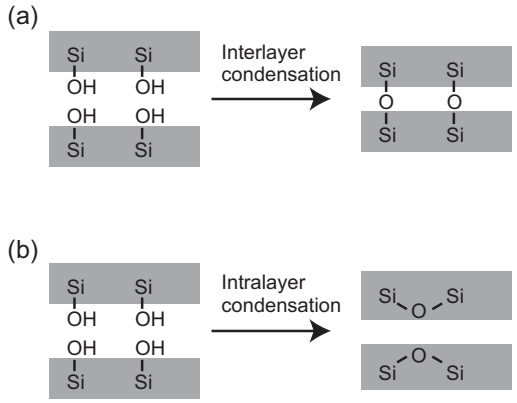

Figure 17. Schmatic model of (a) interlayer condensation and (b) intralayer condensation.

layered silicates. However, the condensation of silanol groups occurs in the same layer, namely *intralayer* condensation (Figure 17b), occurs in only a few cases. Intralayer condensation should create a new siloxane network with distortion by the formation of strained rings, such as three- or four-membered rings.

The silicate layer of kanemite composed of only single SiO_4 sheets is flexible. For example, C_{16}TMA-kanemite is transformed to a 2-D orthorhombic structure (KSW-2) via the bending,[91] which has been reported for only kanemite so far. Apperley *et al.* reported that protonated kanemite (H-kanemite) has Q^3 and Q^4 environmental Si.[170] Because Si atoms of kanemite are only Q^3 environment, condensation of silanol groups by acid treatment is suggested. However, the details of the condensation (inter- or intralayer) were not clear. Kimura *et al.* investigated the silicate structure of kanemite after intercalation with C_{16}TMA cations with high temperature.[90] The environments of Si atoms are Q^3 and Q^4 in spite of the lamellar structure of C_{16}TMA-kanemite. Because additional intercalation of *n*-decanol into C_{16}TMA-kanemite leads to the expansion of basal spacing, the intralayer condensation occurs between silanol groups on the same layers. The flexible layer of kanemite allows distortion of the layer, including the formation of new four-membered

rings. The intralayer condensation of layered silicates is reported for only kanemite, and other cases have not been investigated so far.

8. Pillaring of Layered Silicates by Silylation Reactions

Layered materials can be converted to microporous materials by intercalation of guest species and the following immobilization. By using clay minerals, microporous materials have been obtained by intercalation of polycations and calcination. These pillared clays with 2-dementionally confined spaces are applicable for catalysts, molecular sieve, supports, and adsorbents.[171-174] Layered silicates, composed only SiO_4 tetrahedra, have also been converted into pillared layered materials by using covalent immobilization. In this section, pillared layered silicates through covalent modifications of $SiOH/SiO^-$ groups are reviewed.

8.1. Pillaring with polymeric silica species

Landis *et al.* and Pinnavaia *et al.* reported the pillaring of magadiite and kenyaite with silica species.[175-176] Alkylamine- or alkylammonium-intercalated layered silicates are reacted with tetraethoxysilane (TEOS). After calcination, silica-pillared layered silicates with micropores are obtained (Figure 18). Expansion with alkylamine or alkylammonium is necessary to obtain a large interlayer space. The increase in the added amount of TEOS makes the larger interlayer spacings. However, microporous surface area reaches to a maximum and then decreased with the increasing amount of TEOS, suggesting the decrease in the lateral separation of the silica pillars. Subsequently, the effect of catalysts for polymerization of silica species was investigated by Jeong *et al*.[177-178] Pillaring with

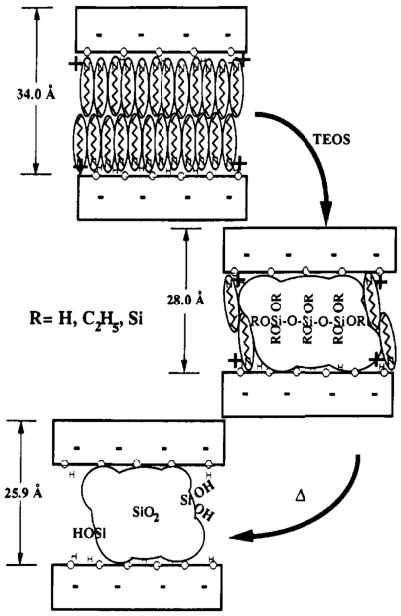

Figure 18. Schematic representation of the pillaring of octylamine solvated octylammonium-magadiite by reaction with TEOS.[176]

polymeric silica is reported for other layered silicates, such as octosilicate,[179] MCM-22,[180-181] kanemite,[182] kenyaite,[183] and potassium layered silicate with kenyaite-like structure.[184] Pillaring of various metal oxides, such as alumina, titania, and zirconia, is achieved by using MCM-22 and octosilicate. [185-186]

Pillaring of layered silicates with silica decreased the crystallinity because of fragmentation and dissolution of silicate layers. Maheshwari and Tsapatsis *et al.* developed the pillaring process at low-temperature for the retention of the crystallinity.[187] C_{16}TMA-intercalated layered MCM-22 is washed with water repeatedly and then treated with ultrasonication. The obtained material has a new ordered layered structure. Interestingly, the swelling procedure is reversible because of restoring back to MCM-22 by acid treatment. The swollen product is pillared, and porous material with the MCM-36 structure is obtained. The swollen sample is partially exfoliated via compounding with polymers.

Although the pillaring with polymeric silica leads to the formation of a two-dimensionally confined porous structure, the size and distribution of pillars are hardly controllable. Therefore, well-ordered arrangement of SiOH/Si^- groups on layered silicates cannot reflect the ordering and size distribution of pores in the products.

8.2. Pillaring with monomeric silylation reagents

Pore size of the products, obtained by topotactic conversion to 3-D structures via condensation of silanol groups of layered silicates, depends on the lateral distance between silanol groups on a silicate layer. For example, PLS-1 has a half ring containing 2 silanol groups and 2 siloxane bonds (Figure 14a right, HOSi-O-Si-O-Si-O-SiOH). On the facing layer, the same half ring is located in a face-to-face manner. By the topotactic condensation of these half rings between facing layers, a new eight-membered ring (8MR) is created (Figure 14b right).

In 2004, Fan and Tatsumi *et al.* reported a concept of *Interlayer-Expanded Zeolite* (IEZ) which is pillared with monomeric pillaring reagents.[188] They synthesized crystalline titanosilicate by pillaring MWW-type layered silicate with monomeric $Ti(OBu)_4$. Inagaki and Tatsumi *et al.* applied this method by using silylation reagents.[189] PLS-1 is silylated with dichlorodimethylsilane and then calcined. The silylation reagent with two reactive groups (Si-Cl) acts as a single molecular pillaring agent. Although direct topotactic conversion of layered silicate PLS-1 leads CDS-1 with 8MRs in a previous report,[63] the pillared product possesses 10MRs because of two additional pillaring molecular reagents. This method has been extended for various layered silicates with MWW, FER, CDO and MCM-47 zeolite precursors by using diethoxydimethylsilane.[190] They determined the crystal structure of the IEZs by electron microscopic investigations (Figure 19B). Although

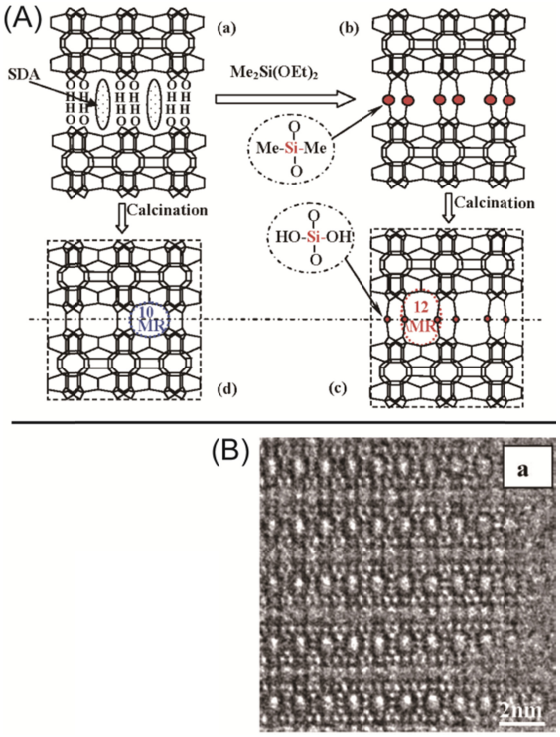

Figure 19. (A): Sequence of postsynthesizing interlayer expanded zeolites through dialkoxysilylation of lamellar precursor (using MWW precursor as a representative). (a) MWW lamellar precursor, (b) the interlayer structure expanded via the reaction of silane with silanols on the layer surface, (c) formation of a novel ordered 3-D crystalline structure with enlarged pore window in comparison to normal 3D MWW structure, and (d) common 3-D MWW structure obtained by a direct interlayer dehydroxylation. (B): HRTEM images of calcined IEZ-MWW taken along the direction of layer stacking.[190]

the direct topotactic conversion of MWW type layered silicate leads the creation of pores with 10MRs, the pillared IEZ has pores with 12MRs (Figure 19A). IEZ of PREFER was also synthesized, and their structures were carefully investigated by Ruan and Terasaki *et al.*[191]

The silylation procedure was improved by Inagaki and Tatsumi from liquid-phase to vapor-phase silylation.[192] Because the conventional liquid-phase silylation was performed in a strongly acidic condition, the number of acid sites in the framework

considerably decreases due to leaching of a part of framework Al during the silylation. In contrast, vapor-phase silylation prevents the decrease of Al in the framework. The product obtained by vapor-phase silylation shows higher catalytic activity than that by the liquid phase. Pillaring reagents also come from the fragmentation of the host layers. Ikeda *et al.* reported that thermal acid treatment of layered silicates (PLS-1, PLS-3, PLS-4, and PREFER) leads monomeric Si pillared structure without silylation reagents.[193]

Pillaring with single molecular species generates small pores with well ordering while pillaring with polymeric silica leads to the formation of lager pores but lower ordering. These two methods are complementary from these points of view. Pillaring with monomeric Si species enables well ordering of pillars and construction of new crystal structures with expanded pores. Although the expansion of pores is limited to the increase by two siloxane bonds, this expansion of pores is effective for the applications of catalysts and adsorbents. For example, IEZs prepared from precursors with MWW topology exhibit higher activities in the redox and solid acid-catalyzed reactions for bulky molecules than those of their counterparts with conventional MWW topology.[190]

8.3. Pillaring with phenylene-bridged silylation reagents

Both of lager pores and well-ordered pillaring has been developed by using phenylene-bridged silylation reagents. Pillaring reagents, especially lager ones, should be rigid to prop interlayer space for the retention of created pores. Ishii *et al.* reported a pillaring of octosilicate with biphenylene-bridged silylation reagents such as 4,4′-bis(triethoxysilyl)biphenyl.[194] The product has porous structure with high surface area (616 m^2 g^{-1}). However, only 33% of silanol groups on the interlayer surface are silylated. Both T^3 and T^2 signals are observed in the spectrum, suggesting the condensation

of hydrolyzed triethoxysilyl groups of silylation reagents in the interlayer space. Pillaring by using biphenylene-bridged silylation reagents with methyldiethoxysilyl groups also results in unwanted condensation among silylation reagents.[195] In the case of using dimethylethoxysilyl groups, the interlayer distance is decreased to 0.60 nm. Díaz *et al*. reported the pillaring of magadiite with 4,4′-bis-(trimethoxysilylpropyl)viologen and 4-nitro-*N*,*N*′-bis(3-trimethoxysilyl)propylaniline.[196] Ordered pores are not obtained because of low degree of silylation (< 20%) and condensation of hydrolyzed trimethoxysilyl groups. Although pillaring with rigid biphenylene-bridged leads to the formation of a porous structure, these alkoxysilyl reagents are not advantageous for well-ordered pillaring and uniform pore size.

As described above, dichlorosilyl reagents can be immobilized onto octosilicate with high degree of silylation (ca. 90%) and uniform bidentate attachment with only T^2 environment.[121] Mochizuki *et al.* reported the pillaring of octosilicate with 1,4-bis(trichlorosilyl)benzene or 1,4-bis(dichloromethylsilyl)benzene (Figure 20).[197] The silylation degrees are from 83% to 88% calculated from Q^3/Q^4 ratio. The high degree of silylation is provided by active silylation reagents with trichlorosilyl groups and suitable

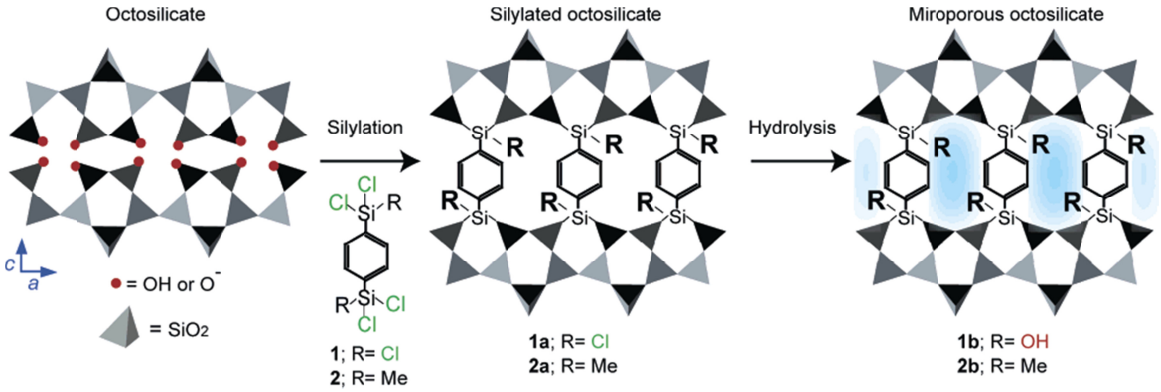

Figure 20. Silylation of octosilicate with 1,4-bis(trichloro- and dichloromethyl-silyl)benzenes.[197]

ordering/distance of SiOH/SiO^- groups on octosilicate. The pore size distribution is narrow, suggesting the formation of uniform pores derived from well-ordered immobilization of silylation reagents. The micropores derived from 1,4-bis-(trichlorosilyl)benzene shows a hydrophilic nature due to remaining Si-OH groups after hydrolysis of chlorosilyl groups. In contrast, those derived from 1,4-bis(dichloromethylsilyl)benzene shows a hydrophobic nature. Adsorption behavior of phenol and water onto these hybrids indicates the difference of the hydrophilicity/hydrophobicity of pores.

Selection of suitable layered silicates and molecular design of pillaring reagents make it possible to synthesize crystalline porous materials with not only larger pores but also well ordering of pores.

Corma *et al.* advanced the pillaring method of layered silicate with zeolite structure by using post treatment for introducing basic groups in the interlayer pillars.[198] MWW-type layered zeolite precursor was pillared with 1,4-bis(triethoxysilyl)benzene for creation of zeolite hybrid with expanded pores. Subsequently, amine groups were additionally immobilized onto benzene bridges by amination post-treatment. This porous material has both acid sites on zeolite layers and base sites of amine groups on benzene bridges. The product can act as a bifunctional catalyst for performing a two-step cascade reaction that involves the catalytic conversion of benzaldehyde dimethylacetal into benzylidene malononitrile.

Pillaring of layered silicates with phenylene-bridged silylation reagents can lead porous structure with expanded pore size. Prevention of the condensation of silylation reagents can be achieved by the design of silylation reagents and selection of layered silicates with suitable distance of SiOH/SiO^- groups. In addition, design of functional groups immobilized on pillars has potential for creation of novel nanospaces because these

functional groups and active sites on the surface of the layers are separated and individually designable. It can be claimed that more precise design of pores will provide unique properties with synergetic effects of two kinds of sites.

9. Summary and Significance of This Thesis

I reviewed material design of layered silicates, whose frameworks are composed of only SiO_4 tetrahedra, through covalent modifications such as silylation, esterification, condensation, and pillaring of silanol groups. The historical development of important discovery in this research area can be summarized as follows. In 1980's, silylation reactions were discovered and studied with simple silylation reagents. In late 1990's, molecular selective adsorption properties were discovered by using 2-D confined spaces designed by silylation reactions. In early 2000's, crystal structure of layered silicates can be designed by precise silylation reactions. In the same decade, immobilization of various functional groups by silylation was developed and their applications were investigated. In middle of 2000's, transformation from 2D to 3D structure was achieved by using topotactic conversion of layered silicates, especially with zeolitic layer. In late 2000's, the pores obtained by topotactic conversion were expanded by well-ordered pillaring with singular silica species. Nowadays, the pillaring of layered silicates has been developed to create the interlayer pores with not only larger size but also functionality on the pillars. Thus, covalent modification of layered silicates makes it possible to design interlayer surfaces, intralayer frameworks, and interlayer spaces.

The interactions, especially electrostatic interactions, between layered host

materials and guest species strongly affect the reactivity and selectivity of intercalation reactions. However, design of layer charge of layered silicate has not been focused in spite of wide variety of reactions of silanol groups. Versatile control of layer charge including anionic-nonionic-cationic will significantly enlarge the versatility of layered silicates. In this thesis, I achieve the covalent modifications of layered silicates for layer-charge control, and their transformations into nanostructured materials.

10. References

[1] D. O'Hare, in *Inorganic Materials, 2nd Edition*, 2nd ed. (Eds.: D. W. Bruce, D. O'Hare), John Wiley & Sons Ltd., Chichester, **1997**, pp. 171-244.

[2] F. Bergaya, B. K. G. Theng, G. Lagaly, *Handbook of Clay Science*, Elsevier Ltd., Amsterdam, **2006**.

[3] S. Yariv, H. Cross, *Organo-clay complexes and interactions*, Marcel Dekker, New York, **2002**.

[4] S. M. Auerbach, K. A. Carrado, P. K. Dutta, *Handbook of Layered Materials*, Marcel Dekker, Inc., New York, **2004**.

[5] M. Ogawa, K. Kuroda, *Chem. Rev.* **1995**, *95*, 399-438.

[6] M. Alexandre, P. Dubois, *Mater. Sci. Eng., R* **2000**, *28*, 1-63.

[7] M. Ogawa, K. Kuroda, *Bull. Chem. Soc. Jpn.* **1997**, *70*, 2593-2618.

[8] E. Ruiz-Hitzky, *Chem. Rec.* **2003**, *3*, 88-100.

[9] S. Sinha Ray, M. Okamoto, *Prog. Polym. Sci.* **2003**, *28*, 1539-1641.

[10] S. K. Parida, S. Dash, S. Patel, B. K. Mishra, *Adv. Colloid Interface Sci.* **2006**, *121*, 77-110.

[11] E. Ruiz-Hitzky, P. Aranda, M. Darder, G. Rytwo, *J. Mater. Chem.* **2010**, *20*, 9306-9321.

[12] W. Schwieger, G. Lagaly, in *Handbook of Layered Materials* (Eds.: S. M. Auerbach, K. A. Carrado, P. K. Dutta), Marcel Dekker, Inc., New York, **2004**, pp. 541-629.

[13] E. Burzo, in *Magnetic Properties · Magnetic Properties of Non-Metallic Inorganic Compounds Based on Transition Elements, Vol. 27I5b* (Ed.: H. P. J. Wijn), Springer-Verlag, Berlin Heidelberg, **2009**.

[14] P. J. Sideris, U. G. Nielsen, Z. Gan, C. P. Grey, *Science* **2008**, *321*, 113-117.

[15] H. P. Eugster, *Science* **1967**, *157*, 1177-1180.

[16] G. W. Brindley, *Am. Mineral.* **1969**, *54*, 1583-&.

[17] J. M. Rojo, E. Ruiz-Hitzky, J. Sanz, *Inorg. Chem.* **1988**, *27*, 2785-2790.

[18] K. Beneke, G. Lagaly, *Am. Mineral.* **1983**, *68*, 818-826.

[19] R. L. Hay, *Contrib. Mineral. Petrol.* **1968**, *17*, 255-274.

[20] R. A. Sheppard, A. J. Gude, R. L. Hay, *Am. Mineral.* **1970**, *55*, 358-366.

[21] H. Annehed, L. Falth, F. J. Lincoln, *Z. Kristallogr.* **1982**, *159*, 203-210.

[22] Z. Johan, G. F. Maglione, *Bull. Soc. Fr. Mineral. Cristallogr.* **1972**, *95*, 371-382.

[23] K. Beneke, G. Lagaly, *Am. Mineral.* **1977**, *62*, 763-771.

[24] H. Gies, B. Marler, S. Vortmann, U. Oberhagemann, P. Bayat, K. Krink, J. Rius, I. Wolf, C. Fyfe, *Microporous Mesoporous Mater.* **1998**, *21*, 183-197.

[25] L. A. J. Garvie, B. Devouard, T. L. Groy, F. Cámara, P. R. Buseck, *Am. Mineral.* **1999**, *84*, 1170-1175.

[26] S. Vortmann, J. Rius, B. Marler, H. Gies, *Eur. J. Mineral.* **1999**, *11*, 125-134.

[27] R. K. Iler, *J. Colloid Sci.* **1964**, *19*, 648-657.

[28] W. Schwieger, D. Heidemann, K.-H. Bergk, *Rev. Chim. Miner.* **1985**, *22*, 639-650.

[29] G. Borbély, H. K. Beyer, H. G. Karge, W. Schwieger, A. Brandt, K.-H. Bergk, *Clays Clay Miner.* **1991**, *39*, 490-497.

[30] S. Vortmann, J. Rius, S. Siegmann, H. Gies, *J. Phys. Chem. B* **1997**, *101*, 1292-1297.

[31] I. Wolf, H. Gies, C. A. Fyfe, *J. Phys. Chem. B* **1999**, *103*, 5933-5938.

[32] U. Brenn, H. Ernst, D. Freude, R. Herrmann, R. Jähnig, H. G. Karge, J. Kärger, T. König, B. Mädler, U. T. Pingel, D. Prochnow, W. Schwieger, *Microporous Mesoporous Mater.* **2000**, *40*,

43-52.

[33] M. Borowski, I. Wolf, H. Gies, *Chem. Mater.* **2002**, *14*, 38-43.

[34] M. Borowski, O. Kovalev, H. Gies, *Microporous Mesoporous Mater.* **2008**, *107*, 71-80.

[35] A. K. Pant, D. W. J. Cruickshank, *Acta Crystallogr., B* **1968**, *24*, 13-19.

[36] A. K. Pant, *Acta Crystallogr., B* **1968**, *24*, 1077-1083.

[37] M. E. Fleet, G. S. Henderson, *J. Solid State Chem.* **1995**, *119*, 400-404.

[38] V. Kahlenberg, G. Dörsam, M. Wendschuh-Josties, R. X. Fischer, *J. Solid State Chem.* **1999**, *146*, 380-386.

[39] W. H. Taylor, S. Naray-Szabo, *Z. Kristallogr.* **1931**, *77*, 146-158.

[40] D. Benbertal, A. Mosset, *J. Solid State Chem.* **1994**, *108*, 340-345.

[41] K. Beneke, P. Thiesen, G. Lagaly, *Inorg. Chem.* **1995**, *34*, 900-907.

[42] B. H. W. S. de Jong, H. T. J. Supèr, A. L. Spek, N. Veldman, G. Nachtegaal, J. C. Fischer, *Acta Crystallogr., B* **1998**, *54*, 568-577.

[43] S. Rakić, V. Kahlenberg, *Eur. J. Mineral.* **2001**, *13*, 1215-1221.

[44] S. Rakić, V. Kahlenberg, B. C. Schmidt, *Z. Kristallogr.* **2003**, *218*, 413-420.

[45] A. L. Spek, B. H. W. S. d. Jong, *Acta Crystallogr., E* **2005**, *61*, i188-i190.

[46] X. Wang, L. Liu, J. Huang, A. J. Jacobson, *J. Solid State Chem.* **2004**, *177*, 2499-2505.

[47] I. Bull, J. B. Parise, *Acta Crystallogr., C* **2003**, *59*, i100-i102.

[48] K. Komura, T. Ikeda, A. Kawai, F. Mizukami, Y. Sugi, *Chem. Lett.* **2007**, *36*, 1248-1249.

[49] T. Ikeda, M. Uenaka, K. Komura, Y. Sugi, *Chem. Lett.* **2010**, *39*, 747-749.

[50] E. Arroyabe, R. Kaindl, D. M. Többens, V. Kahlenberg, *Inorg. Chem.* **2009**, *48*, 11929-11934.

[51] A. J. Blake, K. R. Franklin, B. M. Lowe, *J. Chem. Soc., Dalton Trans.* **1988**, 2513-2517.

[52] S. J. Andrews, M. Z. Papiz, R. McMeeking, A. J. Blake, B. M. Lowe, K. R. Franklin, J. R. Helliwell, M. M. Harding, *Acta Crystallogr., B* **1988**, *44*, 73-77.

[53] M. E. Leonowicz, J. A. Lawton, S. L. Lawton, M. K. Rubin, *Science* **1994**, *264*, 1910-1913.

[54] L. Schreyeck, P. Caullet, J. C. Mougenel, J. L. Guth, B. Marler, *Microporous Mater.* **1996**, *6*,

259-271.

[55] L. Schreyeck, P. Caullet, J. C. Mougenel, J. L. Guth, B. Marler, *Stud. Surf. Sci. Catal.* **1997**, *105*, 1949-1956.

[56] U. Oberhagemann, P. Bayat, B. Marler, H. Gies, J. Rius, *Angew. Chem., Int. Ed.* **1996**, *35*, 2869-2872.

[57] Z. Li, B. Marler, H. Gies, *Chem. Mater.* **2008**, *20*, 1896-1901.

[58] Y. Akiyama, F. Mizukami, Y. Kiyozumi, K. Maeda, H. Izutsu, K. Sakaguchi, *Angew. Chem., Int. Ed.* **1999**, *38*, 1420-1422.

[59] T. Ikeda, Y. Akiyama, F. Izumi, Y. Kiyozumi, F. Mizukami, T. Kodaira, *Chem. Mater.* **2001**, *13*, 1286-1295.

[60] A. Burton, R. J. Accardi, R. F. Lobo, M. Falcioni, M. W. Deem, *Chem. Mater.* **2000**, *12*, 2936-2942.

[61] L. D. Rollmann, J. L. Schlenker, S. L. Lawton, C. L. Kennedy, G. J. Kennedy, *Microporous Mesoporous Mater.* **2002**, *53*, 179-193.

[62] D. L. Dorset, G. J. Kennedy, *J. Phys. Chem. B* **2004**, *108*, 15216-15222.

[63] T. Ikeda, Y. Akiyama, Y. Oumi, A. Kawai, F. Mizukami, *Angew. Chem., Int. Ed.* **2004**, *43*, 4892-4896.

[64] R. Millini, L. C. Carluccio, A. Carati, G. Bellussi, C. Perego, G. Cruciani, S. Zanardi, *Microporous Mesoporous Mater.* **2004**, *74*, 59-71.

[65] T. V. Whittam, in *U. S. Patent*, Inperial Chemical Industries PLC, U. S., **1983**.

[66] S. Zanardi, A. Alberti, G. Cruciani, A. Corma, V. Fornés, M. Brunelli, *Angew. Chem., Int. Ed.* **2004**, *43*, 4933-4937.

[67] Y. X. Wang, H. Gies, J. H. Lin, *Chem. Mater.* **2007**, *19*, 4181-4188.

[68] H.-K. Jeong, S. Nair, T. Vogt, L. C. Dickinson, M. Tsapatsis, *Nat. Mater.* **2003**, *2*, 53-58.

[69] M. Choi, K. Na, J. Kim, Y. Sakamoto, O. Terasaki, R. Ryoo, *Nature* **2009**, *461*, 246-249.

[70] K. Na, M. Choi, W. Park, Y. Sakamoto, O. Terasaki, R. Ryoo, *J. Am. Chem. Soc.* **2010**, *132*,

4169-4177.

[71] E. N. Coker, L. V. C. Rees, *J. Mater. Chem.* **1993**, *3*, 523-529.

[72] A. de Lucas, L. Rodríguez, J. Lobato, P. Sánchez, *Chem. Eng. Sci.* **2002**, *57*, 479-486.

[73] Y. Ide, N. Ochi, M. Ogawa, *Angew. Chem., Int. Ed.* **2011**, *50*, 654-656.

[74] N. Mizukami, M. Tsujimura, K. Kuroda, M. Ogawa, *Clays Clay Miner.* **2002**, *50*, 799-806.

[75] M. Ogawa, Y. Ide, M. Mizushima, *Chem. Commun.* **2010**, *46*, 2241-2243.

[76] G. Lagaly, K. Beneke, P. Dietz, A. Weiss, *Angew. Chem., Int. Ed.* **1974**, *13*, 819-821.

[77] K. Beneke, G. Lagaly, *Am. Mineral.* **1989**, *74*, 224-229.

[78] G. Lagaly, K. Beneke, A. Weiss, *Am. Mineral.* **1975**, *60*, 650-658.

[79] G. Lagaly, K. Beneke, A. Weiss, *Am. Mineral.* **1975**, *60*, 642-649.

[80] T. Yanagisawa, T. Shimizu, K. Kuroda, C. Kato, in *Abstract of 56th Annual Meeting of The Chemical Society of Japan*, Tokyo, **1988**, p. 761.

[81] T. Yanagisawa, T. Shimizu, K. Kuroda, C. Kato, *Bull. Chem. Soc. Jpn.* **1990**, *63*, 988-992.

[82] C. T. Kresge, M. E. Leonowicz, W. J. Roth, J. C. Vartuli, J. S. Beck, *Nature* **1992**, *359*, 710-712.

[83] T. Kimura, K. Kuroda, *Adv. Funct. Mater.* **2009**, *19*, 511-527.

[84] S. Inagaki, Y. Fukushima, K. Kuroda, *J. Chem. Soc., Chem. Commun.* **1993**, 680-682.

[85] T. Kimura, D. Itoh, T. Shigeno, K. Kuroda, *Langmuir* **2002**, *18*, 9574-9577.

[86] M. Kato, T. Shigeno, T. Kimura, K. Kuroda, *Chem. Mater.* **2004**, *16*, 3224-3230.

[87] T. Kimura, D. Itoh, T. Shigeno, K. Kuroda, *Bull. Chem. Soc. Jpn.* **2004**, *77*, 585-590.

[88] T. Kimura, M. Suzuki, T. Ikeda, K. Kato, M. Maeda, S. Tomura, *Microporous Mesoporous Mater.* **2006**, *95*, 146-153.

[89] H. Tamura, D. Mochizuki, T. Kimura, K. Kuroda, *Chem. Lett.* **2007**, *36*, 444-445.

[90] T. Kimura, D. Itoh, N. Okazaki, M. Kaneda, Y. Sakamoto, O. Terasaki, Y. Sugahara, K. Kuroda, *Langmuir* **2000**, *16*, 7624-7628.

[91] T. Kimura, T. Kamata, M. Fuziwara, Y. Takano, M. Kaneda, Y. Sakamoto, O. Terqasaki, Y.

Sugahara, K. Kuroda, *Angew. Chem., Int. Ed.* **2000**, *39*, 3855-3859.

[92] T. Kimura, S. Huang, A. Fukuoka, K. Kuroda, *J. Mater. Chem.* **2009**, *19*, 3859-3866.

[93] T. Kimura, H. Tamura, M. Tezuka, D. Mochizuki, T. Shigeno, T. Ohsuna, K. Kuroda, *J. Am. Chem. Soc.* **2008**, *130*, 201-209.

[94] R. García, I. Díaz, C. Márquez-Álvarez, J. Pérez-Pariente, *Chem. Mater.* **2006**, *18*, 2283-2292.

[95] N. Alam, R. Mokaya, *J. Mater. Chem.* **2008**, *18*, 1383-1391.

[96] G. Pál-Borbély, H. K. Beyer, Y. Kiyozumi, F. Mizukami, *Microporous Mater.* **1997**, *11*, 45-51.

[97] G. Pál-Borbély, H. K. Beyer, Y. Kiyozumi, F. Mizukami, *Microporous Mesoporous Mater.* **1998**, *22*, 57-68.

[98] M. Salou, Y. Kiyozumi, F. Mizukami, P. Nair, K. Maeda, S. Niwa, *J. Mater. Chem.* **1998**, *8*, 2125-2132.

[99] G. Pál-Borbély, Á. Szegedi, H. K. Beyer, *Microporous Mesoporous Mater.* **2000**, *35-36*, 573-584.

[100] T. Selvam, B. Bandarapu, G. T. P. Mabande, H. Toufar, W. Schwieger, *Microporous Mesoporous Mater.* **2003**, *64*, 41-50.

[101] F. Feng, K. J. Balkus, *Microporous Mesoporous Mater.* **2004**, *69*, 85-96.

[102] T. Selvam, G. T. P. Mabande, W. Schwieger, Y. Sugi, I. Toyama, Y. Kubota, H. S. Lee, J. H. Kim, *Catal. Lett.* **2004**, *94*, 17-24.

[103] T. Ikeda, S. Kayamori, F. Mizukami, *J. Mater. Chem.* **2009**, *19*, 5518-5525.

[104] Y. Wang, Y. Shang, J. Wu, J. Zhu, Y. Yang, C. Meng, *J. Chem. Technol. Biotechnol.* **2010**, *85*, 279-282.

[105] H. P. Boehm, *Angew. Chem., Int. Ed.* **1966**, *5*, 533-544.

[106] E. F. Vansant, P. Van Der Voort, K. C. Vrancken, *Characterization and Chemical Modification of the Silica Surface*, Elsevier, Amsterdam, **1995**.

[107] E. Ruiz-Hitzky, J. M. Rojo, *Nature* **1980**, *287*, 28-30.

[108] E. Ruiz-Hitzky, J. M. Rojo, G. Lagaly, *Colloid Polym. Sci.* **1985**, *263*, 1025-1030.

[109] T. Yanagisawa, K. Kuroda, C. Kato, *React. Solids* **1988**, *5*, 167-175.

[110] T. Yanagisawa, K. Kuroda, C. Kato, *Bull. Chem. Soc. Jpn.* **1988**, *61*, 3743-3745.

[111] K. Endo, Y. Sugahara, K. Kuroda, *Bull. Chem. Soc. Jpn.* **1994**, *67*, 3352-3355.

[112] S. Okutomo, K. Kuroda, M. Ogawa, *Appl. Clay Sci.* **1999**, *15*, 253-264.

[113] K.-W. Park, J. H. Jung, S.-K. Kim, O.-Y. Kwon, *Appl. Clay Sci.* **2009**, *46*, 251-254.

[114] M. Ogawa, S. Okutomo, K. Kuroda, *J. Am. Chem. Soc.* **1998**, *120*, 7361-7362.

[115] I. Fujita, K. Kuroda, M. Ogawa, *Chem. Mater.* **2003**, *15*, 3134-3141.

[116] I. Fujita, K. Kuroda, M. Ogawa, *Chem. Mater.* **2005**, *17*, 3717-3722.

[117] Y. Ide, M. Ogawa, *Angew. Chem., Int. Ed.* **2007**, *46*, 8449-8451.

[118] S. Toriya, S. Kobayashi, T. Takei, M. Fuji, T. Watanabe, M. Chikazawa, *Colloid. Polym. Sci.* **2003**, *281*, 1121-1126.

[119] M. Ogawa, M. Miyoshi, K. Kuroda, *Chem. Mater.* **1998**, *10*, 3787-3789.

[120] A. Shimojima, D. Mochizuki, K. Kuroda, *Chem. Mater.* **2001**, *13*, 3603-3609.

[121] D. Mochizuki, A. Shimojima, K. Kuroda, *J. Am. Chem. Soc.* **2002**, *124*, 12082-12083.

[122] D. Mochizuki, A. Shimojima, T. Imagawa, K. Kuroda, *J. Am. Chem. Soc.* **2005**, *127*, 7183-7191.

[123] D. Mochizuki, K. Kuroda, *New J. Chem.* **2006**, *30*, 277-284.

[124] K.-W. Park, S.-Y. Jeong, O.-Y. Kwon, *Appl. Clay Sci.* **2004**, *27*, 21-27.

[125] S.-F. Wang, M.-L. Lin, Y.-N. Shieh, Y.-R. Wang, S.-J. Wang, *Ceram. Int.* **2007**, *33*, 681-685.

[126] C.-M. Leu, Z.-W. Wu, K.-H. Wei, *Chem. Mater.* **2002**, *14*, 3016-3021.

[127] Z. Zhang, S. Saengkerdsub, S. Dai, *Chem. Mater.* **2003**, *15*, 2921-2925.

[128] V. S. O. Ruiz, G. C. Petrucelli, C. Airoldi, *J. Mater. Chem.* **2006**, *16*, 2338-2346.

[129] T. R. Macedo, C. Airoldi, *Dalton Trans.* **2009**, 7402-7409.

[130] T. R. Macedo, C. Airoldi, *New J. Chem.* **2009**, *33*, 2081-2089.

[131] T. R. Macedo, C. Airoldi, *Microporous Mesoporous Mater.* **2010**, *128*, 158-164.

[132] T. R. Macedo, G. C. Petrucelli, C. Airoldi, *Thermochim. Acta* **2010**, *502*, 30-34.

[133] R. Ishii, T. Ikeda, F. Mizukami, *J. Colloid Interface Sci.* **2009**, *331*, 417-424.

[134] Y. Ide, A. Fukuoka, M. Ogawa, *Chem. Mater.* **2007**, *19*, 964-966.

[135] Y. Ide, M. Ogawa, *Bull. Chem. Soc. Jpn.* **2007**, *80*, 1624-1629.

[136] Y. Ide, G. Ozaki, M. Ogawa, *Langmuir* **2009**, *25*, 5276-5281.

[137] Y. Ide, M. Matsuoka, M. Ogawa, *J. Am. Chem. Soc.* **2010**, *132*, 16762-16764.

[138] Y. Guo, Y. Wang, Q.-X. Yang, G.-D. Li, C.-S. Wang, Z.-C. Cui, J.-S. Chen, *Solid State Sci.* **2004**, *6*, 1001-1006.

[139] T. Yanagisawa, M. Harayama, K. Kuroda, C. Kato, *Solid State Ionics* **1990**, *42*, 15-19.

[140] K. Isoda, K. Kuroda, M. Ogawa, *Chem. Mater.* **2000**, *12*, 1702-1707.

[141] I. Shindachi, H. Hanaki, R. Sasai, T. Shichi, T. Yui, K. Takagi, *Chem. Lett.* **2004**, *33*, 1116-1117.

[142] I. Shindachi, H. Hanaki, R. Sasai, T. Shichi, T. Yui, K. Takagi, *Res. Chem. Intermed.* **2007**, *33*, 143-153.

[143] Y. Matsuo, Y. Yamada, M. Nishikawa, T. Fukutsuka, Y. Sugie, *J. Fluorine Chem.* **2008**, *129*, 1150-1155.

[144] K. M. Specht, M. Jackson, B. Sunkel, M. A. Boucher, *Appl. Clay Sci.* **2010**, *47*, 212-216.

[145] A. Schlossbauer, D. Schaffert, J. Kecht, E. Wagner, T. Bein, *J. Am. Chem. Soc.* **2008**, *130*, 12558-12559.

[146] K. Patel, S. Angelos, W. R. Dichtel, A. Coskun, Y.-W. Yang, J. I. Zink, J. F. Stoddart, *J. Am. Chem. Soc.* **2008**, *130*, 2382-2383.

[147] J. Nakazawa, T. D. P. Stack, *J. Am. Chem. Soc.* **2008**, *130*, 14360-14361.

[148] H. C. Kolb, M. G. Finn, K. B. Sharpless, *Angew. Chem., Int. Ed.* **2001**, *40*, 2004-2021.

[149] L. Mercier, G. A. Facey, C. Detellier, *J. Chem. Soc., Chem. Commun.* **1994**, 2111-2112.

[150] Y. Mitamura, Y. Komori, S. Hayashi, Y. Sugahara, K. Kuroda, *Chem. Mater.* **2001**, *13*, 3747-3753.

[151] S. Kiba, T. Itagaki, T. Nakato, K. Kuroda, *J. Mater. Chem.* **2010**, *20*, 3202-3210.

[152] J. J. Tunney, C. Detellier, *Chem. Mater.* **1993**, *5*, 747-748.

[153] J. J. Tunney, C. Detellier, *J. Mater. Chem.* **1996**, *6*, 1679-1685.

[154] Y. Komori, Y. Sugahara, K. Kuroda, *J. Mater. Res.* **1998**, *13*, 930-934.

[155] Y. Komori, H. Enoto, R. Takenawa, S. Hayashi, Y. Sugahara, K. Kuroda, *Langmuir* **2000**, *16*, 5506-5508.

[156] J. E. F. C. Gardolinski, G. Lagaly, *Clay Minerals* **2005**, *40*, 537-546.

[157] Y. Komori, Y. Sugahara, K. Kuroda, *Chem. Mater.* **1998**, *11*, 3-6.

[158] T. Itagaki, Y. Komori, Y. Sugahara, K. Kuroda, *J. Mater. Chem.* **2001**, *11*, 3291-3295.

[159] R. Takenawa, Y. Komori, S. Hayashi, J. Kawamata, K. Kuroda, *Chem. Mater.* **2001**, *13*, 3741-3746.

[160] Y. Kuroda, K. Ito, K. Itabashi, K. Kuroda, *Langmuir* **in press**, DOI: 10.1021/la1047134.

[161] W. Roth, D. Dorset, *Struct. Chem.* **2010**, *21*, 385-390.

[162] R. Millini, G. Perego, W. O. Parker, G. Bellussi, L. Carluccio, *Microporous Mater.* **1995**, *4*, 221-230.

[163] Y. X. Wang, H. Gies, B. Marler, U. Müller, *Chem. Mater.* **2005**, *17*, 43-49.

[164] K. Komura, T. Murase, Y. Sugi, M. Koketsu, *Chem. Lett.* **2010**, *39*, 948-949.

[165] B. Marler, N. Ströter, H. Gies, *Microporous Mesoporous Mater.* **2005**, *83*, 201-211.

[166] Y. Oumi, T. Takeoka, T. Ikeda, T. Yokoyama, T. Sano, *New J. Chem.* **2007**, *31*, 593-597.

[167] T. Ikeda, Y. Oumi, T. Takeoka, T. Yokoyama, T. Sano, T. Hanaoka, *Microporous Mesoporous Mater.* **2008**, *110*, 488-500.

[168] Y. Oumi, K. Takagi, T. Ikeda, H. Sasaki, T. Yokoyama, T. Sano, *J. Porous Mater.* **2009**, *16*, 641-649.

[169] T. Moteki, W. Chaikittisilp, A. Shimojima, T. Okubo, *J. Am. Chem. Soc.* **2008**, *130*, 15780-15781.

[170] D. C. Apperley, M. J. Hudson, M. T. J. Keene, J. A. Knowles, *J. Mater. Chem.* **1995**, *5*, 577-582.

[171] T. J. Pinnavaia, M.-S. Tzou, S. D. Landau, R. H. Raythatha, *J. Mol. Catal.* **1984**, *27*, 195-212.

[172] K. Ohtsuka, *Chem. Mater.* **1997**, *9*, 2039-2050.

[173] J. T. Kloprogge, *J. Porous Mater.* **1998**, *5*, 5-41.

[174] A. Gil, L. M. Gandia, M. A. Vicente, *Catal. Rev.-Sci. Eng.* **2000**, *42*, 145-212.

[175] M. E. Landis, B. A. Aufdembrink, P. Chu, I. D. Johnson, G. W. Kirker, M. K. Rubin, *J. Am. Chem. Soc.* **1991**, *113*, 3189-3190.

[176] J. S. Dailey, T. J. Pinnavaia, *Chem. Mater.* **1992**, *4*, 855-863.

[177] S.-Y. Jeong, O.-Y. Kwon, J.-K. Suh, H. Jin, J. M. Lee, *J. Colloid Interface Sci.* **1995**, *175*, 253-255.

[178] S.-Y. Jeong, J.-K. Suh, H. Jin, J.-M. Lee, O.-Y. Kwon, *J. Colloid Interface Sci.* **1996**, *180*, 269-275.

[179] K. Kosuge, A. Tsunashima, *J. Chem. Soc., Chem. Commun.* **1995**, 2427-2428.

[180] Y. J. He, G. S. Nivarthy, F. Eder, K. Seshan, J. A. Lercher, *Microporous Mesoporous Mater.* **1998**, *25*, 207-224.

[181] S. Maheshwari, C. Martínez, M. Teresa Portilla, F. J. Llopis, A. Corma, M. Tsapatsis, *J. Catal.* **2010**, *272*, 298-308.

[182] S. Toriya, Y. Tamura, T. Takei, M. Fuji, T. Watanabe, M. Chikazawa, *J. Colloid Interface Sci.* **2002**, *255*, 171-176.

[183] K.-W. Park, J. H. Jung, S.-Y. Jeong, O.-Y. Kwon, *J. Nanosci. Nanotechnol.* **2009**, *9*, 3160-3165.

[184] P. Thiesen, K. Beneke, G. Lagaly, *J. Mater. Chem.* **2002**, *12*, 3010-3015.

[185] J.-O. Barth, J. Kornatowski, J. A. Lercher, *J. Mater. Chem.* **2002**, *12*, 369-373.

[186] K. Kosuge, P. S. Singh, *Chem. Mater.* **2000**, *12*, 421-427.

[187] S. Maheshwari, E. Jordan, S. Kumar, F. S. Bates, R. L. Penn, D. F. Shantz, M. Tsapatsis, *J. Am. Chem. Soc.* **2008**, *130*, 1507-1516.

[188] W. Fan, P. Wu, S. Namba, T. Tatsumi, *Angew. Chem., Int. Ed.* **2004**, *43*, 236-240.

[189] S. Inagaki, T. Yokoi, Y. Kubota, T. Tatsumi, *Chem. Commun.* **2007**, 5188-5190.

[190] P. Wu, J. Ruan, L. Wang, L. Wu, Y. Wang, Y. Liu, W. Fan, M. He, O. Terasaki, T. Tatsumi, *J. Am. Chem. Soc.* **2008**, *130*, 8178-8187.

[191] J. Ruan, P. Wu, B. Slater, Z. Zhao, L. Wu, O. Terasaki, *Chem. Mater.* **2009**, *21*, 2904-2911.

[192] S. Inagaki, T. Tatsumi, *Chem. Commun.* **2009**, 2583-2585.

[193] T. Ikeda, S. Kayamori, Y. Oumi, F. Mizukami, *J. Phys. Chem. C* **2010**, *114*, 3466-3476.

[194] R. Ishii, Y. Shinohara, *J. Mater. Chem.* **2005**, *15*, 551-553.

[195] R. Ishii, T. Ikeda, T. Itoh, T. Ebina, T. Yokoyama, T. Hanaoka, F. Mizukami, *J. Mater. Chem.* **2006**, *16*, 4035-4043.

[196] U. Díaz, Á. Cantín, A. Corma, *Chem. Mater.* **2007**, *19*, 3686-3693.

[197] D. Mochizuki, S. Kowata, K. Kuroda, *Chem. Mater.* **2006**, *18*, 5223-5229.

[198] A. Corma, U. Díaz, T. García, G. Sastre, A. Velty, *J. Am. Chem. Soc.* **2010**, *132*, 15011-15021.

Chapter 2

Intercalation of Poly(oxyethylene) Alkyl Ether into Kanemite

1. Introduction

Intercalation of organic substances into inorganic layered materials affords two-dimensionally arranged inorganic-organic nanostructures.[1-4] Such nanostructures are potentially applicable for adsorbents and reaction media utilizing two-dimensionally confined nanospaces.[3,5-9] The control of interlayer environments is quite important for exploring the possibility of such applications. The hydrophobicity and hydrophilicity of interlayer region can be controlled by intercalation of various organic substances, and the kind of such intercalated organic substances is crucial to determine the interactions with adsorbates or reactants.[8,10]

Layered silicates, such as kenyaite, magadiite, and kanemite, whose frameworks are composed of only SiO_4 tetrahedra, have exchangeable metal cations in the interlayer space and $SiOH/SiO^-$ groups at the interlayer surfaces of silicate sheets.[11-12] The

interlayer environments can be modified in various ways including ion exchange of interlayer metal cations with organoammonium ions, adsorption of polar molecules by ion-dipole interaction and/or hydrogen bonding, acid-base reactions with amines, and silylation of SiOH/SiO^- groups.[1] The hydrophobicity and hydrophilicity of the interlayer spaces can be controlled by varying the amount of grafting alkylsilyl groups[6-7] and by carefully choosing silylating agents.[8] Covalently immobilized grafting groups are stable, but hydrophilic sites such as SiOH groups generated from chlorosilyl groups by hydrolysis are forced to be located at the interlayer surfaces of silicate sheets. Thus, the control of hydrophobicity and hydrophilicity in the entire interlayer environment by silylation is quite difficult.

Hydrophobicity and hydrophilicity of oligomeric surfactants and block copolymers are controllable by adjusting the chain lengths of both the hydrophobic and hydrophilic moieties. Poly(oxyethylene) alkyl ether ($C_nH_{2n+1}(OC_2H_4)_mOH$: C_nEO_m) is composed of hydrophobic alkyl chain and hydrophilic poly(oxyethylene) (EO) chain, and is versatile as a typical nonionic surfactant.[13-15] Then, it is expected that the hydrophobicity and hydrophilicity of the interlayer region can be controlled by intercalation of C_nEO_m into inorganic layered materials. Intercalation of C_nEO_m into layered clay minerals was reported,[10,16-18] and the modified interlayer region can accommodate both hydrophobic and hydrophilic molecules.[10,18] Actually, intercalation of C_nEO_m was induced by the interactions between EO units and metal cations.[10] In this case, metal cations remain in the interlayer space, and this hinders the applications utilizing coordination of EO chains with other guest species. In addition, C_nEO_m–clay intercalation compounds are disadvantageous for detailed characterization because natural layered clay minerals contain metal cations as impurities.[9] C_nEO_m is also intercalated into clay

minerals modified organically with alkyltrimethylammonium ions (C_nTMA).[19] Such C_nEO_m–C_nTMA–clay composites showed relatively higher basal spacings and higher densities of organic molecules, though the surfactants remained after the intercalation of C_nEO_m and the interlayer region was highly hydrophobic. Therefore, intercalation compounds composed of pure silicate sheets and C_nEO_m molecules without interlayer cations are very important from the viewpoints of the control of hydrophobicity, detailed characterization of these materials, mechanical and thermal stabilities of surfactants, and nanomaterials design.

In this study, such intercalation compounds are synthesized through intercalation of C_nEO_m into a layered silicate kanemite with simultaneous removal of interlayer cations. Kanemite is composed of flexible single silicate sheets and interlayer hydrated sodium cations.[11,20] Depending on the reaction conditions with various cationic species, the silicate framework is transformed to various mesostructures with lamellar,[21-22] 2-D hexagonal,[23-26] and 2-D orthorhombic phases.[27] The reaction between kanemite and C_nEO_m would also produce novel mesostructures different from simple intercalation compounds. However, it is difficult to intercalate C_nEO_m molecules into the layered silicates. The layer charge density of the layered silicate is normally higher than that of clay minerals, which also suppresses the intercalation of various guest species. C_nEO_m molecules are only adsorbed on the external surface of magadiite.[28] Direct intercalation of C_nEO_m into kanemite was also unsuccessful under various conditions (time, temperature, solvent, and pH) in a preliminary study. Therefore, I adopted a different strategy for the intercalation of C_nEO_m by using a layered $C_{16}TMA$–kanemite as an intermediate. Because first intercalation of C_nEO_m only yields an incomplete intercalation compound (C_nEO_m–$C_{16}TMA$–kanemite), further intercalation of C_nEO_m was performed by subsequent acid

treatment under the presence of an excess amount of C_nEO_m to form an intercalation compound consisting of silicate sheets and C_nEO_m molecules, resulting in the simultaneous removal of remaining C_{16}TMA ions. (Figure 1)

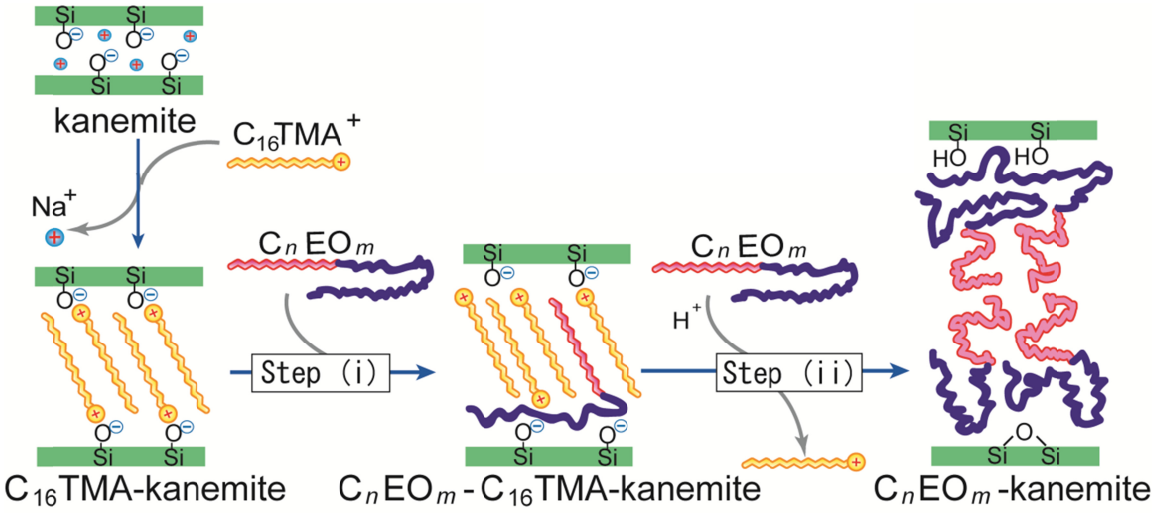

Figure 1. Synthetic pathway of C_nEO_m–kanemite intercalation compounds.

2. Experimental

Materials

Kanemite ($NaHSi_2O_5 \cdot 3H_2O$) was obtained through dispersing δ-$Na_2Si_2O_5$ (1.0 g) in deionized water (50 mL) with stirring for 0.5 h.[22] The Na/Si molar ratio of kanemite was ca. 0.5 (ICP). The XRD pattern was consistent with that of JCPDS file (25-1309). Hexadecyltrimethylammonium chloride ($C_{16}H_{33}N(CH_3)_3Cl$, denoted as C_{16}TMACl, Tokyo Kasei Kogyo Co.) and C_nEO_m (n = 12, m = 10, Sigma-Aldrich; n = 16, m = 10; and n = 18, m = 10, Aldrich) were used as received. An aqueous solution of HCl (1.0 M) was used for the acid treatment.

Synthesis of layered C_{16}TMA–kanemite intermediate

Layered C_{16}TMA–kanemite was prepared by the ion-exchange of interlayer Na cations in kanemite with C_{16}TMA cations. Kanemite (0.2 g) was added to an aqueous solution (40 mL) of 0.1 M C_{16}TMACl, where the C_{16}TMA/Si molar ratio was 2.0. After the mixture was stirred at room temperature for 2 days, the product was separated by centrifugation and air-dried. Because the Na content of C_{16}TMA–kanemite was virtually zero (ICP), complete ion-exchange reaction with C_{16}TMA cations was confirmed. After the reaction, the XRD peaks assigned to kanemite disappeared and new peaks with the *d*-spacings of 2.92, 1.45, and 0.97 nm appeared, indicating the formation of layered C_{16}TMA–kanemite.[22] The C_{16}TMA/Si molar ratio was 0.30 (CHN analysis and TG-DTA) and the value is similar to that (0.28) reported previously.[22] The ^{29}Si MAS NMR spectrum of the C_{16}TMA–kanemite showed three Q^3 signals with a weak Q^4 signal. The $Q^4/(Q^3+Q^4)$ ratio was 0.08, and the value was slightly lower than that reported previously.[22]

Intercalation of C_nEO_m into layered C_{16}TMA–kanemite

Intercalation of C_nEO_m was carried out by the following two step reactions.

Step (i): C_{16}TMA–kanemite (0.2 g) was dispersed in an aqueous solution of C_nEO_m (0.1 M, 40 mL). The mixture was stirred for 2 days at room temperature and centrifuged to remove the supernatant. At this step, the slurry is treated as described in the second step. However, to characterize the products obtained in the first step, the slurry was washed by dispersion in deionized water, stirred for 5 min, and centrifuged. This procedure was repeated twice to remove residual C_nEO_m completely and air-dried. Further repeated washings did not affect the organic content of this sample. The product is denoted as C_nEO_m–C_{16}TMA–kanemite.

Step (ii): The slurry C_nEO_m–$C_{16}TMA$–kanemite obtained before washing (0.2 g as dried $C_{16}TMA$–kanemite) was dispersed in an aqueous solution of C_nEO_m (0.1 M, 40 mL). The pH value of this mixture was 8.9. The pH value was then decreased down to 3.0 by adding 1.0 M HCl slowly over 0.5 h. The mixture was stirred for 1 day to complete the reaction. The slurry was centrifuged, washed twice with deionized water, and air-dried. The product is denoted as C_nEO_m–kanemite.

Characterization

X-ray powder diffraction patterns (XRD) were obtained with a Rigaku Rint-Ultima III powder diffractometer (CuKα, λ = 0.15418 nm) by using a parallel beam geometry equipped with a parabolic multilayer solar slit. The scanning electron microscopic (SEM) images were obtained by using a JEOL JSM-5500LV microscope at an accelerating voltage of 15 kV. The amounts of organic constituents were determined by CHN analysis (Perkin Elmer, 2400 Series II). Thermogravimetry (TG) measurements were carried out with a Rigaku Thermo Plus 2 instrument under a dry air flow at a heating rate of 10 °C min^{-1}, and the amounts of SiO_2 fractions in the products were calculated from the residual weights after heating up to 900 °C. Silicon and sodium contents in the samples were determined by inductively coupled plasma emission spectroscopy (ICP) (Varian Technology Japan Ltd. Vista-MPX). Each sample was decomposed in a melted $LiBO_2$ and then dissolved in 0.02 M HNO_3. Solid-state ^{13}C CP/MAS NMR spectra were recorded on a JEOL JNM-CMX-400 spectrometer at a resonance frequency of 100.4 MHz and a recycle delay of 5 s. The samples were put into a 7.5 mm (or 5 mm) zirconia rotor and spun at 5 kHz. Solid-state ^{29}Si MAS NMR spectra were also recorded on the same spectrometer at a resonance frequency of 79.42 MHz with a 45° pulse and a recycle delay of 100 s. It was

confirmed that the signals were fully relaxed under these conditions so that quantitative analysis was possible. The ^{13}C and ^{29}Si chemical shifts were referenced to tetramethylsilane.

3. Results and Discussion

3.1. Intercalation of $C_{16}EO_{10}$ into $C_{16}TMA$–kanemite ($C_{16}EO_{10}$–$C_{16}TMA$–kanemite)

The XRD pattern of $C_{16}EO_{10}$–$C_{16}TMA$–kanemite (Figure 2b) exhibits the peaks with the *d*-spacings of 3.34, 1.65, and 1.10 nm. The basal spacing of 3.34 nm is larger than that of the $C_{16}TMA$–kanemite intermediate (2.92 nm, Figure 2a) by 0.42 nm, suggesting the intercalation of $C_{16}EO_{10}$. The peaks can be assigned to (010), (020), and (030) peaks of a layered structure, respectively. The layered structure of $C_{16}EO_{10}$–$C_{16}TMA$–kanemite is also consistent with the result that all of the peaks disappeared after calcination at 550 °C for 6 h.

The $C_{16}TMA$/Si and $C_{16}EO_{10}$/Si molar ratios, calculated from the CHN analysis and TG data, are summarized in Table 1. The $C_{16}TMA$/Si ratio of $C_{16}EO_{10}$–$C_{16}TMA$–kanemite was 0.26. Because the ratio of $C_{16}TMA$–kanemite was 0.30, 85% of $C_{16}TMA$ cations remained in the $C_{16}EO_{10}$–$C_{16}TMA$–kanemite. The C/N ratio of the $C_{16}EO_{10}$–$C_{16}TMA$–kanemite (C/N = 29) is higher than that of the $C_{16}TMA$–kanemite (C/N = 19), indicating the presence of $C_{16}EO_{10}$ molecules in the product. The $C_{16}EO_{10}$/Si ratio of the $C_{16}EO_{10}$–$C_{16}TMA$–kanemite was 0.07, revealing that $C_{16}EO_{10}$ molecules are not so much intercalated in $C_{16}TMA$–kanemite. It is known that $C_{16}TMA$ cations are released from

C_{16}TMA–kanemite by cation exchange with H^+ by decreasing the pH value in a medium.[27] When the C_{16}TMA–kanemite intermediate was dispersed in an aqueous solution containing $C_{16}EO_{10}$, the pH value of the suspension became 8.9 (very low H^+ concentration) and then C_{16}TMA cations were poorly exchanged with H^+.

Because C_{16}TMA–kanemite can take up *n*-decanol into the interlayer,[22] the interlayer silicate surface is considered to be hydrophilic, though the interlayer is hydrophobic because of the presence of alkyl chains. Therefore, the driving forces for the intercalation of $C_{16}EO_{10}$ molecules into C_{16}TMA–kanemite are thought to be the followings: hydrophobic interaction among alkyl chains of both C_{16}TMA ions and $C_{16}EO_{10}$ molecules, and hydrogen bonding between the silicate layers and EO chains.

All of the ^{13}C CP/MAS NMR signals (15.6, 25.0, 28.6, 33.5, 34.8, 54.2, and 66.9 ppm) of C_{16}TMA–kanemite (Figure 3a) are assigned to carbon atoms in C_{16}TMA ions.[29] The ^{13}C CP/MAS NMR spectrum of $C_{16}EO_{10}$–C_{16}TMA–kanemite (Figure 3b) shows the additional signals (62.3, 71.5, 71.8, and 73.6 ppm) due to EO units in addition to those due to C_{16}TMA ions, indicating the presence of $C_{16}EO_{10}$. Therefore, it is quite obvious that $C_{16}EO_{10}$ molecules are intercalated into C_{16}TMA-kanemite, as proved by the increase in the *d*-value (XRD; Figure 2) with the increase in the amount of $C_{16}EO_{10}$ (Table 1). It is known that the signal assigned to the interior methylene carbons with an all-trans conformation appears at 33 ppm and shifts up field to 30 ppm for the trans/gauche conformation.[30] In the ^{13}C CP/MAS NMR spectrum of C_{16}TMA–kanemite, the signal due to the interior methylene carbons appears at 33.5 ppm, indicating that the conformation of the alkyl chains is all-trans. The molecular length of C_{16}TMA is calculated to be 2.47 nm,[31] and the thickness of silicate layer of kanemite is 0.60 nm.[32] If I assume that the arrangement of C_{16}TMA is monolayer, C_{16}TMA ions are inclined to the interlayer surface

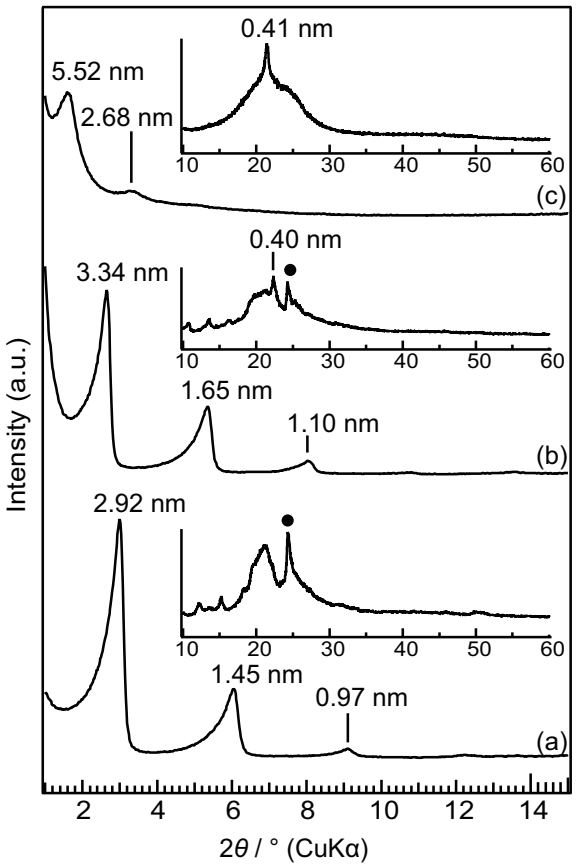

Figure 2. XRD patterns of (a) C_{16}TMA–kanemite, (b) $C_{16}EO_{10}$–C_{16}TMA–kanemite, and (c) $C_{16}EO_{10}$–kanemite. The insets show the profiles in higher 2θ regions.

Table 1. Summary of CHN analysis, SiO_2 contents, amount of organic species.

Sample	C / mass%	N / mass%	C / N	SiO_2 / mass%	C_{16}TMA / Si	C_nEO_{10} / Si	Formula*
C_{16}TMA–kanemite	42.7	2.6	19	36.2	0.30	–	$(C_{16}TMA)_{0.60}H_{1.24}Si_2O_{4.92}$
$C_{16}EO_{10}$–C_{16}TMA –kanemite	46.7	1.9	29	33.9	0.26	0.07	$(C_{16}EO_{10})_{0.14}(C_{16}TMA)_{0.52}$ $H_{0.96}Si_2O_{4.74}$
$C_{16}EO_{10}$–kanemite	41.8	0.0	–	30.6	0.00	0.19	$(C_{16}EO_{10})_{0.38}H_{1.04}Si_2O_{4.52}$
$C_{12}EO_{10}$–kanemite	34.1	0.1	–	41.7	0.01	0.12	–
$C_{18}EO_{10}$–kanemite	39.0	0.1	–	37.4	0.02	0.13	–

* The Si/O ratio was determined by the intensity ratio of the Q^3 and Q^4 signals of ^{29}Si MAS NMR data, and the hydrogen content was calculated by subtraction of remaining negative charge from the total charge balance.

at an angle of 70 °. The ^{13}C CP/MAS NMR spectrum of $C_{16}EO_{10}$–C_{16}TMA–kanemite shows the signal due to the interior methylene carbons at 33.6 ppm as well as a small signal at 30.9 ppm. Thus, the conformation of the interior methylene carbons of C_{16}TMA

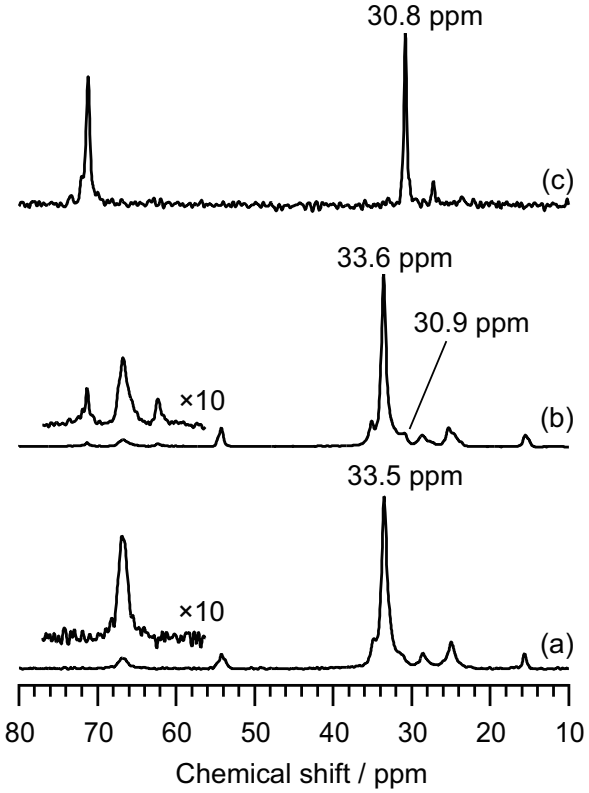

Figure 3. ^{13}C CP/MAS NMR spectra of (a) $C_{16}TMA$–kanemite, (b) $C_{16}EO_{10}$–$C_{16}TMA$–kanemite, and (c) $C_{16}EO_{10}$–kanemite.

ions and $C_{16}EO_{10}$ molecules is mostly all-trans, even though trans/gauche conformation is slightly present. Therefore, the conformation of alkyl chains is not transformed so largely with the intercalation of $C_{16}EO_{10}$ molecules into $C_{16}TMA$–kanemite.

The XRD pattern of $C_{16}EO_{10}$–$C_{16}TMA$–kanemite (Figure 2b inset) also shows a peak with the *d*-spacing of 0.40 nm assignable to closely packed alkyl chains.[33-36] In contrast, a similar peak was not observed in the XRD pattern of $C_{16}TMA$–kanemite (Figure 2a inset). Because the total amount of organic substances in $C_{16}EO_{10}$–$C_{16}TMA$–kanemite ($C_{16}TMA/Si + C_{16}EO_{10}/Si = 0.26 + 0.07 = 0.33$; Table 1) was larger than that of $C_{16}TMA$–kanemite (0.30), the alkyl chains in $C_{16}EO_{10}$–$C_{16}TMA$–kanemite should be packed more closely than those in $C_{16}TMA$–kanemite.

The condensation of silanol groups within the individual silicate sheets (*intra*layer condensation) was examined by ^{29}Si MAS NMR. The ^{29}Si MAS NMR spectrum of $C_{16}EO_{10}$–C_{16}TMA–kanemite (Figure 4b) shows both Q^3 and Q^4 peaks, and the $Q^4/(Q^3+Q^4)$ ratio (= 0.26) was increased relative to that of C_{16}TMA–kanemite (Figure 4a, $Q^4/(Q^3+Q^4)$ = 0.08). Therefore, the condensation of SiOH/SiO$^-$ groups of the silicate layer proceeded during the reaction of C_{16}TMA–kanemite with $C_{16}EO_{10}$. In the higher 2θ angles of the XRD pattern of $C_{16}EO_{10}$–C_{16}TMA–kanemite (Figure 2b inset), a peak at 2θ = 24.3°, attributed to (002) lattice plane (denoted as ●) was observed. Because the *c* axis of kanemite is directed parallel to the layer, the structural regularity originating from kanemite is retained in $C_{16}EO_{10}$–C_{16}TMA–kanemite.

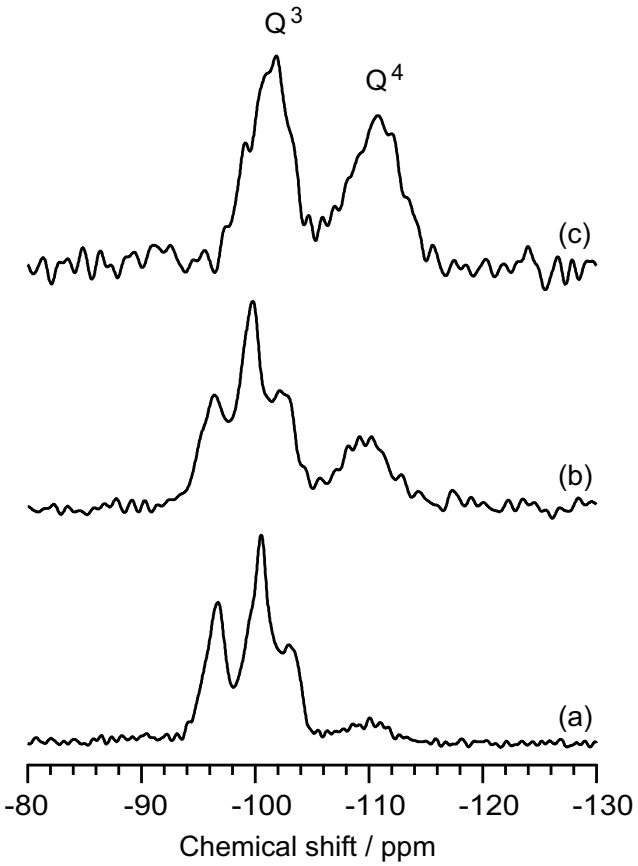

Figure 4. ^{29}Si MAS NMR spectra of (a) C_{16}TMA–kanemite, (b) $C_{16}EO_{10}$–C_{16}TMA–kanemite, and (c) $C_{16}EO_{10}$–kanemite.

The head groups of C_{16}TMA ions interact with SiO^- groups electrostatically on the interlayer surfaces of silicate layers.[22] Because the C_{16}TMA/Si ratio was decreased only 15% after the reaction with $C_{16}EO_{10}$, the headgroups of C_{16}TMA ions in the $C_{16}EO_{10}$–C_{16}TMA–kanemite should have a similar electrostatic interaction with SiO^- groups. Assuming that the headgroup of the C_{16}TMA ion is spherical, the space that one headgroup can occupy is 0.34 nm^2 on the interlayer surfaces of silicate layers.[37] On the basis of the C_{16}TMA/Si ratio in $C_{16}EO_{10}$–C_{16}TMA–kanemite and the lattice constant of kanemite (a = 0.4946 nm, c = 0.7227 nm), the silicate surface of $C_{16}EO_{10}$–C_{16}TMA–kanemite is calculated to be occupied with C_{16}TMA headgroups by 49%. Therefore, 51% of the surface of the silicate layer is not occupied. Intercalation of poly(oxyethylene) (without alkyl ether groups) into H–magadiite was investigated, and the proposed structural model shows that the EO chains lie flat and take a monolayer arrangement, because the d-value was increased by only 0.44–0.46 nm after the intercalation.[1] If the EO chains of $C_{16}EO_{10}$–C_{16}TMA–kanemite similarly lie flat and take a monolayer arrangement, the interlayer silicate surfaces are covered with the EO chains by 61% at the maximum because each EO chain can occupy the surface by 0.16 nm^2 $unit^{-1}$. Accordingly, the total occupied interlayer surface area is estimated to be 49% + 61% = 110 %. Because of the electrostatic interactions between C_{16}TMA ions and the silicate layers, C_{16}TMA ions are not likely to be apart from the silicate layers. Thus, some EO chains may be present apart from the interlayer silicate surface. The increase of the d-value (0.42 nm) can be explained by the assumption that a part of the EO chains changes the arrangement of the alkyl chains after intercalation of $C_{16}EO_{10}$ molecules into C_{16}TMA–kanemite.

3.2. Synthesis and structure of C_nEO_{10}–kanemite

The XRD pattern of the final product (named as $C_{16}EO_{10}$–kanemite), which was prepared from $C_{16}EO_{10}$–C_{16}TMA–kanemite by acid treatment in an aqueous solution of $C_{16}EO_{10}$ (**step (ii)**), shows the peaks with the *d*-spacings of 5.52 and 2.68 nm (Figure 2c) assignable to (010) and (020) of a layered structure. Indeed, these two peaks disappeared after calcination at 550 °C for 6 h. The basal spacing of 5.52 nm is much larger than that of $C_{16}EO_{10}$–C_{16}TMA–kanemite (3.34 nm, Figure 2b). The result suggests further intercalation of $C_{16}EO_{10}$ molecules by the acid treatment in the presence of $C_{16}EO_{10}$.

The nitrogen content of the product was zero (Table 1), indicating complete elimination of C_{16}TMA ions by the acid treatment. The $C_{16}EO_{10}$/Si ratio (0.19) of the $C_{16}EO_{10}$–kanemite is much larger than that of $C_{16}EO_{10}$–C_{16}TMA–kanemite (0.07), indicating further intercalation of $C_{16}EO_{10}$ molecules. On the basis of these results, it is confirmed that only $C_{16}EO_{10}$ molecules are present in the interlayer space.

All of the signals in the ^{13}C CP/MAS NMR spectrum of $C_{16}EO_{10}$–kanemite (Figure 3c) are assignable to carbon atoms in $C_{16}EO_{10}$ molecule.[38] The signal due to the interior methylene carbons appears at 30.8 ppm, suggesting the trans/gauche conformation of the alkyl chains. The EO chains of $C_{16}EO_{10}$ are flexible and tend to take a random conformation in the $C_{16}EO_{10}$–kanemite. The XRD pattern of the $C_{16}EO_{10}$–kanemite (Figure 2c inset) shows the peak with the *d*-spacing of 0.41 nm, indicating that alkyl chains of $C_{16}EO_{10}$ are closely packed in the interlayer region.[33-36]

The ^{29}Si MAS NMR spectrum of the $C_{16}EO_{10}$–kanemite (Figure 4c) shows Q^3 and Q^4 peaks. The $Q^4/(Q^3+Q^4)$ ratio (= 0.48) was increased from that of $C_{16}EO_{10}$–C_{16}TMA–kanemite ($Q^4/(Q^3+Q^4)$ = 0.26). The result indicates that SiOH/SiO^- groups in the silicate framework were condensed further during the acid treatment. Kimura *et al.* reported that

layered C_{16}TMA–kanemite is transformed into a mesostructured precursor for 2-D orthorhombic mesoporous silica (KSW-2) through the bending of silicate layers with inter- and intralayer condensation induced by acid treatment in the absence of C_nEO_m.[27] In the present case, the intralayer condensation occurs within the individual silicate sheets, as reported previously for the formation of layered C_{16}TMA–silicates.[22] In the higher 2θ angles of the XRD pattern of $C_{16}EO_{10}$–kanemite (Figure 2c inset), a peak attributed to the (002) lattice plane due to the structure of original kanemite was not observed. Therefore, the structural regularity of the original silicate layer was deteriorated by the intralayer condensation. Condensation of SiOH/SiO^- groups on layered silicate is crucial for the intercalation of $C_{16}EO_{10}$ molecules, therefore, this successful method is limited to kanemite. I tried to synthesize $C_{16}EO_{10}$-intercalated layered silicates by using other layered silicates, such as octosilicate and magadiite, that do not exhibit intralayer condensation. Though the intercalation of $C_{16}EO_{10}$ molecules into C_{16}TMA–octosilicate and C_{16}TMA–magadiite was confirmed after the acid treatment, the amounts of intercalated $C_{16}EO_{10}$ molecules were much lower ($C_{16}EO_{10}$/Si = 0.06 and 0.03, respectively) than that in $C_{16}EO_{10}$–kanemite. Also, the powder XRD profiles were very broad, suggesting poor intercalation ability for these cases.

C_nEO_{10}–kanemite complexes (n = 12 and 18) were also synthesized in a manner similar to that of the $C_{16}EO_{10}$–kanemite. The XRD patterns (Figure 5) of $C_{12}EO_{10}$– and $C_{18}EO_{10}$–kanemites (after the acid treatment in the presence of C_nEO_{10}) exhibit the peaks with the d-spacings of 4.96 and 6.40 nm, respectively. The nitrogen contents of $C_{12}EO_{10}$– and $C_{18}EO_{10}$–kanemite are less than 0.1 mass % (Table 1). The carbon contents of $C_{12}EO_{10}$– and $C_{18}EO_{10}$–kanemite are 34.1 and 39.0 mass %, respectively. Therefore, C_nEO_m–kanemite with different alkyl chain lengths can also be synthesized similarly.

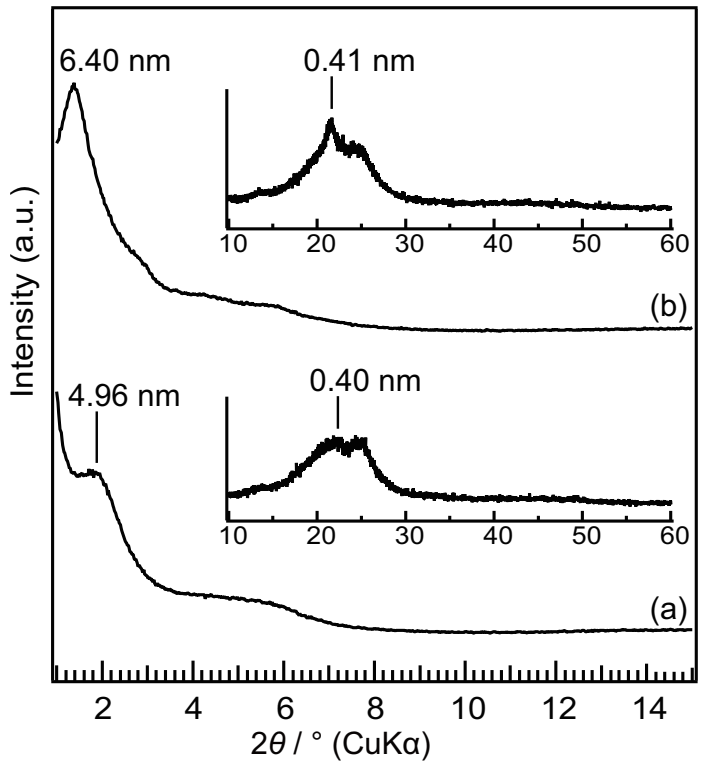

Figure 5. XRD patterns of C_nEO_m–kanemite (a) n = 12; m = 10 and (b) n = 18; m = 10.

Accordingly, the selection of the alkyl chain length and the number of the EO units in C_nEO_m molecules is possible, which may play a role in controlling the hydrophobicity and hydrophilicity in the interlayer spaces. As expected, the basal spacing of C_nEO_{10}–kanemite is increased with the alkyl chain length of C_nEO_m. The $C_{12}EO_{10}$/Si (0.12) and $C_{18}EO_{10}$/Si (0.13) ratios are lower than the $C_{16}EO_{10}$/Si (0.19) ratio. The XRD patterns of $C_{12}EO_{10}$– and $C_{18}EO_{10}$–kanemites (Figure 5 inset) showed the peaks with the *d*-spacings of 0.40 and 0.41 nm assignable to closely packed alkyl chains, respectively.[33-36] These peaks are relatively weaker and broader than that of $C_{16}EO_{10}$–kanemite (Figure 2c inset), implying that the packing of alkyl chains in the interlayer region corresponds to the amount of C_nEO_m.

3.3. Adsorption of *n*-decane and water

The hydrophobicity and hydrophilicity of $C_{16}EO_{10}$–kanemite was examined by adsorption experiments of *n*-decane and water. A few drops of *n*-decane or water were added to $C_{16}EO_{10}$–kanemite (0.05 g), and then the samples were covered with a slide and allowed to stand for 1 day at room temperature. The XRD patterns of the samples after the treatment show the peaks at 6.30 and 6.59 nm, respectively (Figure 6). The larger *d*-values than that of $C_{16}EO_{10}$–kanemite (d = 5.52 nm) before adsorption suggest the adsorption of these adsorbates. These samples were dried in vacuum, and then the *d*-values decreased to 5.60 and 5.59 nm, respectively. Therefore, the interlayer region of $C_{16}EO_{10}$–kanemite has both hydrophobic and hydrophilic characters to exhibit reversible adsorption. The stability of intercalated $C_{16}EO_{10}$ in the interlayer space is rather high. In fact, the deintercalation of $C_{16}EO_{10}$ was not observed for these measurements, though $C_{16}EO_{10}$ was finally deintercalated from $C_{16}EO_{10}$–kanemite when it was stirred in *n*-decane for 1 day. However, the deintercalation of $C_{16}EO_{10}$ did not occur in water even under a similar condition.

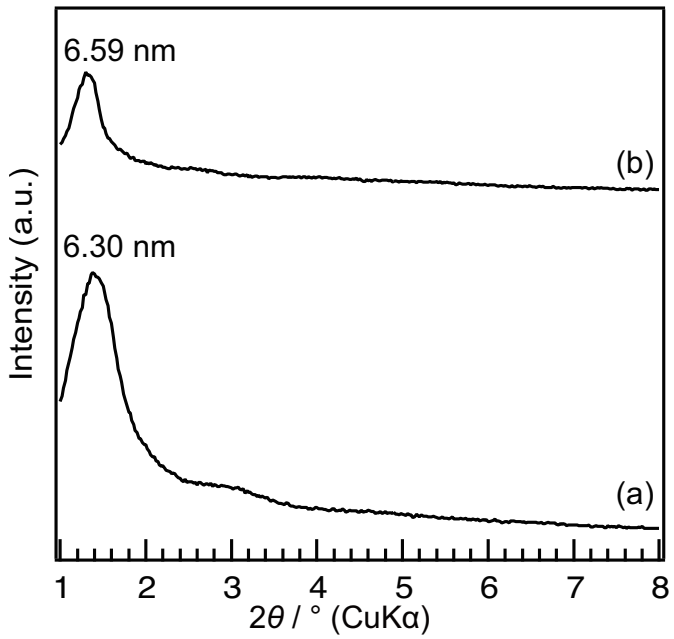

Figure 6. XRD patterns of $C_{16}EO_{10}$–kanemite after the adsorption of (a) *n*-decane and (b) water.

3.4. Formation mechanism of $C_{16}EO_{10}$–kanemite

The SEM images of kanemite, C_{16}TMA–kanemite, and $C_{16}EO_{10}$–C_{16}TMA –kanemite show plate-like morphologies with 2–5 μm in size (Figure 7a–c), indicating that the original morphology of kanemite is preserved after the reactions with C_{16}TMA and $C_{16}EO_{10}$. The particle size of C_nEO_m–kanemite (Figure 7d) is smaller and the shape is rounded. However, the loss in the product yield by the acid treatment was low (ca. 10%). Therefore, the dissolution of silicate layers may very partially occur by the acid treatment. I also think that the process of exfoliation and reassembly of silicate layers is unlikely, because the XRD pattern of hydrated slurry of $C_{16}EO_{10}$–kanemite is quite similar to that of dried powders of $C_{16}EO_{10}$–kanemite (though the *d*-values are slightly larger due to the adsorption of water). Also, there are no data indicating unlimited swelling of the product in water and decane as described above.

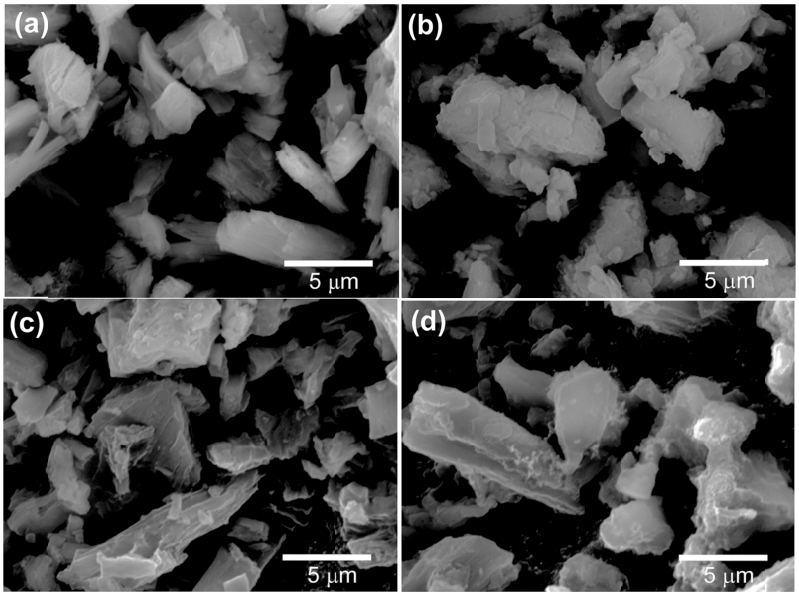

Figure 7. SEM images of (a) kanemite, (b) C_{16}TMA–kanemite, (c) $C_{16}EO_{10}$–C_{16}TMA–kanemite, and (d) $C_{16}EO_{10}$–kanemite. The scale bar represents 5 μm.

Figure 8 shows the variations in both the amount of the organic species (C_{16}TMA/Si or $C_{16}EO_{10}$/Si ratio) and *d*-value with the acid treatment of the preparation **step (ii)**. The C_{16}TMA/Si ratio was decreased from 0.26 at pH 8.9 to 0.01 at pH 4.0 and then became constant at almost zero. The amount of SiO^- groups should be decreased with the decrease of the pH value, because SiOH/SiO^- groups are condensed mainly in the vicinity of the neutral region, and the equilibrium between SiOH and $SiO^- + H^+$ is shifted to the left. Therefore, the electrostatic interactions between C_{16}TMA cations and silicate layers were decreased with pH value, causing the decrease in the C_{16}TMA/Si ratio. However, it is difficult to remove C_{16}TMA cations completely from C_{16}TMA–kanemite by acid treatment. In previous report, the C_{16}TMA/Si ratio was not decreased to zero at pH 3.0 (C_{16}TMA/Si = 0.12) by the acid treatment of C_{16}TMA–kanemite with acetic acid (1 M).[27]

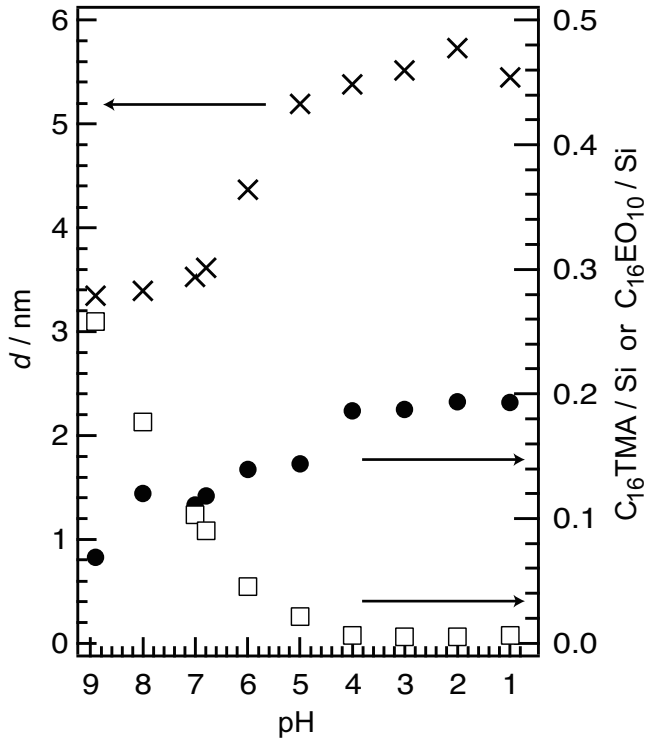

Figure 8. Variation in the *d*-values and amounts of organic species (C_{16}TMA cations and $C_{16}EO_{10}$) during acid treatment in **Step (ii)**. ×: *d*-value in XRD patterns, □: C_{16}TMA/Si ratio, ●: $C_{16}EO_{10}$/Si ratio.

In the present study, the acid treatment in the absence of $C_{16}EO_{10}$ was also performed for $C_{16}EO_{10}$–C_{16}TMA–kanemite. The C_{16}TMA/Si ratio of this sample was 0.06 at pH 3.0 ($C_{16}EO_{10}$/Si = 0.10, d = 3.84 nm). Consequently, $C_{16}EO_{10}$ molecules in the aqueous solution promote the elimination of C_{16}TMA cations because C_{16}TMA cations are strongly interacted with C_nEO_m molecules in aqueous solutions through hydrophobic interaction of the alkyl chains and hydrophilic ones between EO chains and trimethylammonium headgroups.[39]

With the decrease in the pH value from 8.9 to 4.0, the $C_{16}EO_{10}$/Si ratio was increased from 0.07 to 0.19 and then became constant at ca. 0.19 (Figure 8). In general, EO chains have hydrogen bonding with SiOH groups.[40-41] The amount of SiOH groups is increased with decreasing pH value, so that the amount of EO chains adsorbed on the silica surface is increased.[41] In the acid treatment of $C_{16}EO_{10}$–C_{16}TMA–kanemite, the $C_{16}EO_{10}$/Si ratio was increased with decreasing pH value because of the increased affinity between the EO chains and the interlayer surface.

As a possible alternative synthetic pathway, a sample was prepared via only **step (ii)** without **step (i)**. The $C_{16}EO_{10}$/Si ratio (= 0.09) of this sample was lower than that of $C_{16}EO_{10}$–kanemite (0.19). Therefore, **step (i)** is important to improve the intercalation of $C_{16}EO_{10}$ molecules because of the affinity of pre-existed $C_{16}EO_{10}$ and the intercalating $C_{16}EO_{10}$. The removal of C_{16}TMA cations should be accompanied by the exchange with H^+. The hydrophilic EO chains in the $C_{16}EO_{10}$–C_{16}TMA–kanemite should enhance the accessibility of H^+ to the interlayer and consequently C_{16}TMA cations are removed with an increase of $C_{16}EO_{10}$.

With the decrease in the pH value from 8.9 to 6.8, the *d*-value was slightly increased from 3.34 to 3.62 nm and rapidly reached up to 5.38 nm at pH 4.0. The *d*-value

was almost constant over the range of pH 4.0 to 1.0 (d = 5.73–5.38 nm). In the range of pH 8.9 to 6.8, where the C_{16}TMA/Si ratio was relatively higher than that of the $C_{16}EO_{10}$/Si ratio, the interactions between the layers are strong owing to the packing of the alkyl chains of C_{16}TMA cations. Accordingly, the d-value of the acid-treated products increased only slightly in this range. In the range of pH 6.8 to 4.0, complete elimination of C_{16}TMA cations caused the decrease of the interactions between the silicate layers. Therefore, the d-value rapidly increased with the decrease of pH value because $C_{16}EO_{10}$ interacting with silicate surface weakly is dominant in the interlayer region.

The chemical formulas of C_{16}TMA–kanemite, $C_{16}EO_{10}$–C_{16}TMA–kanemite, and $C_{16}EO_{10}$–kanemite are listed in Table 1. The oxygen content (δ) in the formula of $(C_{16}EO_{10})_x(C_{16}TMA)_yH_zSi_2O_{5-\delta}$ corresponds to the intralayer condensation. The value of δ increases (δ = 0.08 to 0.26) during the first step and further increases to 0.48 during the intercalation of $C_{16}EO_{10}$. The value x was initially increased from 0 to 0.14 and further increased to 0.38. Therefore, the intercalation of $C_{16}EO_{10}$ is basically related to the intralayer condensation but the degree of the intercalation exceeds the degree of condensation, which means other factors, such as hydrogen bonding between intercalated species and guest molecules, contribute to the intercalation.

4. Conclusion

Poly(oxyethylene) alkyl ether is intercalated into the interlayer region of a layered silicate kanemite by using layered C_{16}TMA–kanemite as the intermediate. Although a small amount of C_nEO_m molecules are intercalated into the C_{16}TMA–kanemite, the

resultant $C_{16}EO_{10}$–C_{16}TMA–kanemite is transformed into pure layered $C_{16}EO_{10}$–kanemite by the acid treatment in an excessive C_nEO_m aqueous solution. C_nEO_m molecules are not directly intercalated into kanemite, but the interactions among C_{16}TMA ions, C_nEO_m molecules, and silicate surface effectively work to induce the intercalation. This method is promising to intercalate a wide variety of functional polymers that have not been reported to be intercalated conventionally. Because the charge density of kanemite was changed during acid treatment, this reaction can be categorized as a sort of intercalation reactions rather than conventional intercalation reactions which proceed without change of crystal structure of layers. $C_{16}EO_{10}$–kanemite shows an interesting reversible hydrophobic and hydrophilic character. Because C_nEO_m is useful as a carrier for drug delivery system and as adsorbents for both hydrophobic organic contaminants and hydrophilic toxic heavy metal cations, C_nEO_m–kanemite, which is easily handled as powders with higher thermal and chemical stabilities, has a potential for such applications.

5. References and Footnotes

[1] W. Schwieger, G. Lagaly, in *Handbook of Layered Materials* (Eds.: S. M. Auerbach, K. A. Carrado, P. K. Dutta), Marcel Dekker, Inc., New York, **2004**, pp. 541-629.

[2] E. Ruiz-Hitzky, *Chem. Rec.* **2003**, *3*, 88-100.

[3] M. Ogawa, K. Kuroda, *Bull. Chem. Soc. Jpn.* **1997**, *70*, 2593-2618.

[4] M. Alexandre, P. Dubois, *Mater. Sci. Eng., R* **2000**, *28*, 1-63.

[5] M. Ogawa, K. Kuroda, *Chem. Rev.* **1995**, *95*, 399-438.

[6] I. Fujita, K. Kuroda, M. Ogawa, *Chem. Mater.* **2003**, *15*, 3134-3141.

[7] I. Fujita, K. Kuroda, M. Ogawa, *Chem. Mater.* **2005**, *17*, 3717-3722.

[8] D. Mochizuki, S. Kowata, K. Kuroda, *Chem. Mater.* **2006**, *18*, 5223-5229.

[9] F. Bergaya, B. K. G. Theng, G. Lagaly, *Handbook of Clay Science*, Elsevier Ltd., Amsterdam, **2006**.

[10] Y. Deng, J. B. Dixon, G. N. White, *Clays Clay Miner.* **2003**, *51*, 150-161.

[11] K. Beneke, G. Lagaly, *Am. Mineral.* **1977**, *62*, 763-771.

[12] G. G. Almond, R. K. Harris, K. R. Franklin, *J. Mater. Chem.* **1997**, *7*, 681-687.

[13] S. A. Bagshaw, E. Prouzet, T. J. Pinnavaia, *Science* **1995**, *269*, 1242-1244.

[14] I. F. Uchegbu, A. T. Florence, *Adv. Colloid Interface Sci.* **1995**, *58*, 1-55.

[15] K. A. Krogh, B. Halling-Sørensen, B. B. Mogensen, K. V. Vejrup, *Chemosphere* **2003**, *50*, 871-901.

[16] W. F. Bradley, *J. Am. Chem. Soc.* **1945**, *67*, 975-981.

[17] H. Schott, *Kolloid-Z. Z. Polym.* **1964**, *199*, 158-169.

[18] L. J. Michot, T. J. Pinnavaia, *Clays Clay Miner.* **1991**, *39*, 634-641.

[19] D. Platikanov, A. Weiss, G. Lagaly, *Colloid. Polym. Sci.* **1977**, *255*, 907-915.

[20] S. Vortmann, J. Rius, B. Marler, H. Gies, *Eur. J. Mineral.* **1999**, *11*, 125-134.

[21] D. C. Apperley, M. J. Hudson, M. T. J. Keene, J. A. Knowles, *J. Mater. Chem.* **1995**, *5*, 577-582.

[22] T. Kimura, D. Itoh, N. Okazaki, M. Kaneda, Y. Sakamoto, O. Terasaki, Y. Sugahara, K. Kuroda, *Langmuir* **2000**, *16*, 7624-7628.

[23] T. Kimura, D. Itoh, T. Shigeno, K. Kuroda, *Langmuir* **2002**, *18*, 9574-9577.

[24] T. Kimura, D. Itoh, T. Shigeno, K. Kuroda, *Bull. Chem. Soc. Jpn.* **2004**, *77*, 585-590.

[25] T. Yanagisawa, T. Shimizu, K. Kuroda, C. Kato, *Bull. Chem. Soc. Jpn.* **1990**, *63*, 988-992.

[26] S. Inagaki, Y. Fukushima, K. Kuroda, *J. Chem. Soc., Chem. Commun.* **1993**, 680-682.

[27] T. Kimura, T. Kamata, M. Fuziwara, Y. Takano, M. Kaneda, Y. Sakamoto, O. Terasaki, Y. Sugahara, K. Kuroda, *Angew. Chem., Int. Ed.* **2000**, *39*, 3855-3859.

[28] H. D. Dörfler, K. Müllier, E. Müller, K. H. Bergk, *Tenside Deterg.* **1984**, *21*, 226-234.

[29] R. Suresh, S. Vasudevan, K. V. Ramanathan, *Chem. Phys. Lett.* **2003**, *371*, 118-124.

[30] A. Shimojima, D. Mochizuki, K. Kuroda, *Chem. Mater.* **2001**, *13*, 3603-3609.

[31] The alkyl chain length of C_{16}TMA ion is 2.03 nm (= 0.127 nm/C-C × 16).

[32] Kanemite is transformed into H-kanemite by acid treatment. The thickness of the individual silicate sheet of kanemite is calculated to be 0.60 nm on the basis of the XRD pattern of H-kanemite. The structure of H-kanemite is described in detail in the reference [21].

[33] Y. Fujimoto, M. Heishi, A. Shimojima, K. Kuroda, *J. Mater. Chem.* **2005**, *15*, 5151-5157.

[34] H. Shi, Y. Zhao, X. Zhang, S. Jiang, D. Wang, C. C. Han, D. Xu, *Macromolecules* **2004**, *37*, 9933-9940.

[35] S. Gestí, A. Almontassir, M. T. Casas, J. Puiggalí, *Polymer* **2004**, *45*, 8845-8861.

[36] G. H. Peters, N. B. Larsen, T. Bjørnholm, S. Toxvaerd, K. Schaumburg, K. Kjaer, *Phys. Rev. E* **1998**, *57*, 3153-3163.

[37] The radius of headgroup was calculated by the software "MS Modeling", Accelrys Co.

[38] S. Mita, S. Kondo, M. Takeda, *Bull. Chem. Soc. Jpn.* **1982**, *55*, 1988-1991.

[39] H. Matsubara, A. Ohta, M. Kameda, N. Ikeda, M. Aratono, *Langmuir* **2000**, *16*, 7589-7596.

[40] S. K. Parida, S. Dash, S. Patel, B. K. Mishra, *Adv. Colloid Interface Sci.* **2006**, *121*, 77-110.

[41] J. Rubio, J. A. Kitchener, *J. Colloid Interface Sci.* **1976**, *57*, 132-142.

Chapter 3

Intercalation Mechanism of Poly(oxyethylene) Alkyl Ether into Kanemite

1. Introduction

Intercalation compounds based on layered silicates have received considerable attention as green and sustainable materials such as catalysts, catalyst supports and adsorbents because of the expandable nanospaces and the inherent high surface areas.[1-2] Such applications have been achieved by controlling interlayer environments including organic modification as well as the variations in layer charge, SiOH density, and polarity. Therefore, a precise control of layered structures is promising for the developments of new functionalities and high performances.

Layered silicates composed of only SiO_4 units, such as kanemite, magadiite, octosilicate, etc. have $SiOH/SiO^-$ groups at the surfaces of the silicate frameworks and exchangeable alkali metal cations in the interlayer spaces[1,3-5]. The design of interlayer spaces has been achieved by various methods such as ion exchange, adsorption of polar

molecules, acid-base reaction and silylation.[1] Nonionic surfactants like poly(oxyethylene) alkyl ether (C_nEO_m) were not directly intercalated into layered silicates, and just adsorbed on the external surfaces[6] because of the high density of SiOH/SiO^- groups and the low polarity of EO chains.

In a previous study, C_nEO_m was successfully intercalated into a layered silicate kanemite[7] by using a hexadecyltrimethylammonium (C_{16}TMA) intercalated kanemite (C_{16}TMA-kenemite[8]) as an intermediate. The acid treatment of the intercalated kanemite in an aqueous solution of C_nEO_m induced further intercalation of C_nEO_m molecules with the elimination of C_{16}TMA cations, resulting in the formation of pure C_nEO_m intercalated kanemite. During the intercalation of C_nEO_m molecules, SiOH groups of kanemite were condensed within the individual silicate sheets (intralayer condensation). We suggested that the density of SiOH/SiO^- groups, which is related to the intensity of Q^3 peaks in ^{29}Si MAS NMR spectra, influences the intercalation of nonionic surfactants. The control of the SiOH/SiO^- density would lead to the precise design of interlayer spaces by intercalation of nonionic surfactants.

In this study, we investigated the intercalation behavior of C_nEO_m molecules into C_{16}TMA−kanemite with different SiOH/SiO^- densities, and the intermediates were obtained by changing the reaction temperature of kanemite with C_{16}TMA cations.[8] The intercalation behavior of C_nEO_m molecules has been investigated only for C_{16}TMA−kanemite prepared at room temperature as an intermediate.[7] Therefore, the insight obtained in this study is useful for further understanding of the intercalation behavior of $C_{16}EO_{10}$ molecules into layered silicates.

2. Experimental

Materials

Kanemite ($NaHSi_2O_5 \cdot 3H_2O$) was obtained by dispersing δ-$Na_2Si_2O_5$ (1.0 g) in deionized water (50 mL) with stirring for 0.5 h.[7-8] Hexadecyltrimethylammonium chloride ($C_{16}H_{33}N(CH_3)_3Cl$, denoted as C_{16}TMACl, Tokyo Kasei Kogyo) and $C_{16}EO_{10}$ ($C_{16}H_{33}(OC_2H_4)_{10}OH$, Aldrich) were used as received.

Synthesis of C_{16}TMA-kanemite (L1)

The synthetic pathway is summarized in Figure 1. C_{16}TMA−kanemites with different SiOH/SiO^- densities were prepared by the reactions of kanemite with C_{16}TMA cations at temperatures ranging from room temperature (r.t.) to 90 °C.[8] Kanemite (1.0 g) was added to an aqueous solution (200 mL) of 0.1 M C_{16}TMACl and the mixture was stirred for 2 days at room temperature, 50 °C, 70 °C, and 90 °C. The resultant solid

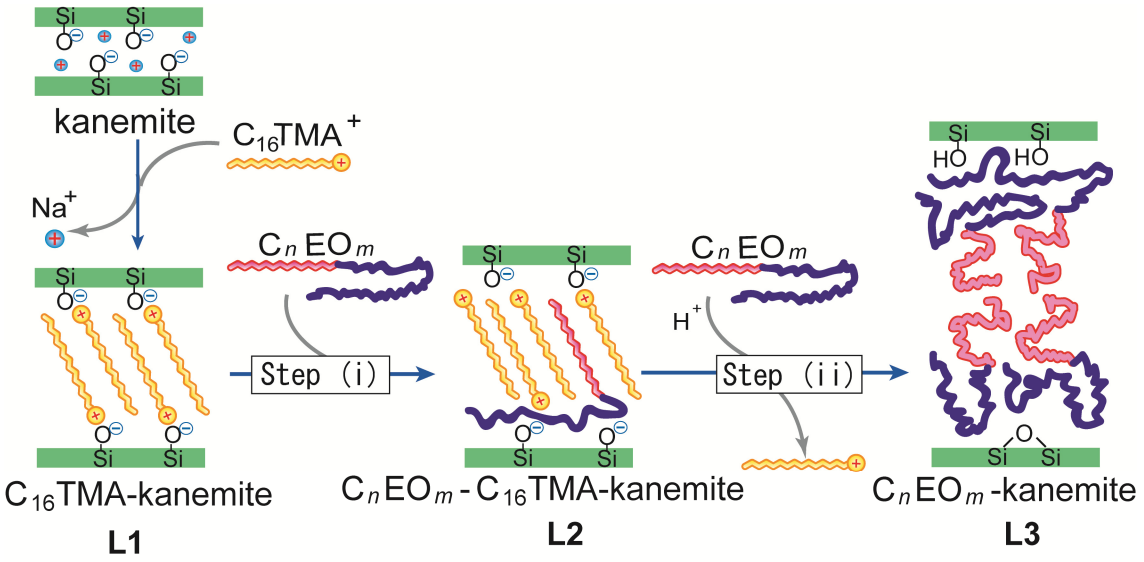

Figure 1. Synthetic pathway of **L1**, **L2**, and **L3**.

products were separated by centrifugation and air-dried, which are denoted as **L1(r.t.)**, **L1(50)**, **L1(70)**, and **L1(90)**, respectively.

Intercalation of $C_{16}EO_{10}$ into L1

L1 was dispersed in an aqueous solution of $C_{16}EO_{10}$ (0.1 M, 40 mL). The mixture was stirred for 2 days at room temperature and centrifuged to recover the resultant product. The slurry was washed by dispersing in deionized water, stirred for 5 min, and centrifuged. This procedure was repeated twice to remove residual $C_{16}EO_{10}$ molecules completely and air-dried. The products are denoted as **L2(r.t.)**, **L2(50)**, **L2(70)**, and **L2(90)**, respectively.

Acid treatment of L2(r.t.)

The wet slurry of **L2(r.t.)** (0.2 g as dried **L1(r.t.)**) was dispersed in an aqueous solution of $C_{16}EO_{10}$ (0.1 M, 40 mL). The pH value was decreased to 3.0 by adding HCl (1.0 M) slowly over 0.5 h. The mixture was stirred for 1 day. The slurry was centrifuged, washed twice with deionized water, and air-dried. The product is denoted as **L3(r.t.)**.

Characterization

X-ray powder diffraction patterns (XRD) were obtained with a Rigaku Rint-Ultima III powder diffractometer (CuKα, λ = 0.15418 nm) by using a parallel beam geometry equipped with a parabolic multilayer solar slit. The amounts of organic constituents were determined by CHN analysis (Perkin Elmer, 2400 Series II). Thermogravimetry (TG) measurements were carried out with a Rigaku Thermo Plus 2 instrument under a dry air flow at a heating rate of 10 °C min^{-1}, and the amounts of SiO_2 fractions in the products were calculated from the residual weights after heating up to

900 °C. Two-dimensional (2D) $^{29}Si\{^{1}H\}$ HETeronuclear chemical shift CORrelation (HETCOR) NMR experiments[9] were performed under conditions of magic-angle sample spinning at 5−6 kHz, using a μs π/2 ^{1}H pulse, followed by a 4.0 ms contact time.

3. Results and Discussion

3.1. Intercalation of $C_{16}EO_{10}$ into L1

The XRD patterns of **L2**s are shown in Figure 2. As reported previously, **L2(r.t.)** has a layered structure having the *d*-spacings of 3.3, 1.6 and 1.1 nm.[7] The XRD patterns of **L2(50)** (3.3, 1.7 and 1.1 nm), **L2(70)** (3.6, 1.8 and 1.2 nm) and **L2(90)** (3.7, 1.8 and 1.2 nm) exhibit successful intercalation into **L1**s because these three peaks are assignable to layered structure and the *d*-spacings of the main peaks are larger than those observed for the corresponding intermediates.

The $C_{16}TMA$/Si and $C_{16}EO_{10}$/Si ratios calculated from the CHN and TG data are summarized in Table 1. The carbon contents of **L2(50)**, **L2(70)**, and **L2(90)** (45.4, 44.8, and 44.3 mass%) are larger than those of **L1(50)**, **L1(70)**, and **L1(90)** (41.4, 40.1, and 40.0 mass%). The results also support the intercalation of $C_{16}EO_{10}$ molecules into **L1**s.

The $C_{16}EO_{10}$/Si molar ratios of **L2(50)**, **L2(70)**, and **L2(90)** are 0.09, 0.10 and 0.10, respectively. The ratios are increased with the increase in the synthetic temperature of **L1**s. The **L1**s obtained at higher temperatures showed higher $Q^4/(Q^3+Q^4)$ ratios, suggesting the proceeding of intralayer condensation of SiOH groups.[8] Therefore, the decrease in the SiOH/SiO^- density enhances the intercalation of $C_{16}EO_{10}$ molecules into **L1**.

The $C_{16}TMA$/Si molar ratios of **L2(50)**, **L2(70)**, and **L2(90)** (0.19, 0.13 and 0.13)

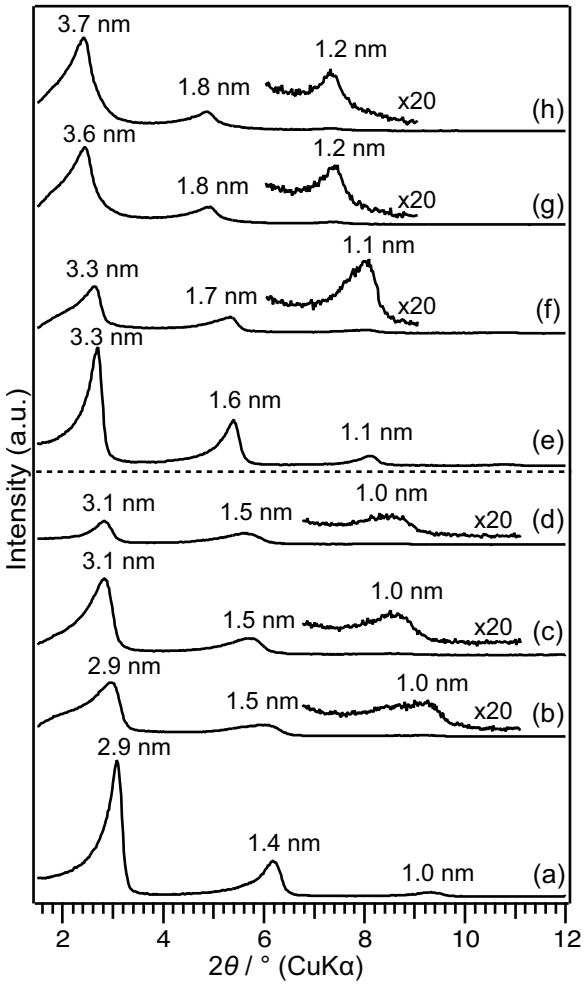

Figure 2. XRD patterns of (a) **L1(r.t.)**, (b) **L1(50)**, (c) **L1(70)**, (d) **L1(90),** (e) **L2(r.t.)**, (f) **L2(50)**, (g) **L2(70)**, and (h) **L2(90)**

Table 1. Amount of organic fractions and SiO_2 in the kanemite-based products

Sample	C/mass%	N/mass%	SiO_2/mass %	C_{16}TMA/Si	$C_{16}EO_{10}$/Si	ΔC_{16}TMA/Si**
L1(r.t.)*	42.7	2.6	36.2	0.30	–	–
L1(50)	41.4	2.4	38.4	0.27	–	–
L1(70)	40.1	2.2	41.0	0.23	–	–
L1(90)	40.0	2.4	40.7	0.25	–	–
L2(r.t.)*	46.7	1.9	33.9	0.26	0.07	0.04
L2(50)	45.4	1.5	33.2	0.19	0.09	0.08
L2(70)	44.8	1.1	36.9	0.13	0.10	0.10
L2(90)	44.3	1.1	36.4	0.13	0.10	0.12

* These data are obtained from our previous paper. [7]
** ΔC_{16}TMA/Si equals to C_{16}TMA/Si of **L1** minus C_{16}TMA/Si of **L2**.

are lower than those of **L1(50)**, **L1(70)**, and **L1(90)** (0.27, 0.23 and 0.25), respectively. C_{16}TMA cations were eliminated partially by the reaction with an aqueous solution of

$C_{16}EO_{10}$. The decrease of $C_{16}TMA$ cations was also observed in the case of **L1(r.t.)**; the $C_{16}TMA$/Si molar ratio decreased from 0.30 to 0.26.[7] The decreased amount of the $C_{16}TMA$/Si molar ratio ($\Delta C_{16}TMA$/Si) in **L2(r.t.)**, **L2(50)**, **L2(70)**, and **L2(90)** are 0.04, 0.08, 0.10 and 0.12, respectively. Because the intralayer condensation within the individual sheets of kanemite causes the decrease of the SiOH/SiO^- density, the electrostatic interaction of $C_{16}TMA$ cations with silicate layers decreases with the condensation. Therefore, the intralayer condensation of the silicate layers can enhance the elimination of $C_{16}TMA$ cations.

The XRD patterns of **L2**s showed that the *d* value of the main peak increased when **L1**s with much condensed frameworks were used. The *d* value and the $C_{16}EO_{10}$/Si ratio of **L2(r.t.)** also increased with the decrease in the pH value during the acid treatment in an aqueous solution of $C_{16}EO_{10}$.[7] We explain the increase in the *d* value by the assumption that weak interaction between $C_{16}EO_{10}$ molecules and silicate surfaces is dominant in the interlayer region. Similarly, in this study, the increase of the *d* value with the increase of the amount of condensed silicate species in **L1**s arises from the increase of the amount of intercalated $C_{16}EO_{10}$.

3.2. Intercalation mechanism

L2(r.t.) was treated with hydrochloric acid in an aqueous solution of $C_{16}EO_{10}$ to remove $C_{16}TMA$ cations completely and to precede the intralayer condensation of SiOH groups (Figure 1). We analyzed the interactions between $C_{16}EO_{10}$ molecules and silicate layers of **L3(r.t.)** by using HETCOR NMR. The 2-D NMR spectrum of **L3(r.t.)** (Figure 3) showed the correlation between water (at 5.0 ppm, ^1H) and Q^3 species, showing the presence of adsorbed water on the silicate surfaces.[10] I observed the correlations arising

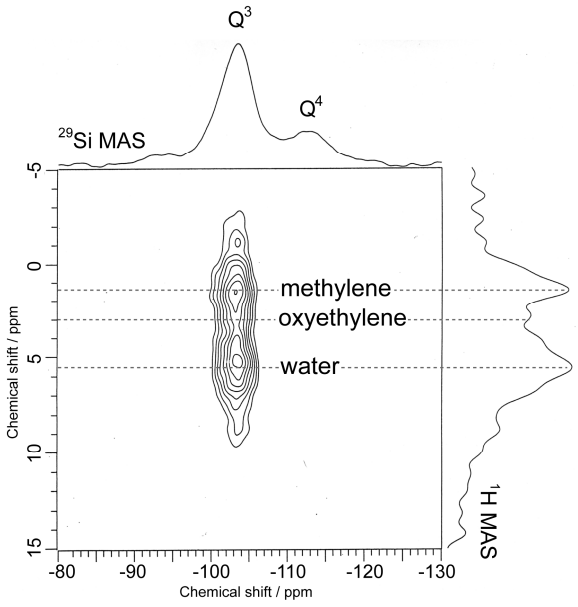

Figure 3. 2-D $^{29}Si\{^{1}H\}$ HETCOR NMR spectrum of **L3(r.t.)**

from the dipole-dipole couplings between methylene protons (1.3 ppm, ^{1}H) and the Q^3 species, and between oxyethylene protons (3.0 ppm, ^{1}H) and the Q^3 species. The correlations display that both oxyethylene chains and alky chains are located closely to the Q^3 species. The intensity of the peak due to methylene protons is higher than that due to oxyethylene chains, despite the number of protons in alkyl chains is less than that in oxyethylene chains. Therefore, it is suggested that alky chains are more closely located to the silicate layers than oxyethylene chains. This closer location of alkyl chains with the silicate layers can be explained by assuming the hydrophobic interaction between the alkyl chains and the silicate layers. **L3(r.t.)** has a higher $Q^4/(Q^3+Q^4)$ ratio (0.48)[7] because of intralayer condensation of SiOH during the acid treatment. In general, silica surfaces composed mainly of Q^4 species are more hydrophobic than those of Q^3 species. We predict that the hydrophobicity of silicate layers due to the presence of more Q^4 species enhances the intercalation of $C_{16}EO_{10}$.

The $C_{16}EO_{10}$/Si molar ratio of **L2(r.t)** was increased with the increase in the

synthetic temperature of **L1**s (Table. 1). The mechanism of intercalation of $C_{16}EO_{10}$ can be explained as follows: **L1**s with higher $Q^4/(Q^3+Q^4)$ ratios can be obtained at higher temperatures because of the progress of intralayer condensation. The surface with larger amount of Q^4 species can provide hydrophobic interlayer surfaces. The amount of $C_{16}EO_{10}$ adsorbed on the silicate surfaces increased according to the hydrophobic interaction between the surfaces and alkyl chains of $C_{16}EO_{10}$. Therefore, the intralayer condensation of SiOH enhances the intercalation of $C_{16}EO_{10}$ in the interlayer spaces of **L1**s. We have already showed the increase of the $C_{16}EO_{10}$/Si ratio with the decrease in the pH value of the reaction medium because of hydrogen bonding between SiOH and EO chains.[7] However, the hydrophobic interaction between alkyl chains and silicate surfaces also affects the intercalation property of $C_{16}EO_{10}$ molecules into **L1**s.

4. Conclusion

Intercalation behavior of $C_{16}EO_{10}$ molecules into layered silicates was investigated by using C_{16}TMA−kaenemites (**L1**s) with different SiOH/SiO^- densities. The decrease in the SiOH/SiO^- densities of C_{16}TMA−kanemites enhances the hydrophobicity of the interlayer surface. The amount of intercalated $C_{16}EO_{10}$ molecules is increased according to the intralayer condensation which induces the hydrophobic interaction between alkyl chains and silicate surfaces. The eliminated amount of C_{16}TMA cations is increased when C_{16}TMA−kaenemites with more condensed frameworks are used. The intercalation of C_nEO_m molecules into layered silicates is controllable depending on the conditions. The design of the interlayer environments of layered materials is promising for

the enhancement of the properties as green and sustainable materials such as catalysts, catalyst supports and adsorbents.

5. References

[1] W. Schwieger, G. Lagaly, in *Handbook of Layered Materials* (Eds.: S. M. Auerbach, K. A. Carrado, P. K. Dutta), Marcel Dekker, Inc., New York, **2004**, pp. 541-629.

[2] F. Bergaya, B. K. G. Theng, G. Lagaly, *Handbook of Clay Science*, Elsevier Ltd., Amsterdam, **2006**.

[3] K. Beneke, G. Lagaly, *Am. Mineral.* **1977**, *62*, 763-771.

[4] S. Vortmann, J. Rius, B. Marler, H. Gies, *Eur. J. Mineral.* **1999**, *11*, 125-134.

[5] G. G. Almond, R. K. Harris, K. R. Franklin, *J. Mater. Chem.* **1997**, *7*, 681-687.

[6] H. D. Dörfler, K. Müllier, E. Müller, K. H. Bergk, *Tenside Deterg.* **1984**, *21*, 226-234.

[7] N. Takahashi, H. Tamura, D. Mochizuki, T. Kimura, K. Kuroda, *Langmuir* **2007**, *23*, 10765-10771.

[8] T. Kimura, D. Itoh, N. Okazaki, M. Kaneda, Y. Sakamoto, O. Terasaki, Y. Sugahara, K. Kuroda, *Langmuir* **2000**, *16*, 7624-7628.

[9] S. C. Christiansen, D. Zhao, M. T. Janicke, C. C. Landry, G. D. Stucky, B. F. Chmelka, *J. Am. Chem. Soc.* **2001**, *123*, 4519-4529.

[10] S. Hayashi, *J. Mater. Chem.* **1997**, *7*, 1043-1048.

Chapter 4

Enlargement of Mesopores of 2-D Orthorhombic KSW-2-type Silica by the Addition of Poly(oxyethylene) Alkyl Ether during the Mesostructural Formation

1. Introduction

Ordered mesoporous silicas[1-2] possess high surface area, large adsorption capacity, and periodic, uniform, and tunable mesopores with 2-50 nm in pore size. Because of the unique structural features, mesoporous silicas have received much attention for practical uses in adsorbents,[3] catalysts,[4-5] electronic devices,[6] optical devices,[7-8] drug delivery carriers,[9-10] and low-*k* materials,[11] etc. For their applications, the control of both mesostructural (pore size, pore shape, etc.) and microstructural (crystallinity and surface structure of mesopore walls) scales is quite important. The mesostructural control,

important for improving selectivity, dispersibility, and accessibility of guest molecules has mainly been developed by the selection and design of surfactants.[12-14] The mesopore size can also be increased by using pore expanders, such as alkylamines[15] and trimethylbenzene,[16] in the presence of structure directing amphiphilic organic molecules.[17] However, in order to develop sophisticated applications of ordered mesoporous silica, simple mesostructural control is insufficient because the density of silanol groups in the pore walls and also the surface structure (microstructural control) greatly affect the activities and reactivities.

The crystallinity of mesopore walls (silicate frameworks) is important as an influential parameter of the microstructural control for enhancing the catalytic activities. It is clear that the presence of large mesopores is quite attractive for effective diffusion of large organic molecules. Recently mesoporous zeolites (formed through dual templating method,[18-19] hard-templating using carbon species,[20-23] organosilane-directed synthesis,[24-26] and so on.) have been reported by several research groups. Another unique synthetic method using crystalline silica precursors is the use of a layered silicate,[27] and various mesoporous silicas have been prepared from kanemite [1,28-31] and other layered silicates.[32-34] In particular, 2-D orthorhombic mesoporous silica (KSW-2)[35] is quite interesting because of their crystalline units of silica wall originating from kanemite. The 2-D orthorhombic structural precursor of KSW-2 (asKSW-2) is obtained by an acid treatment of hexadecyltrimethylammonium-intercalated kanemite (C_{16}TMA-kanemite[36]). The bending of the silicate layers was proved by transmission electron microscopy by the Terasaki group.[35] Although calcination of as-KSW-2 leads to the deformation of the periodicity in the silicate frameworks, the crystal structure can be retained by using precise modification of as-KSW-2 using molecularly designed silylating agents.[37] Accordingly,

KSW-2-type mesoporous silica is quite attractive as high-performance catalysts according to the unique structural features, such as the periodicity in the designed silicate framework and square-shaped mesopores.[38] However, the pore size control of KSW-2 has not been achieved yet. KSW-2 type mesoporous silica can be obtained only when C_{16}TMACl and C_{14}TMACl are used because the solubility mainly influences the mesostructural transformation of lamellar intermediates into 2-D orthorhombic structures.

From the viewpoint of intercalation chemistry, the adjustment of interlayer distance of intercalation compounds has been well demonstrated through co-intercalation of additional guest species.[39-40] We reported the expansion of interlayer distance of lamellar C_{16}TMA-kanemite by further intercalation of nonionic surfactants, such as poly(oxy ethylene) alkyl ether (C_nEO_m; n = 16, m = 10).[41] $C_{16}EO_{10}$-intercalated kanemite (without C_{16}TMA cations) was also obtained by an acid treatment at pH 3 with hydrochloric acid in an aqueous solution of $C_{16}EO_{10}$. The acid treatment in the $C_{16}EO_{10}$ solution promoted both the intercalation of $C_{16}EO_{10}$ and the deintercalation of C_{16}TMA cations and then pure $C_{16}EO_{10}$-intercalated kanemite with a large d_{001}-spacing of 5.5 nm was obtained. Accordingly, intercalation of $C_{16}EO_{10}$ with acid treatment is a quite attractive method for controlling the interlayer distance of such lamellar surfactant-kanemite materials. A mixed surfactant system using both $C_{16}EO_{10}$ and C_{16}TMACl was also used for the expansion of the pore size of MCM-41 type mesoporous silica.[42]

The thickness of mesopore walls of KSW-2 is thin because the mesopore walls of KSW-2 are basically composed of single silicate layers of SiO_4 tetrahedra, as derived from kanemite. Therefore, the expansion of mesopores of KSW-2 should increase pore/wall ratio with constant thickness of pore walls. It is known in general that the enhancement of

pore/wall ratio will be advantageous for low-*k* materials.[11] Thus, the mesostructural control of KSW-2 is highly demanded. In this paper, the preparation of KSW-2-type silica with expanded mesopores is reported by utilizing intercalation of poly(oxyethylene) alkyl ether into C_{16}TMA-kanemite, as illustrated in Figure 1. The acid treatment of C_{16}TMA-kanemite in an aqueous solution of $C_{16}EO_{10}$ induces the simultaneous reaction of intercalation of $C_{16}EO_{10}$ into the interlayer of C_{16}TMA-kanemite, deintercalation of C_{16}TMA cations, and mesostructural transformation of lamellar into 2-D orthorhombic structures, which could open a precise and continuous mesostructural control of KSW-2 type mesoporous silica.

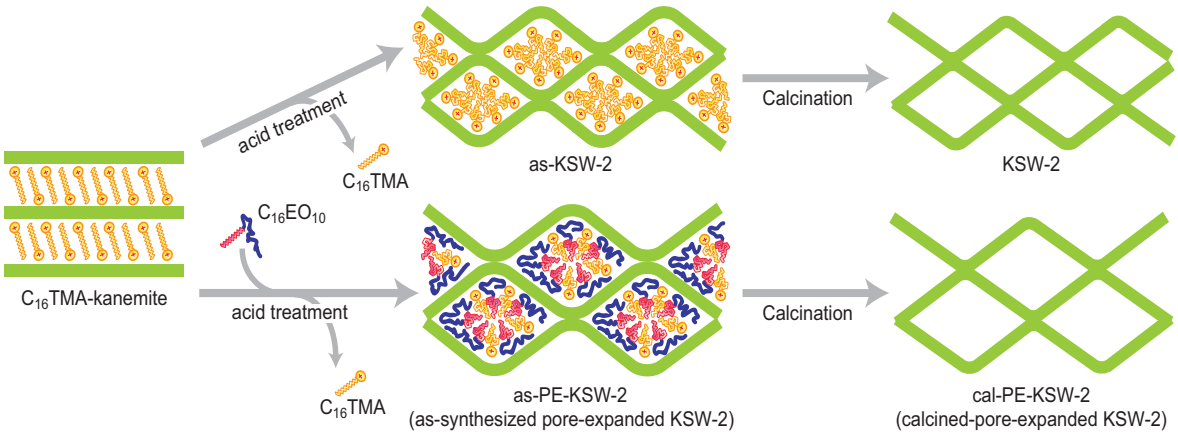

Figure 1. Schematic formation mechanism of KSW-2 and pore-expanded KSW-2.

2. Experimental

Preparation of C_{16}TMA-kanemite

A layered silicate kanemite ($NaHSi_2O_5 \cdot 3H_2O$) was prepared by dispersing δ-$Na_2Si_2O_5$ (1.0 g) in deionized water (50 mL) with stirring for 0.5 h.[36] The Na/Si molar ratio of kanemite was checked to be ca. 0.5 by inductively coupled plasma emission

spectroscopy (ICP). The XRD pattern of the resultant kanemite was consistent with that recorded in the JCPDS file (25-1309). A hexadecyltrimethylammonium-intercalated kanemite (C_{16}TMA-kanemite) was prepared by ion-exchange of interlayer Na^+ with C_{16}TMA cations. Kanemite (0.2 g) was dispersed in an aqueous solution of C_{16}TMACl (0.1 M, 40 mL, Tokyo Kasei Kogyo Co.). The suspension was stirred at room temperature for 2 d, and then C_{16}TMA-kanemite was recovered by centrifugation and air-drying.[36,41] The amount of remaining Na^+ after the ion-exchange was virtually zero (ICP).

Synthesis of pore-expanded KSW-2

Poly(oxyethylene) alkyl ether (C_nEO_m; n = 16, m = 10; Aldrich) was used as a pore expander. The acid treatment of C_{16}TMA-kanemite was done in an aqueous solution of $C_{16}EO_{10}$ with concentrations of 0, 1, 5, 10, 50, and 100 mM. An aqueous solution of acetic acid (0.1 M) was added dropwise to each mixture to adjust the pH value to 5.5 for 30 min. Each mixture was stirred for another 30 min and centrifuged. The resultant solid products were washed twice with deionized water (40 mL) and air-dried for 1 day. As-synthesized KSW-2 type silica is denoted as as-PE-KSW-2_x (x = concentration of $C_{16}EO_{10}$). As-PE-KSW-2_0 means conventional as-synthesized KSW-2 (as-KSW-2[35]) without the addition of $C_{16}EO_{10}$. As-PE-KSW-2_x were calcined at 550 °C for 5 h to remove organic fractions completely and named as cal-PE-KSW-2_x.

Characterizations

X-ray powder diffraction (XRD) measurements were performed on a Rigaku Rint-Ultima III diffractometer with Cu Kα (λ = 0.15418 nm) radiation by using a parallel beam geometry equipped with a parabolic multilayer solar slit. The contents of Na and Si

were measured by ICP with a Vista-MPX instrument (Varian Technology Japan Ltd.). Solid-state ^{13}C CP/MAS NMR spectra were recorded on a JEOL JNM-CMX-400 spectrometer at a resonance frequency of 100.5 MHz and a recycle delay of 5 s. Samples were put into a 5 mm zirconia rotor and spun at 8 kHz. The chemical shift was externally referenced to hexamethylbenzene at 17.4 ppm (-$\underline{C}H_3$). The amount of surfactants (C_{16}TMA and $C_{16}EO_{10}$) was determined by CHN analysis (Perkin Elmer, 2400 Series II). Thermogravimetry (TG) measurements were carried out with a Rigaku Thermo Plus 2 instrument under a dry air flow (200 mL·min^{-1}) at a heating rate of 10 °C·min^{-1}. Transmission electron micrographs (TEM) were recorded with a JEOL JEM 2010 instrument, operated at 200 kV. Nitrogen adsorption-desorption isotherms were recorded by using a Quantachrome Autosorb-1 at 77 K. Samples were dried by heating at 120 °C for 3 h under vacuum prior to the measurement. Specific surface areas (S_{BET}) were calculated by the BET method using adsorption data. Inner surface areas (S_{inner}) and total pore volumes (V) were estimated by the *t*-plot method, and then pore sizes were calculated by an equation of $4V/S_{inner}$.[35,37] Pore size (D_{BJH}) distributions were calculated by the BJH method on the basis of an assumption of a structural model with cylindrical mesopores.

3. Results and Discussion

3.1. Mesostructural control of as-PE-KSW-2

C_{16}TMA-kanemite is a lamellar material showing the diffraction peaks of 2.9, 1.4, and 1.0 nm in the XRD pattern (Figure 2a), and the acid treatment of C_{16}TMA-kanemite (as-PE-KSW-2_0 which is equivalent to as-KSW-2[35]) induced the mesostructural change

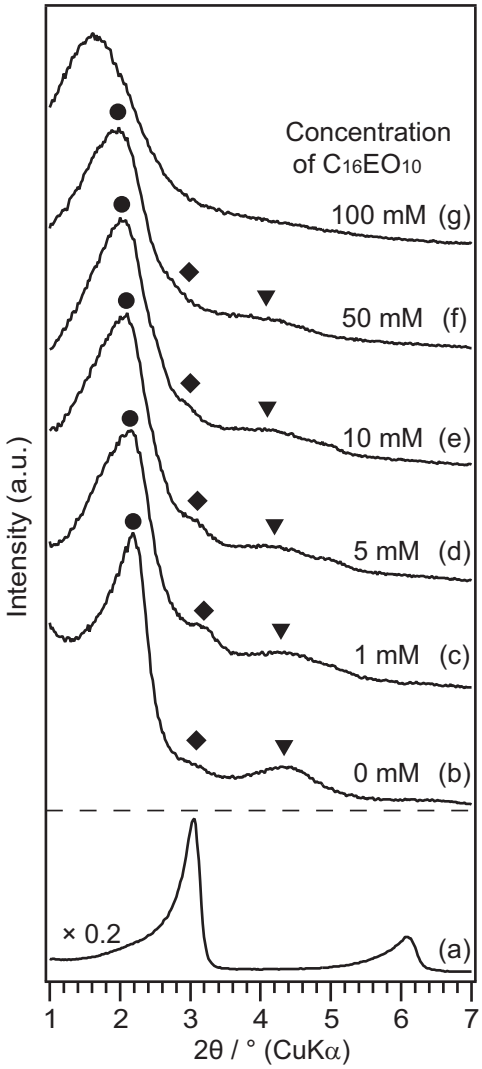

Figure 2. XRD patterns of (a) C_{16}TMA-kanemite; and (b) as-PE-KSW-2_0, (c) _1, (d) _5, (e) _10, (f) _50, and (g) _100. Symbols indicate the assignment of diffraction peaks to ●: (11), ▼: (20), and ♦: (22) of the 2-D orthorhombic structure.

to a 2-D orthorhombic phase in water without $C_{16}EO_{10}$ (Figure 2b), as reported previously.[41] The lamellar structure of C_{16}TMA-kanemite disappeared completely by the acid treatment in an aqueous solution of $C_{16}EO_{10}$ as in the case without using $C_{16}EO_{10}$. The XRD patterns of as-PE-KSW-2_1 after the acid treatment in aqueous solution of $C_{16}EO_{10}$ (1 mM) showed the peaks at 4.1, 2.8, and 2.0 nm (Figure 2c). The ratio of the *d*-values was

2:√2:1, and these peaks are assignable to (11), (20) and (22) planes of a 2-D orthorhombic structure.[35] In the XRD patterns of as-PE-KSW-2_5, _10, and _50, the (11), (20), and (22) peaks were also observed (Figure 2d-f). The *d*-values of the (11) lattice plane of as-PE-KSW-2_0, _1, _5, _10, and _50 were 4.0, 4.1, 4.2, 4.3, and 4.6 nm, respectively. The acid treatment with higher concentration of $C_{16}EO_{10}$ produces the higher *d*-values of the 2-D orthorhombic phase.

Typical TEM images of as-PE-KSW-2_10 are displayed in Figure 3. A rectangle grid pattern (Figure 3a) and one-dimensionally ordered stripe patterns (Figure 3b) were observed clearly, being in good agreement with the XRD pattern of as-PE-KSW-2_10 (Figure 2c). The rectangle size was ca. 3 nm × 3 nm on the basis of the FFT image of the grid pattern and the d_{11} value was calculated to be 4.4 nm, being similar to the corresponding d_{11}-value (4.3 nm) in the XRD pattern (Figure 2e).

The XRD peaks of as-PE-KSW-2_*x* (*x* = 1~100) were broadened with the increase in the $C_{16}EO_{10}$ concentration. It is difficult to assign the higher order peaks, (20) and (22),

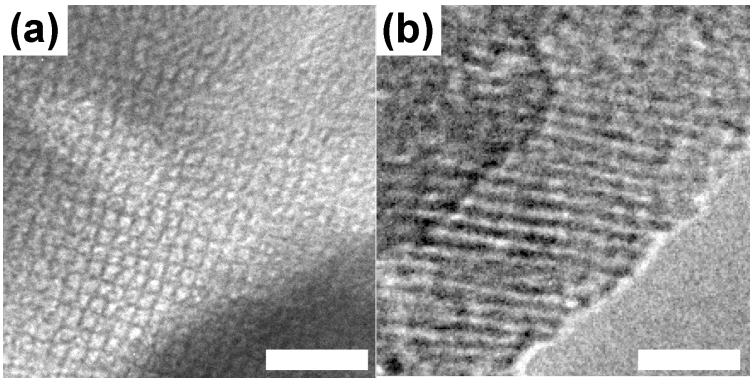

Figure 3. TEM images of as-PE-KSW-2_10 taken along with (a) parallel and (b) perpendicular directions to 1-D mesochannels.

for as-PE-KSW-2_100 because of the broadening. Electrostatic interactions between C_{16}TMA ions and silicate layers are stronger than hydrogen bonding between EO chains and silicate layers. The regularity of mesostructure was decreased because the interactions between surfactants and silicate layers decreased due to the increase in the amount of intercalated $C_{16}EO_{10}$. We have already reported the intercalation of $C_{16}EO_{10}$ into C_{16}TMA-kanemite without the acid treatment.[41] C_{16}TMA-kanemite was dispersed into an aqueous solution of $C_{16}EO_{10}$ (100 mM), and then the mixture was just stirred. The obtained sample showed sharp XRD peaks at the *d*-spacings of 3.3, 1.7, and 1.1 nm. These peaks were assignable to (001), (002), and (003) planes of the lamellar structure. On the basis of these results, it can be summarized that all the as-PE-KSW-2_*x* samples after acid treatment showed lager d_{11}-values (4.0~4.6 nm) that cannot be assigned to lamellar but to 2-D orthorhombic phases. Thus, the addition of $C_{16}EO_{10}$ in the acid treatment is necessary to control the mesostructure through the transformation from the lamellar to the 2-D orthorhombic.

All the signals (14.7, 23.7, 25.3, 27.4, 31.0, 33.0, 54.3, and 67.2 ppm) in the ^{13}C CP/MAS NMR spectrum of as-PE-KSW-2_0 are assignable to C_{16}TMA (Figure 4a),[41] revealing the presence of only C_{16}TMA cations in as-PE-KSW-2_0. The ^{13}C CP/MAS NMR spectra of as-PE-KSW-2_*x* (*x* = 1~100) showed additional signal at 71.3 ppm that can be assigned to poly(oxyethylene) chain (-O$\underline{C}$H$_2\underline{C}$H$_2$-) (Figure 4b-g). The additional small signals at 62.1 and 73.1 ppm due to other carbon atoms in $C_{16}EO_{10}$, such as HO$\underline{C}$H$_2$CH$_2$- and -O$\underline{C}$H$_2$C$_{15}$H$_{32}$, respectively, are observed for as-PE-KSW-2_50 and _100. Therefore, the presence of $C_{16}EO_{10}$ in as-PE-KSW-2_*x* (*x* = 1~100) was confirmed by ^{13}C CP/MAS NMR. The chemical shift due to the interior methylene groups should be changed according to the conformation. The signal due to carbon atoms in methylene groups with

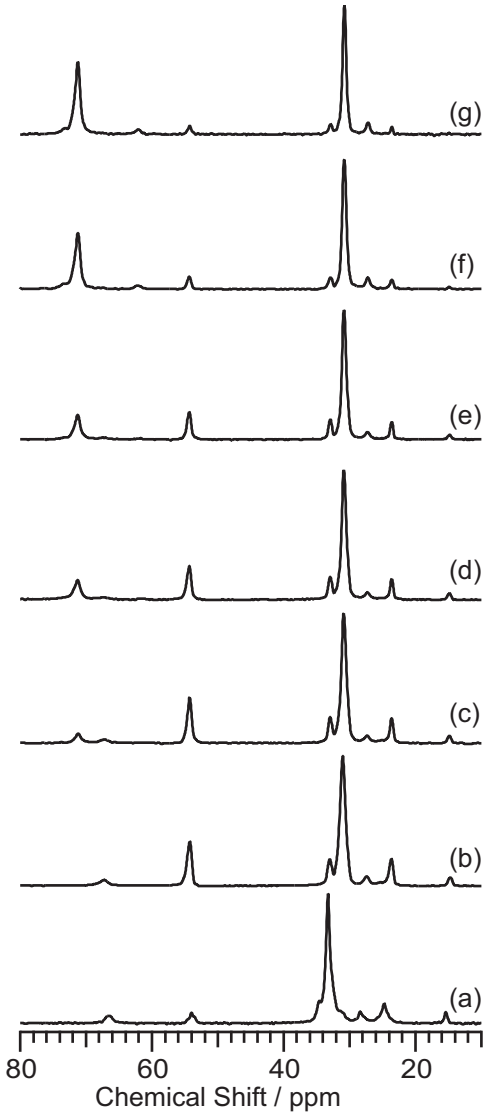

Figure 4. ^{13}C CP/MAS NMR spectra of (a) C_{16}TMA-kanemite and (b) as-PE-KSW-2_0, (c) _1, (d) _5, (e) _10, (f) _50, and (g) _100.

all-*trans* conformation is observed at 33 ppm, while it is shifted to 31 ppm by changing the conformation to *trans/gauche*.[43-44] The signals due to the interior methylene groups in hexadecyl chains of C_{16}TMA and $C_{16}EO_{10}$ are overlapped. The chemical shifts of interior methylene carbons of all as-PE-KSW-2_*x* (*x* = 0~100) were 33.0 ppm, though that of C_{16}TMA-kanemite was 31.0 ppm, meaning that the methylene chains were changed from all-*trans* to *trans/gauche* through the acid treatment with the deintercalation of C_{16}TMA

cations. In lamellar $C_{16}EO_{10}$-intercalated C_{16}TMA-kanemite (without acid treatment), almost all the methylene carbons take all-*trans* conformation.[41] The difference in the alkyl chain conformations can be explained by the formation of rod-like micelles through the deintercalation of C_{16}TMA cations and the accompanying structural transformation by the acid treatment (See Figure 1 and ref. 35).

The C_{16}TMA/Si and $C_{16}EO_{10}$/Si molar ratios, calculated from the CHN analysis and TG data, are summarized in Table 1, and are plotted with the concentration of $C_{16}EO_{10}$ (Figure 5). The C_{16}TMA/Si molar ratios were calculated on the basis of the nitrogen and Si contents. As reported previously,[35] the C_{16}TMA/Si molar ratio of C_{16}TMA-kanemite was decreased from 0.30 to 0.19 by an acid treatment (without $C_{16}EO_{10}$). C_{16}TMA cations were ion-exchanged with H^+ and deintercalated, accompanied with the mesostructural

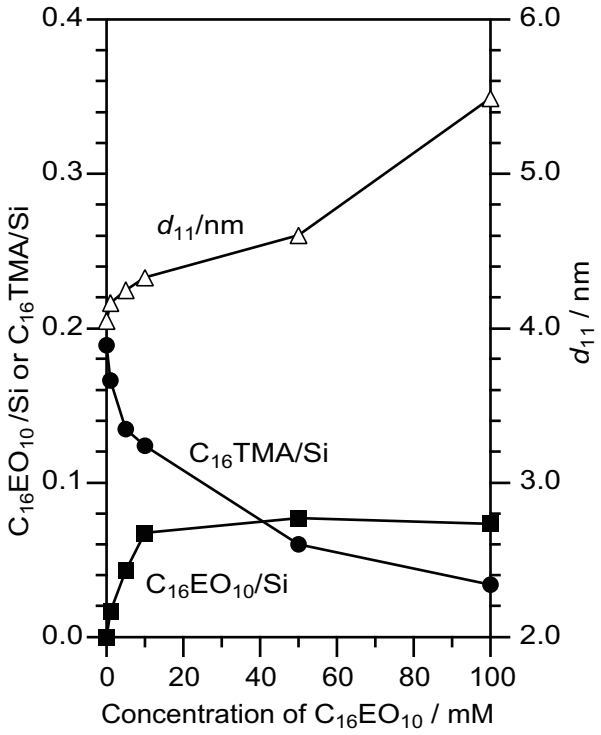

Figure 5. Variations in the d_{11}-value and amount of $C_{16}EO_{10}$ and C_{16}TMA in as-PE-KSW-2_*x*.

Table 1. Composition of C_{16}TMA-kanemite and as-PE-KSW-2_*x*

Sample	C/mass%	N/mass%	SiO_2/mass%*	C_{16}TMA/Si	$C_{16}EO_{10}$/Si	$C_{16}EO_{10}$/C_{16}TMA
C_{16}TMA-kanemite	42.7	2.6	36.2	0.30	-	-
as-PE-KSW-2_0	35.2	2.1	49.0	0.19	0.00	0.0
as-PE-KSW-2_1	33.5	1.7	44.7	0.17	0.02	0.1
as-PE-KSW-2_5	35.8	1.4	43.7	0.13	0.04	0.3
as-PE-KSW-2_10	37.7	1.1	39.5	0.12	0.07	0.5
as-PE-KSW-2_50	37.5	0.7	47.9	0.06	0.08	1.3
as-PE-KSW-2_100	31.6	0.4	48.1	0.03	0.07	2.2

* Residual amount after heating the samples at 900 °C by TG.

variation of C_{16}TMA-kanemite. The C_{16}TMA/Si molar ratios of as-PE-KSW-2_1, _5, _10, _50, and 100 were 0.17, 0.13, 0.12, 0.06, and 0.03, respectively.

On the basis of the charge compensation of the interlayer region, C_{16}TMA cations were exchanged with H^+ in the solution, and the reaction was enhanced by the different H^+ concentrations between the solution and the interlayer of C_{16}TMA-kanemite. However, the pH values of the acid treatment were same at pH 5.5 for all the samples. Therefore, the decrease of C_{16}TMA/Si with the concentration of $C_{16}EO_{10}$ cannot be explained by the concentration of H^+. It is assumed that the presence of $C_{16}EO_{10}$ molecules in a solution enhanced deintercalation of C_{16}TMA cations because the headgroup of C_{16}TMA cations is considered to interact with poly(oxyethylene) chain of $C_{16}EO_{10}$ in the aqueous solution regardless of the micelle formation.[41] Thus, the acid treatment of C_{16}TMA-kanemite leads to simultaneous reactions of (1) intercalation of $C_{16}EO_{10}$ into the interlayer of C_{16}TMA-kanemite, (2) deintercalation of C_{16}TMA cations, and (3) mesostructural change from lamellar to 2-D orthorhombic phases.

The $C_{16}EO_{10}$/Si molar ratios were calculated from the residual carbon content excluding that of C_{16}TMA cations. The $C_{16}EO_{10}$/Si molar ratios of as-PE-KSW-2_1, _5,

_10, _50, and 100 are 0.02, 0.04, 0.07, 0.08, and 0.07, respectively. The variation in the $C_{16}EO_{10}$/Si molar ratio can be categorized into two parts as follows. The $C_{16}EO_{10}$/Si molar ratio was increased up to 0.07 with the concentration of $C_{16}EO_{10}$ from 0 to 10 mM, and was constant about 0.08 with the concentration from 10 to 100 mM. In the range from 0 to 10 mM, it is supposed that the increase of the $C_{16}EO_{10}$ concentration elevates the concentration gradient between the solution and the interlayer of C_{16}TMA-kanemite, and promotes the intercalation of $C_{16}EO_{10}$. A possible interpretation of the plateau of $C_{16}EO_{10}$/Si molar ratio is that the interaction of the silicate framework with oxyethylene chain is mainly hydrogen bonding and weaker than electrostatic interaction between SiO^- groups and trimethylammonium headgroups. Therefore, the amount of $C_{16}EO_{10}$ intercalated into the interlayer was saturated at higher $C_{16}EO_{10}$ concentrations.

The d_{11}-value of as-PE-KSW-2_ *x* (*x* = 0~100) was increased with the concentration of $C_{16}EO_{10}$. The d_{11}-value is not proportional to the C_{16}TMA/Si and $C_{16}EO_{10}$/Si molar ratios. In contrast, the d_{11}-value was linearly increased with the $C_{16}EO_{10}/C_{16}$TMA molar ratio in the as-PE-KSW-2_*x* samples after drying, as plotted in

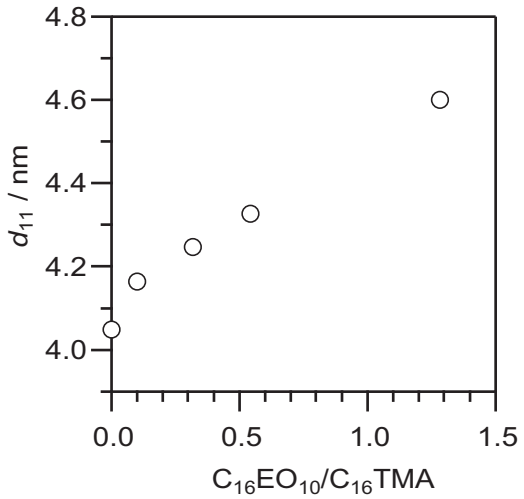

Figure 6. Dependence of the d_{11} value as a function of $C_{16}EO_{10}/C_{16}$TMA in as-PE-KSW-2_*x*. The value for as-PE-KSW-2_100 was omitted because of the less ordered mesostructure.

Figure 6. Hence, the increase of the $C_{16}EO_{10}/C_{16}TMA$ molar ratio is a key parameter, which is probably explained by loose packing of micelles including $C_{16}EO_{10}$ and/or swelling of oxyethylene chains with water molecules provided from the aqueous solution. We reported that lamellar $C_{16}EO_{10}$-intercalated kanemite ($C_{16}TAM/Si$ = 0, $C_{16}EO_{10}/Si$ = 0.19) after complete removal of $C_{16}TMA$ cations showed larger d_{001}-value (5.5 nm) than that of $C_{16}EO_{10}$-intercalated $C_{16}TMA$-kanemite (d_{001} = 3.3 nm, $C_{16}TAM/Si$ = 0.26, $C_{16}EO_{10}/Si$ = 0.07) even though the total organic contents were decreased.[41] In addition, $C_{16}EO_{10}$-intercalated kanemite indicated the expansion of the interlayer space by adsorption of water. Thus, as-PE-KSW-2 type silica was mesostructurally controlled by the adjustment of intercalation of $C_{16}EO_{10}$ molecules and deintercalation of $C_{16}TMA$ cations by acid treatment in this mixed surfactant system.

3.2. Pore-expansion of cal-PE-KSW-2

The XRD patterns of the sample after calcination exhibited the peaks assignable to the (11) plane of 2-D orthorhombic structure, and the *d*-spacings were 3.5, 3.5, 3.7, 3.8, 4.4, and 4.8 nm for cal-PE-KSW-2_0, _1, _5, _10, _50, and _100, respectively (Figure 7). The existence of the peak after calcination strongly supports the structural transformation into 2-D orthorhombic by the acid treatment. Compared with those observed for as-PE-KSW-2_*x*, the *d*-values of cal-PE-KSW-2_*x* were decreased by the shrinkage of the silicate frameworks during calcination. With the increase in the $C_{16}EO_{10}$ concentration, the peaks in the XRD patterns of cal-PE-KSW-2_*x*, especially cal-PE-KSW-2_100 were broadened (Figure 7f), being related to the deformation of the mesostructure with the increase in $C_{16}EO_{10}/C_{16}TMA$ molar ratio. This decrease of the mesostructural ordering depends on the ordering of samples before calcination (as-PE-KSW-2_*x*). Therefore, the

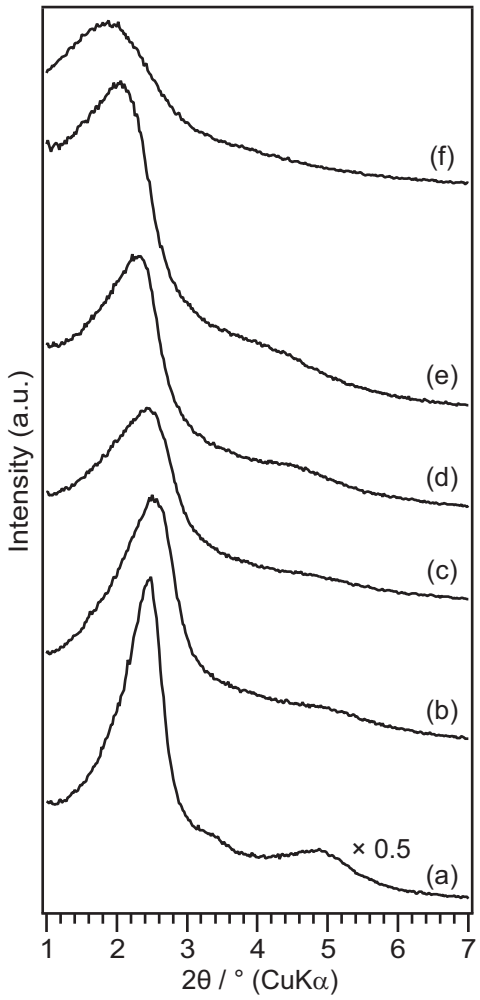

Figure 7. XRD patterns of (a) cal-PE-KSW-2_0, (b) _1, (c) _5, (d) _10, (e) _50, and (f) _100.

increase of the $C_{16}EO_{10}/C_{16}TMA$ molar ratio probably disturbs the formation of regularly arranged 2-D orthorhombic mesostructure of cal-PE-KSW-2_*x*.

The TEM images of cal-PE-KSW-2_0, _1, _5, _10, and _50 are shown in Figure 8, proving the formation of ordered and less ordered rectangular grid mesopores after calcination. The ordering of the patterns was decreased with the increase of *x*, which agrees with the broadening of the XRD peaks (Figure 7). In the TEM image of cal-PE-KSW-2_100, rectangle patterns were partially distorted and crushed. In the case of MCM-41 type mesoporous silica synthesized using mixed surfactants of $C_{16}EO_{10}$ and

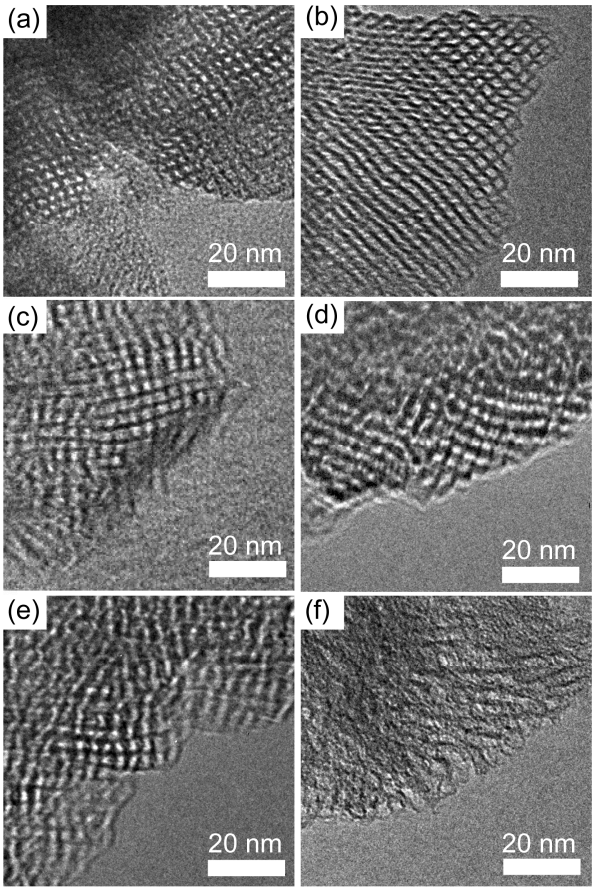

Figure 8. TEM images of (a) cal-PE-KSW-2_0, (b) _1, (c) _5, (d) _10, (e) _50, and (f) _100.

C_{16}TMA (molar ratio = 1.0: the same ratio for the structural deterioration of the above system), a 2-D hexagonal mesostructure was successfully observed.[42] The difference is probably caused by the different thicknesses of silica walls. The thickness of the silica walls of KSW-2 type mesoporous silica is independent of pore size, and is thinner than that of MCM-41 type mesoporous silica.[35] Therefore, the partial disordering of cal-PE-KSW-2_100 comes from the mechanical weakness because this sample possesses larger pores despite the thin silica walls. Nevertheless, the pore size of the samples is continuously controlled in the range from 3.5 to 4.4 nm with the retention of the 2-D orthorhombic structure by varying the concentration of $C_{16}EO_{10}$.

All the N_2 adsorption-desorption isotherms of cal-PE-KSW-2_*x* showed type IV behavior (Figure 9) characteristic of mesoporous materials.[45] The BET surface area, pore volume, and pore size of cal-PE-KSW-2_*x* are summarized in Table 2. The BET surface areas of cal-PE-KSW-2_*x* are almost constant in the range of *x* = 0~50, while cal-PE-KSW-2_100 exhibits a reduced surface area because of the deformation of the mesostructure. The pore volume (*V*) of cal-PE-KSW-2_100 is also relatively smaller than

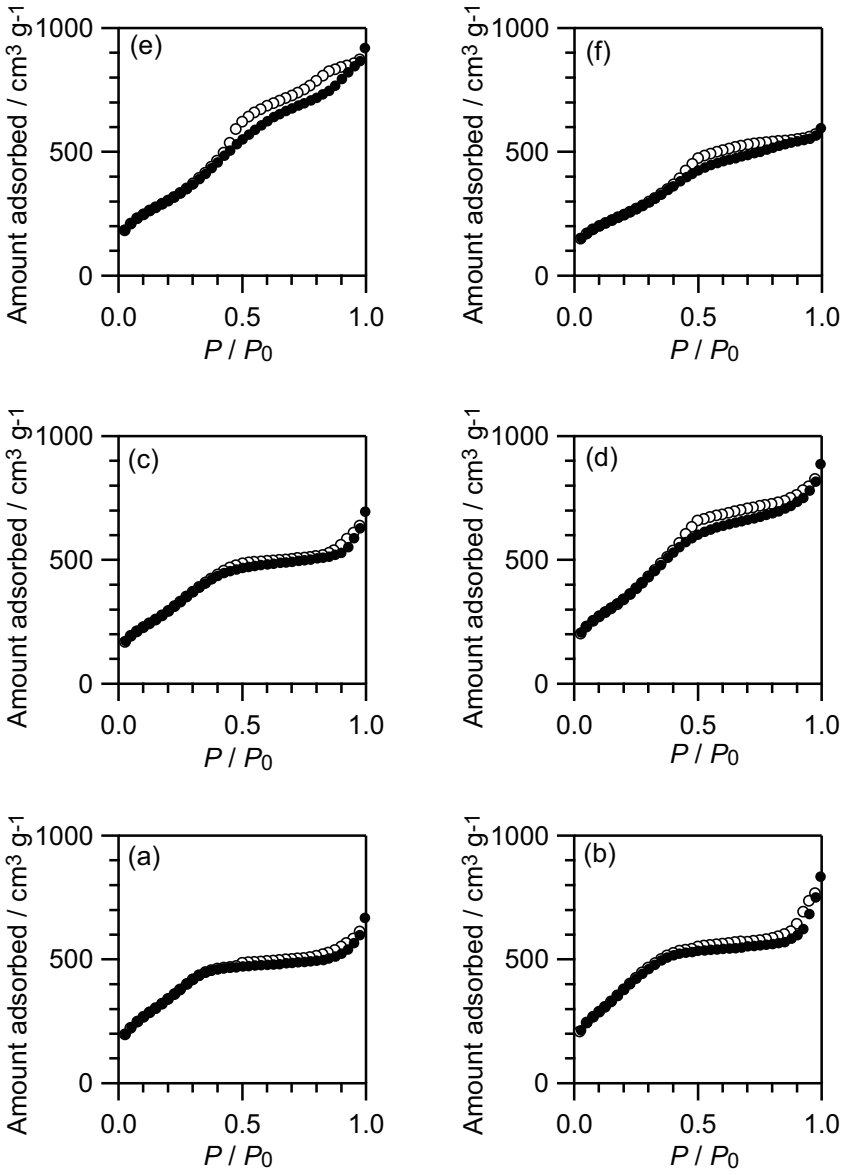

Figure 9. N_2 adsorption-desorption isotherms of (a) cal-PE-KSW-2_0, (b) _1, (c) _5, (d) _10, (e) _50, and (f) _100. ●: adsorption, ○: desorption.

Table 2. Surface area, pore volume, and pore size of cal-PE-KSW-2_*x*.

sample	BET surface area S_{BET} /m^2 g^{-1}	Pore volume V /cm^3 g^{-1}	Inner surface area S_{inner} /m^2 g^{-1}	Pore size $4V/S_{inner}$ /nm
cal-PE-KSW-2_0	1400	0.64	1200	2.1
cal-PE-KSW-2_1	1500	0.75	1400	2.1
cal-PE-KSW-2_5	1200	0.63	1100	2.3
cal-PE-KSW-2_10	1400	0.77	1100	2.7
cal-PE-KSW-2_50	1200	0.71	800	3.6
cal-PE-KSW-2_100	900	0.51	700	-*

* The data for cal-PE-KSW-2_100 was omitted because of the less ordered 2-D orthorhombic structure.

those of the others. These decreases are due to partial distortion and crushing of the mesopore. The pore size, which is calculated by $4V/S_{inner}$, corresponds to the average length of one side of rectangular mesopores. In the range of x = 1~50, the pore size was increased and in good agreement with the increase of the d_{11}-value.

The D_{BJH} distribution is meaningful for the discussion on the uniformity of pores of cal-PE-KSW-2_*x* samples, though the D_{BJH} distribution does not fully indicate true values because the mesopores of cal-PE-KSW-2 are not cylindrical but rectangular. With the increase of the concentration of $C_{16}EO_{10}$, the width of the distribution of cal-PE-KSW-2_*x* is broadened and the distributions are shifted to larger size (Figure 10). The arithmetic mean values of D_{BJH} of cal-PE-KSW-2_0, _1, _5, _10, _50, and _100 were 2.3, 2.4, 2.6, 2.9, 3.4, and 3.0 nm, respectively. This tendency of D_{BJH} in the range of x = 0~50 is in good agreement with that of $4V/S_{inner}$. Thus, the pore size of KSW-2 type mesoporous silica is varied in the range from 2.1 to 3.6 nm ($4V/S_{inner}$) though the expansion is limited by the decrease of the structural regularity with larger pore size.

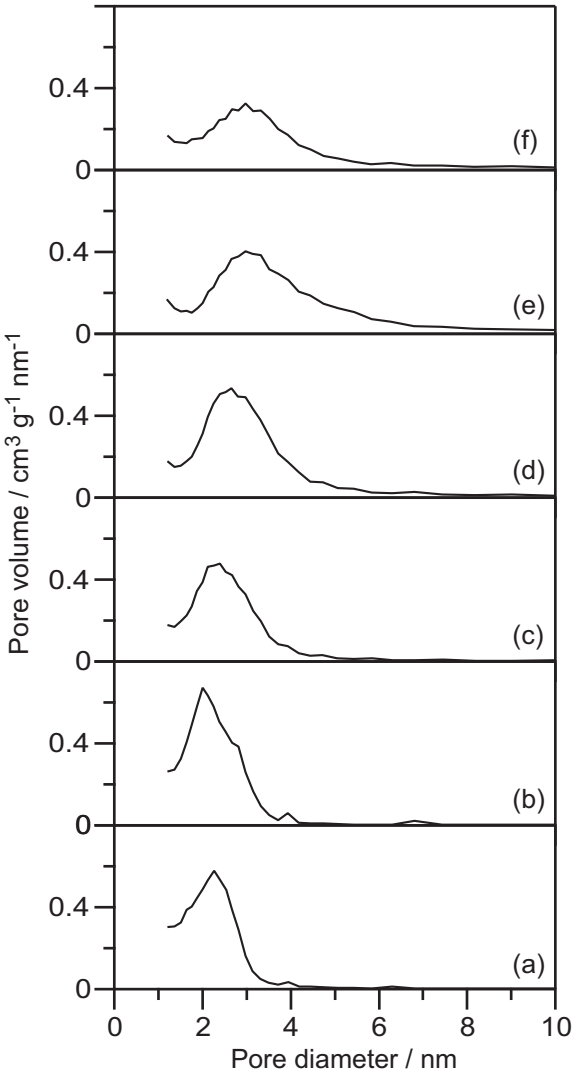

Figure 10. BJH pore size (D_{BJH}) distributions of (a) cal-PE-KSW-2_0, (b) _1, (c) _5, (d) _10, (e) _50, and (f) _100.

4. Conclusion

The acid treatment of lamellar C_{16}TMA-kanemite in an aqueous solution containing $C_{16}EO_{10}$ leads to simultaneous reactions, such as (1) intercalation of $C_{16}EO_{10}$, (2) deintercalation of C_{16}TMA cations, and (3) mesostructural transformation into a 2-D orthorhombic phase. The presence of $C_{16}EO_{10}$ in the aqueous solution promotes the pore

expansion of KSW-2 type mesoporous silica, which is varied with the $C_{16}EO_{10}$ concentration. This unique method, consisting of intercalation and deintercalation of organic guest species, will contribute to precise control of mesopore size of KSW-2 with retaining the silicate ordering of starting silicate materials.

5. References

[1] T. Yanagisawa, T. Shimizu, K. Kuroda, C. Kato, *Bull. Chem. Soc. Jpn.* **1990**, *63*, 988-992.

[2] C. T. Kresge, M. E. Leonowicz, W. J. Roth, J. C. Vartuli, J. S. Beck, *Nature* **1992**, *359*, 710-712.

[3] L. Mercier, T. J. Pinnavaia, *Adv. Mater.* **1997**, *9*, 500-503.

[4] P. T. Tanev, M. Chibwe, T. J. Pinnavaia, *Nature* **1994**, *368*, 321-323.

[5] T. Maschmeyer, F. Rey, G. Sankar, J. M. Thomas, *Nature* **1995**, *378*, 159-162.

[6] C. G. Wu, T. Bein, *Science* **1994**, *264*, 1757-1759.

[7] T. Q. Nguyen, J. J. Wu, V. Doan, B. J. Schwartz, S. H. Tolbert, *Science* **2000**, *288*, 652-656.

[8] C. Sanchez, B. Lebeau, F. Chaput, J.-P. Boilot, *Adv. Mater.* **2003**, *15*, 1969-1994.

[9] M. Hartmann, *Chem. Mater.* **2005**, *17*, 4577-4593.

[10] M. Vallet-Regí, F. Balas, D. Arcos, *Angew. Chem. Int. Ed.* **2007**, *46*, 7548-7558.

[11] S. Baskaran, J. Liu, K. Domansky, N. Kohler, X. Li, C. Coyle, G. E. Fryxell, S. Thevuthasan, R. E. Williford, *Adv. Mater.* **2000**, *12*, 291-294.

[12] S. A. Bagshaw, E. Prouzet, T. J. Pinnavaia, *Science* **1995**, *269*, 1242-1244.

[13] D. Zhao, Q. Huo, J. Feng, B. F. Chmelka, G. D. Stucky, *J. Am. Chem. Soc.* **1998**, *120*, 6024-6036.

[14] D. Zhao, J. Feng, Q. Huo, N. Melosh, G. H. Fredrickson, B. F. Chmelka, G. D. Stucky, *Science* **1998**, *279*, 548-552.

[15] M. Kruk, M. Jaroniec, A. Sayari, *J. Phys. Chem. B* **1999**, *103*, 4590-4598.

[16] M. J. Kim, R. Ryoo, *Chem. Mater.* **1999**, *11*, 487-491.

[17] Y. Wan, D. Y. Zhao, *Chem. Rev.* **2007**, *107*, 2821-2860.

[18] B. T. Holland, L. Abrams, A. Stein, *J. Am. Chem. Soc.* **1999**, *121*, 4308-4309.

[19] F. S. Xiao, *Angew. Chem. Int. Ed.* **2006**, *45*, 3090-3093.

[20] C. J. H. Jacobsen, C. Madsen, J. Houzvicka, I. Schmidt, A. Carlsson, *J. Am. Chem. Soc.* **2000**, *122*, 7116-7117.

[21] Y. S. Tao, H. Kanoh, K. Kaneko, *J. Am. Chem. Soc.* **2003**, *125*, 6044-6045.

[22] Y. Fang, H. Hu, *J. Am. Chem. Soc.* **2006**, *128*, 10636-10637.

[23] W. Fan, *Nat. Mater.* **2008**, *7*, 984-991.

[24] M. Choi, *Nat. Mater.* **2006**, *5*, 718-723.

[25] H. Wang, T. J. Pinnavaia, *Angew. Chem. Int. Ed.* **2006**, *45*, 7603-7606.

[26] M. Choi, K. Na, J. Kim, Y. Sakamoto, O. Terasaki, R. Ryoo, *Nature* **2009**, *461*, 246-249.

[27] T. Kimura, K. Kuroda, *Adv. Funct. Mater.* **2009**, *19*, 511-527.

[28] S. Inagaki, Y. Fukushima, K. Kuroda, *J. Chem. Soc., Chem. Commun.* **1993**, 680-682.

[29] T. Kimura, D. Itoh, T. Shigeno, K. Kuroda, *Langmuir* **2002**, *18*, 9574-9577.

[30] T. Kimura, D. Itoh, T. Shigeno, K. Kuroda, *Bull. Chem. Soc. Jpn.* **2004**, *77*, 585-590.

[31] T. Kimura, M. Suzuki, T. Ikeda, K. Kato, M. Maeda, S. Tomura, *Microporous Mesoporous Mater.* **2006**, *95*, 146-153.

[32] M. Kato, T. Shigeno, T. Kimura, K. Kuroda, *Chem. Mater.* **2004**, *16*, 3224-3230.

[33] M. Kato, T. Shigeno, T. Kimura, K. Kuroda, *Chem. Mater.* **2005**, *17*, 6416-6421.

[34] H. Tamura, D. Mochizuki, T. Kimura, K. Kuroda, *Chem. Lett.* **2007**, *36*, 444-445.

[35] T. Kimura, T. Kamata, M. Fuziwara, Y. Takano, M. Kaneda, Y. Sakamoto, O. Terqasaki, Y. Sugahara, K. Kuroda, *Angew. Chem. Int. Ed.* **2000**, *39*, 3855-3859.

[36] T. Kimura, D. Itoh, N. Okazaki, M. Kaneda, Y. Sakamoto, O. Terasaki, Y. Sugahara, K. Kuroda, *Langmuir* **2000**, *16*, 7624-7628.

[37] T. Kimura, H. Tamura, M. Tezuka, D. Mochizuki, T. Shigeno, T. Ohsuna, K. Kuroda, *J. Am. Chem. Soc.* **2007**, *130*, 201-209.

[38] T. Kimura, S. Huang, A. Fukuoka, K. Kuroda, *J. Mater. Chem.* **2009**, *19*, 3859-3866.

[39] M. Ogawa, K. Kuroda, *Chem. Rev.* **1995**, *95*, 399-438.

[40] M. Alexandre, P. Dubois, *Mater. Sci. Eng., R* **2000**, *28*, 1-63.

[41] N. Takahashi, H. Tamura, D. Mochizuki, T. Kimura, K. Kuroda, *Langmuir* **2007**, *23*, 10765-10771.

[42] M.-G. Song, J.-Y. Kim, S.-H. Cho, J.-D. Kim, *Langmuir* **2002**, *18*, 6110-6115.

[43] W. Gao, L. Reven, *Langmuir* **1995**, *11*, 1860-1863.

[44] M. Pursch, L. C. Sander, K. Albert, *Anal. Chem.* **1996**, *68*, 4107-4113.

[45] M. Kruk, M. Jaroniec, A. Sayari, *Langmuir* **1997**, *13*, 6267-6273.

Chapter 5

Anion Exchangeable Layered Silicates Modified with Ionic Liquids on the Interlayer Surface

1. Introduction

Inorganic layered materials are quite attractive because of a wide variety of applications, including adsorbents, catalyst supports, porous materials, and building units for nano/meso-structured materials utilizing their unique two-dimensionally confined space.[1] The interactions, especially electrostatic interactions, between layered host materials and guest species strongly affect the reactivity and selectivity of intercalation reactions. Among a large number of layered materials, anion exchangeable layered materials figure prominently in this field and have been studied as hosts or carriers for not only inorganic anions but also drug substances[2] and biological species.[3-4] Despite the demanding requirement for the creation of such functional materials, there are few kinds of

anion exchangeable layered materials. A typical one is layered double hydroxides (LDHs)[5-7] in which anion exchangeable sites come from substituted trivalent cations in divalent metal hydroxides. Because the property of anion exchangeable sites is limited to the kind of substituting trivalent metal cations, the affinity for various intercalating guest species is almost fixed.[8-10] In addition, LDHs are unstable in acid media.

Recently, another method of the incorporation of anion exchangeable sites into interlayer spaces has been achieved through the hybridization of cation exchangeable layered clay minerals with calix[4]areneoctols,[11] chitosan,[12] or cationic polyelectrolytes with amine groups.[13-14] Hata *et al.* reported that the color of intercalated anionic dye can be tuned through choosing the optimal polyelectrolyte and the reaction pH.[14] However, because cation sites are generally distributed throughout the whole of the interlayer spaces, the distance and arrangement of anion exchangeable sites cannot be controlled with incorporated polycations. Furthermore, these hybrids possess much lower anion exchange capacity (AEC: 0.2 meqiv/g of host) than that of LDH (2−4.5 meqiv/g of host)[6] because their AEC values rely on the degree of overcompensation of polycations and the degree is limited by steric hindrance of the polymer and repulsion of cations.

Ionic liquids[15-16] have attracted keen interest as “designer solvents”,[17] such as ionic conductors,[18-19] as well as solvents for synthesis and catalysis.[20-21] As an anion exchanger, ionic liquids immobilized onto solid supports have received much attention as stationary phases of liquid chromatography[22-24] and catalyst supports.[25-34] Ionic liquids as liquid chromatography stationary phases can separate a wide variety of mixtures, such as nonpolar and polar molecules, cations and anions because of the wide range of properties of the ionic liquids.[24,35] Anionic catalysts on ionic liquids immobilized onto silica supports exhibit high selectivities and activities because of the homogeneous-like state of

the catalysts with liquid-state ionic liquids.[29-32] However, silica supports for ionic liquids are so far limited to amorphous ones, such as silica gel,[25,27,31] silica nanoparticles,[29-30] and mesoporous silica.[25,33-34,36] Therefore, immobilized ionic liquid molecules are located randomly on such amorphous supports.

Layered silicates,[37] composed of SiO_4 tetrahedra only, possess SiOH/SiO^- groups on the interlayer surfaces which are reactive for organic modification including silylation.[38-48] In particular, a layered octosilicate[49-50] ($Na_8[Si_{32}O_{64}(OH)_8 \cdot 32H_2O]$, also known as ilerite or RUB-18) possesses confronting SiOH/SiO^- groups arranged along one axis on the interlayer surfaces (Figure 1).[50] The confronting groups preferentially induce a bidentate silylation which provides organic groups in a well-arranged manner reflecting the surface structure of the silicate layers.[44-46] More than 90% of the confronting SiOH/SiO^- groups of octosilicate are silylated with alkoxytrichlorosilanes[45] and the value is higher than that of another layered silicate kanemite[51] ($NaHSi_2O_5 \cdot 3H_2O$)[42] though the density of the SiOH/SiO^- groups of kanemite is higher than that of octosilicate. Therefore,

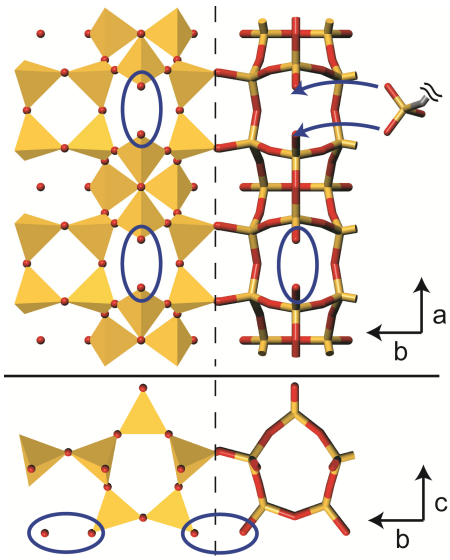

Figure 1. Crystal structure of layered octosilicate. The ellipsoids indicate confronting SiOH/SiO^- groups

octosilicate is an ideal host for immobilization of organic species with optimal arrangement and high density.

From the viewpoint of the highest utilization of ionic liquids on solid supports, it is extremely important to select and/or design supports possessing a high surface area, high accessibility, confined space, and controllability of immobilized sites;[33] and all these requirements can be provided by well-defined layered silicates. The distance of immobilized sites can be controlled by choosing the kind of layered silicates and modifying agents. Hybridization of layered materials and ionic liquids has been reported for a few cases; ionic liquids are intercalated into clays such as montmorillonite[52-53] and kaolinite.[54-55] However, these studies have not focused on the control of layer charge and covalent immobilization. From the viewpoint of the layered materials, well-designed anion exchangeable sites are quite essential for developing advanced functional nanomaterials. Consequently, the immobilization of ionic liquids in the interlayer space of layered silicates can satisfy all the requirements described above because the structure of the ionic liquids is diverse and the hydrophilicity/hydrophobicity is controllable.

Here, I report the synthesis of anion exchangeable layered silicate via immobilization of ionic liquids onto the interlayer surfaces of octosilicate (Figure 2). I utilized ionic liquids containing three specific functional groups as follows; (i) butyl or octyl group attached on the imidazolium group for the control of hydrophobicity, (ii) triethoxysilyl group for immobilization, and (iii) imidazolium group for bridging both the alkyl chain and triethoxysilylpropyl group (Figure 2). Because of two quaternized nitrogens, imidazolium groups are more useful for bridging two functional groups than trimethylammonium groups which are also used conventionally.[56-57] In addition, imidazolium groups can form metal complexes, and, in particular, complexes with Pd or Ir

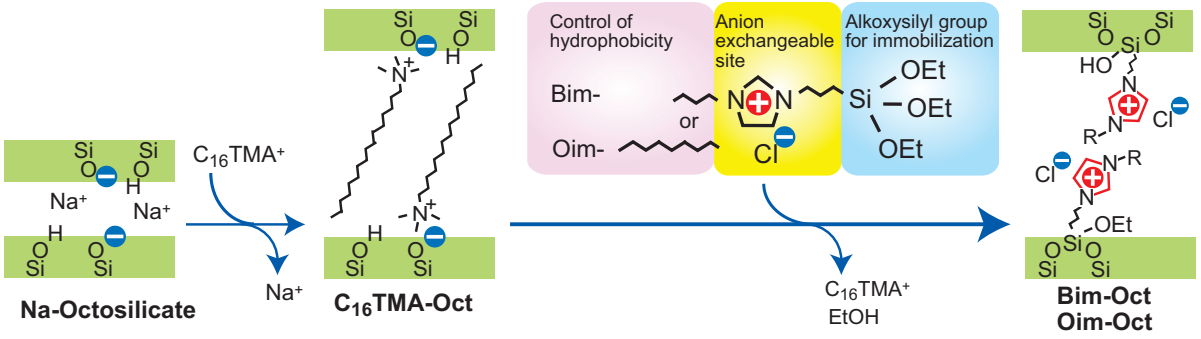

Figure 2. Synthetic pathway of anion exchangeable layered silicates. The first step is the intercalation of hexadecyltrimethylammonium ions for the expansion of the interlayer distance. The second step is immobilization of triethoxysilyl-terminated imidazolium salts with butyl or octyl groups.

species are useful as catalysts for cross-coupling reactions.[33,58] I can expect that the cation exchangeable sites of the SiOH/SiO^- groups can be converted to anion exchangeable sites of the imidazolium salts via silylation. The derivatized layered hybrids should have the following expected properties, such as a relatively high AEC, high durability in acid solution, and controllability of the affinity for guest species. Finally, I investigated the possibility of using the derivatives as a drug delivery carrier for an anti-inflammatory prodrug, sulfasalazine,[59] in oral administration, which needs high capacity, accessibility, and durability in gastric fluid, because oral administration needs high dosage, and sulfasalazine is metabolized into the active form in the colon.

2. Experimental

Materials

Layered Na-octosilicate ($Na_8[Si_{32}O_{64}(OH)_8 \cdot 32H_2O]$) was synthesized according to previous reports.[44-46] Na-Octosilicate (3.0 g) was dispersed in an aqueous solution (0.1 mol L^{-1}, 100 mL) of hexadecyltrimethylammonium chloride (C_{16}TMACl, Tokyo Chemical

Industry Co.). The mixture was stirred at room temperature for 1 day and then centrifuged to remove the supernatant. This procedure was repeated three times in total. The resulting slurry was washed with water and air-dried at room temperature to obtain the intermediate product (C_{16}TMA-Oct) for silylation.[44-46]

The silylating reagent was synthesized according to a previously reported method.[29-30] All reactions were performed under a nitrogen atmosphere using a vacuum line and Schlenk technique. A mixture of 3-(2-imidazolin-1-yl)propyltriethoxysilane (denoted as ImSi, Gelest, Inc.) and three equiv. of alkyl chloride (1-chlorobutane or 1-chlorooctane, Aldrich) was stirred at 70 °C for 1 day. The mixture was washed with *n*-hexane (100 mL) five times. The mixture was evaporated under a reduced pressure at room temperature for 2 h, and then at 70 °C for 3 h. 1-Butyl-3-(3-triethoxysilylpropyl)-4,5-dihydroimidazolium chloride ($BimSi(OEt)_3Cl$) and 1-octyl-3-(3-triethoxysilylpropyl)-4,5-dihydroimidazolium chloride ($OimSi(OEt)_3Cl$) were obtained as orange-colored waxy solids. The physical state of $BimSi(OEt)_3Cl$ and $OimSi(OEt)_3Cl$ depends on the amount of water in the system. $BimSi(OEt)_3Cl$ and $OimSi(OEt)_3Cl$, dried in vacuum and obtained as waxy solids, rapidly change to viscous liquids at ambient atmosphere by the absorption of water vapor. These viscous liquids can be transformed again to waxy solids by drying in vacuum. These ionic liquids were identified by ^1H, ^{13}C, and ^{29}Si NMR as well as mass spectroscopy as follows.[29-30]

$BimSi(OEt)_3Cl$: ^1H NMR: (500 MHz, $CDCl_3$, TMS, 25 °C) δ 10.1 (1H, s, NC**H**N), 3.92−3.93 (4H, m, NC**H**$_2$C**H**$_2$N), 3.82 (6H, q, $CH_3C\mathbf{H}_2O$), 3.67 (4H, m, $SiCH_2CH_2C\mathbf{H}_2N$, NC**H**$_2CH_2CH_2CH_3$), 1.39−1.76 (6H, m, methylene), 1.23 (9H, t, C**H**$_3CH_2O$), 0.97 (3H, t, $CH_2CH_2C\mathbf{H}_3$), 0.62 (2H, m, SiC**H**$_2CH_2$). ^{13}C NMR: (125.7 MHz, $CDCl_3$, TMS, 25 °C) δ 159.1 (N**C**HN), 58.6 ($CH_3\mathbf{C}H_2O$), 50.4, 48.4, 48.1, 48.1

(N**C**$H_2CH_2CH_2CH_3$, SiCH_2CH_2**C**H_2N, N**C**H_2**C**H_2N), 29.4, 21.3, 19.7 (methylene), 18.3 (**C**H_3CH_2O), 13.6 (CH_2CH_2**C**H_3), 7.3 (Si**C**H_2). ^{29}Si NMR (99.3 MHz, $CDCl_3$ TMS, 25 °C): δ −47.1 (T^0). MS (FAB^+): Calcd for $[C_{16}H_{35}N_2O_3Si]^+$, 331; found, 331.

OimSi(OEt)$_3$Cl: ^{1}H NMR: (500 MHz, $CDCl_3$, TMS, 25 °C) δ 9.94 (1H, s, NC**H**N), 3.99 (4H, m, NC**H**$_2$C**H**$_2$N), 3.82 (6H, q, CH_3C**H**$_2$O), 3.64−3.66 (4H, m, SiCH_2CH_2C**H**$_2$N, NC**H**$_2(CH_2)_6CH_3$), 1.26−1.77 (14H, m, methylene), 1.23 (9H, t, C**H**$_3CH_2O$), 0.88 (3H, t, CH_2CH_2C**H**$_3$), 0.61 (2H, m, SiC**H**$_2CH_2$). ^{13}C NMR: (125.7 MHz, $CDCl_3$, TMS, 25 °C) δ 159.1 (N**C**HN), 58.6 (CH_3**C**H_2O), 50.4, 48.4, 48.1 (N**C**$H_2(CH_2)_6CH_3$, SiCH_2CH_2**C**H_2N, N**C**H_2**C**H_2N), 31.7, 29.1, 27.5, 26.5, 22.6, 21.3 (methylene), 18.3 (**C**H_3CH_2O), 14.1 (CH_2CH_2**C**H_3), 7.3 (Si**C**H_2). ^{29}Si NMR (99.3 MHz, $CDCl_3$ TMS, 25 °C): δ -47.0 (T^0). MS (FAB^+): Calcd for $[C_{20}H_{43}N_2O_3Si]^+$, 387; found, 387.

Immobilization of ionic liquids onto C_{16}TMA-Oct.

Silylation of C_{16}TMA-Oct was performed under a N_2 atmosphere. Toluene (100 mL; anhydrous, Wako Pure Chemical Industries, Ltd.) and BimSi(OEt)$_3$Cl (3.7 g) or OimSi(OEt)$_3$Cl (4.2 g) was added to C_{16}TMA-Oct (1.0 g) which was dried in vacuum at 120 °C for 2 h beforehand. The amount of added ionic liquids equals to 2.5 equiv. of SiOH/SiO^- groups of C_{16}TMA-Oct. The mixtures were stirred at 70 °C for 1 day. After being cooled at room temperature, they were centrifuged and washed with acetonitrile, acetone, and *n*-hexane three times for each solvent with 100 mL. The products were dried under reduced pressure at room temperature for 1 day to yield silylated derivatives denoted as Bim-Oct (with a butyl group) and Oim-Oct (with an octyl group) as white powders.

Synthesis of Bim-kane

Layered silicate kanemite ($NaHSi_2O_5 \cdot 3H_2O$) was obtained through dispersing δ-$Na_2Si_2O_5$ (1.0 g) in deionized water (50 mL) with stirring for 0.5 h.[3] The slurry was centrifuged to remove supernatant, and dried. Obtained kanemite (0.2 g) was added to an aqueous solution of C_{16}TMACl (0.1 M, 40 mL), where the C_{16}TMA/Si molar ratio was 2.0. After the mixture was stirred at room temperature for 2 d, hexadecyltrimethylammonium-exchanged kanemite (C_{16}TMA-kane) was obtained by centrifugation and drying.[60] Silylation of C_{16}TMA-kane was performed by according to that of Bim-Oct. Anhydrous toluene (100 mL) and $BimSi(OEt)_3Cl$ (6.0 g) was added to C_{16}TMA-kane (1.0 g) which was dried in vacuo at 120 °C for 2 h beforehand. The added amount of $BimSi(OEt)_3Cl$ equals to 2.5 equivalent of $SiOH/SiO^-$ groups in C_{16}TMA-kane. The mixture was stirred at 70 °C for 1 d. After cooling at room temperature, the mixture was centrifuged for separation of solid, and the solid was washed with acetonitrile, acetone, and hexane three times for each solvent with 100 mL. The product was dried under a reduced pressure at room temperature for 1 day.

Sorption of anionic dye into Bim-Oct or Oim-Oct by anion exchange

The sorption isotherms were obtained by the following procedure. Bim-Oct or Oim-Oct (2.5 mg) was dispersed into 2.0 mL of an aqueous solution of Orange II (4-[(2-hydroxy-1-naphthyl)azo]benzenesulfonic acid, monosodium salt; Tokyo Chemical Industry Co.) with various concentrations (0.50−8.0 mM), and the mixtures were shaken at 25 °C for 2 days.[61] The solids were separated by centrifugation at 9700 × *g* (12000 rpm) for 5 min. The supernatants were diluted with deionized water and analyzed with a UV−Vis spectrometer. The amount of Orange II loaded into the samples was calculated

from the concentration of the dye in the supernatants by measuring the absorbance at 485 nm with a calibration curve. For the characterization of the exchanged products by powder XRD, Bim-Oct and Oim-Oct (0.15 g) were treated with 200 mL of the solution of Orange II (2.75 mM) for 1 day in the same manner.

Anion exchange with various inorganic anions

A solution containing four anions was prepared by dissolving NaCl, NaBr, NaI, and $NaNO_3$ (25 mM, respectively) into deionized water.[62] Bim-Oct or Oim-Oct (0.10 g) was dispersed into the solution, and stirred for 2 days at room temperature. After centrifugation for the removal of the supernatant, the slurry was washed with water four times.[63] The solid was dried for 1 day under reduced pressure at room temperature, and white powders were obtained from Bim-Oct and Oim-Oct that are denoted as Bim-Oct_A and Oim-Oct_A, respectively.

Investigation of the stability of Bim-Oct in an acid solution

Bim-Oct was dispersed into an aqueous solution of HCl (pH 1.0) and stirred for 50 h at room temperature. The mixture was centrifuged at 4800 × *g* (5000 rpm) for 15 min for the separation of the supernatant and solids. The supernatant was filtered through a Mixed Cellulose Esters Filter (Millipore^{TM}) with pore size of 0.1 μm to remove the solid. The Si content in this solution was determined by inductively coupled plasma emission spectroscopy (Vista-MPX, Varian Technology Japan Ltd.) with a calibration curve. The Si content in the acid solution was 26.7 ppm. On the basis of this concentration, it is calculated that 2.9% of Si species in Bim-Oct were dissolved into the acid solution. On the other hand, the solid after centrifugation was dried for 2 d in vacuum at room temperature.

The powdery sample was obtained and analyzed by XRD.

Sorption and release of prodrug in Bim-Oct.

Bim-Oct (50 mg) was dispersed into an aqueous solution (1 L, 40.0 μM) of sulfasalazine (2-hydroxy-5-[[4-[(2-pyridinylamino)sulfonyl]phenyl]azo] benzoic acid; Sigma) and stirred at 25 °C for 1 day. After filtration and drying for 1 day at room temperature under reduced pressure, yellow colored powders were obtained. The sorbed amount of sulfasalazine was determined in the decrease of the absorbance at 360 nm of the residual solution with a calibration curve. An in vitro release experiment was performed in a simulated gastric fluid (aqueous solution of HCl at pH 1.2) and an intestinal fluid (Ringer's solution at pH 7.4).[64] The sulfasalazine-loaded sample (10 mg) was dispersed into the simulated fluids (100 mL), and stirred (200 rpm) at 37 °C. To determine the time course of the release behavior of sulfasalazine, a part of the suspension (1.6 mL) was centrifuged at 9700 × *g* (12000 rpm) for 5 min, and the concentration of sulfasalazine in the supernatant was measured by the variation of the absorbance at 360 nm. After the measurement, the precipitates and supernatants were returned to the suspensions.

Characterization.

Powder X-ray diffraction (XRD) measurements were performed on a Rigaku Rint-Ultima III powder diffractometer with a radiation of CuKα (λ = 0.15418 nm) by using parallel beam geometry equipped with a parabolic multilayer solar slit. Liquid-state NMR spectra were recorded on a JEOL Lambda-500 spectrometer. Solid-state ^{13}C CP/MAS NMR spectra were recorded on a JEOL JNM-CMX-400 spectrometer at a resonance frequency of 100.40 MHz and a recycle delay of 5 s. The samples were put into a 5 mm

zirconia rotor and spun at 8 kHz. Solid-state ^{29}Si MAS NMR spectra were also recorded on the same spectrometer at a resonance frequency of 79.42 MHz with a 45° pulse and a recycle delay of 200 s with a 7.5 mm zirconia rotor by spinning at 5 kHz. It was confirmed that the signals were fully relaxed under these conditions so that quantitative analysis was possible.[45] The ^{13}C and ^{29}Si chemical shifts were externally referenced to hexamethylbenzene at 17.4 ppm (-**C**H$_3$) and poly(dimethylsiloxane) at −33.8 ppm, respectively. The amounts of organic constituents were determined by CHN analysis (Perkin Elmer, 2400 Series II). Positive FAB mass spectra were obtained by using a JEOL JMS-GCmateII mass spectrometer. The halogen contents were measured by ion chromatography with an SX-Elements microanalyzer YS-10 (Yanaco New Science Inc.). Thermogravimetry (TG) measurements were carried out with a Rigaku Thermo Plus 2 instrument under a dry air flow at a heating rate of 10 °C min^{-1}. The scanning electron microscopy (SEM) images were obtained by using a JEOL JSM-6500F microscope at an accelerating voltage of 15 kV. UV−Vis absorption spectra were measured with a JASCO V-530 UV/vis spectrophotometer. Raman spectra were obtained with a Renishaw inVia Reflex Raman Microscope.

3. Results and Discussion

3.1. Immobilization of ionic liquids onto layered octosilicate

The presence of imidazolium groups on octosilicate was confirmed by the ^{13}C CP/MAS NMR spectra (Figure 3). All signals (158.9, 59.3, 49.2−48.7, 30.0, 21.6, 21.2, 20.3, 14.4, and 10.9 ppm) in the ^{13}C CP/MAS NMR spectrum of Bim-Oct are assignable to

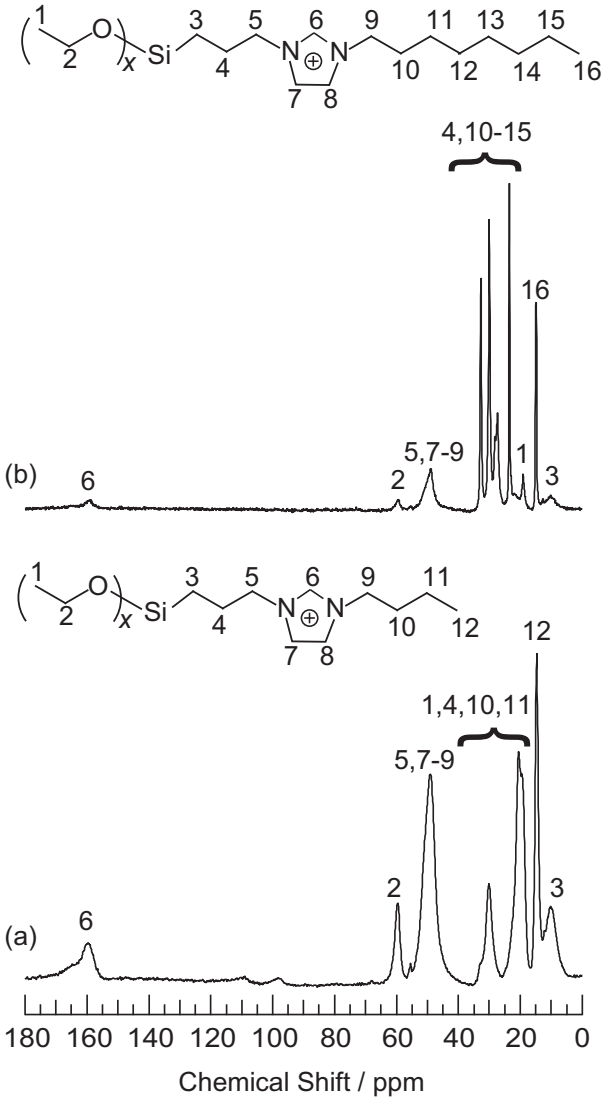

Figure 3. ^{13}C CP/MAS NMR spectra of (a) Bim-Oct and (b) Oim-Oct.

BimSi(OEt)$_{3-x}$ (x = 1−3) cation. In the ^{13}C CP/MAS NMR spectrum of Oim-Oct, all of the observed signals (159.1, 59.4, 52.5−49.0, 32.8, 30.1, 28.1, 27.4, 23.5, 18.5, 14.9, 12.6, and 10.2 ppm) are attributed to the Oim(OEt)$_{3-x}$ cation. No peaks assignable to C_{16}TMA cation were observed. Therefore, C_{16}TMA cations were completely removed from Bim-Oct and Oim-Oct during the silylation with ethoxy-terminated imidazolium cations.

As reported previously,[45] the ^{29}Si MAS NMR spectrum of C_{16}TMA-Oct (Figure 4a) shows two narrow signals at −100 ppm and −110 ppm, corresponding to the Q^3(**Si**(OSi)$_3$OH/O$^-$) and Q^4(**Si**(OSi)$_4$) units with an integral ratio of 1:1, which is the same as that of pristine Na-Octosilicate. The ^{29}Si MAS NMR spectrum of Bim-Oct (Figure 4b) indicates broad Q^3 (−102 ppm) and Q^4 (−111 ppm) signals with the integral ratio (Q^3 : Q^4) of 18:182. Therefore, 82% of the SiOH/SiO$^-$ groups in C_{16}TMA-Oct were silylated and converted to Q^4 units. The spectrum also shows new signals at −50, −57, and −66 ppm, which are attributed to the T^1, T^2, and T^3 sites of grafted Bim**Si**≡ groups with the integral ratio of T^1:T^2:T^3 = 7:44:20. No signal assignable to the T^0 environment was observed. The Si species with T^2 units are dominant in the immobilized silylation reagent, which is in accordance with the bidentate grafting of confronting SiOH/SiO$^-$ groups.[44-45,50] Because

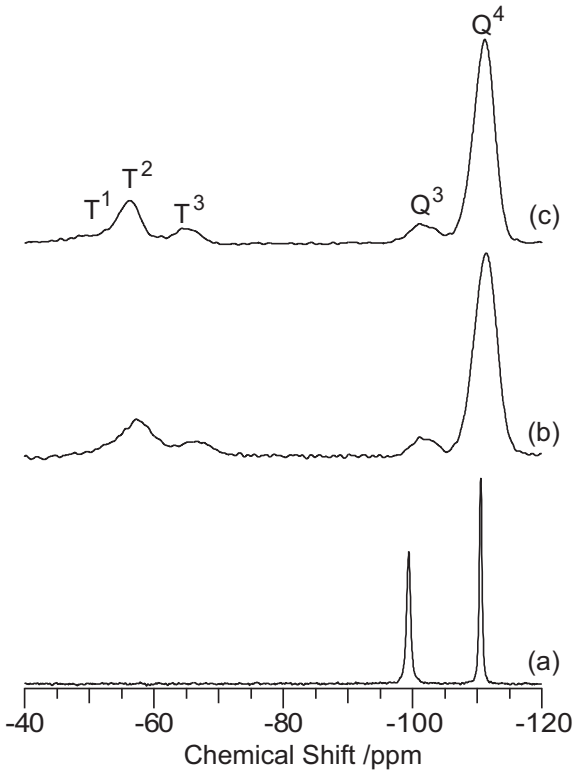

Figure 4. ^{29}Si MAS NMR spectra of (a) C_{16}TMA-Oct, (b) Bim-Oct, and (c) Oim-Oct.

the SiOH/SiO$^-$ groups are highly silylated, the imidazolium groups are probably located on the silicate layers in an ordered arrangement reflecting the confronting SiOH/SiO$^-$ groups arranged along one axis. The ^{29}Si MAS NMR spectrum of Oim-Oct (Figure 4c) shows similar signals (T^1:T^2:T^3:Q^3:Q^4 = 9:36:21:17:183). It should be noted that the presence of T^3 units in Bim-Oct and Oim-Oct indicates the condensation that occurs between the ethoxy groups of the coupling agents. This condensation may be the cause of contamination by water because of the hygroscopic property of BimSi(OEt)$_3$Cl and OimSi(OEt)$_3$Cl, as described in the experimental section.

For comparison, C$_{16}$TMA-Oct was allowed to react with a nonionic ImSi (3-(2-imidazolin-1-yl)propyltriethoxysilane, before quaternization). The ^{29}Si MAS NMR spectrum of the product (imidazol-Oct) showed the integral ratio of Q^3:Q^4 = 86:114 (Figure 5), indicating the low reactivity of the nonionic reagent. The electrostatic interaction between the SiO$^-$ and cationic imidazolium groups probably enhances the intercalation of BimSi(OEt)$_3$Cl and OimSi(OEt)$_3$Cl into the anionic interlayer space of the

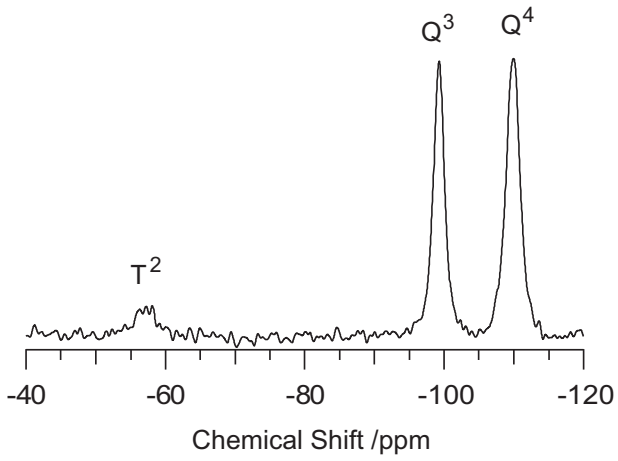

Figure 5. ^{29}Si MAS NMR spectrum of imidazol-Oct prepared by silylation of C$_{16}$TMA-Oct with 3-(2-imidazolin-1-yl)propyltriethoxy silane.

silicate hosts. Actually, it was found that the C_{16}TMA cations remained in imidazol-Oct after the reaction, which was confirmed by the ^{13}C CP/MAS NMR spectrum (Figure 6).

In addition, I investigated the hydrolysis behavior of the triethoxy groups of $BimSi(OEt)_3Cl$ and $OimSi(OEt)_3Cl$ without the addition of any acid.[65] The ethoxy groups were partially (about 10% and 30%, respectively) hydrolyzed after stirring for 1 day at room temperature, whereas $MeSi(OEt)_3$ was not hydrolyzed under the same condition. It is highly possible for $BimSi(OEt)_3Cl$ and $OimSi(OEt)_3Cl$, which are hygroscopic (see experiment 2), to adsorb water, and the adsorbed water (weak acid) may hydrolyze the ethoxy groups. Thus, imidazolium chloride groups are effective not only for the creation of anion exchangeable sites, but also for hydrolysis of the ethoxy groups and the following siloxane bond formation leading to the immobilization of imidazolium groups.

I investigated the effect of the density and ordering of silanol groups on the surface of the silicate layer by using another layered silicate of kanemite. Kanemite consists of only SiO_4 tetrahedra with a Q^3 environment.[51] The density of the $SiOH/SiO^-$

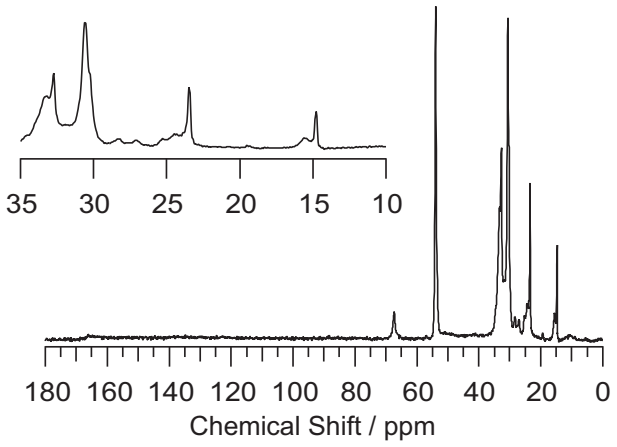

Figure 6. ^{13}C CP/MAS NMR spectrum of imidazol-Oct

groups on the interlayer surface of kanemite (5.6 groups nm^{-2}) is higher than that of octosilicate (3.7 groups nm^{-2}) when they are calculated on the basis of their crystal structures.[50-51] Immobilization of $BimSi(OEt)_3Cl$ onto kanemite was performed in the same manner as that onto octosilicate. The sample is denoted as Bim-kane. The ^{29}Si MAS NMR spectrum of Bim-kane (Figure 7) shows the signals assignable to the T^1, T^2, T^3, Q^3, and Q^4 environments with the integral ratio of 8:18:9:37:63 (This ratio is normalized as $Q^3 + Q^4 = 100$). The spectrum of C_{16}TMA-kanemite before silylation shows the Q^3 and Q^4 signals with the integral ratio of 92:8.[66] Therefore, ca. 55% (63 – 8 = 55) of the $SiOH/SiO^-$ groups were silylated. The amount of imidazolium groups immobilized onto Bim-kane is 1.4 groups nm^{-2} and the data are calculated from the CHN and TG data (Table 1). In spite of the higher density of the $SiOH/SiO^-$ groups of kanemite than octosilicate, the

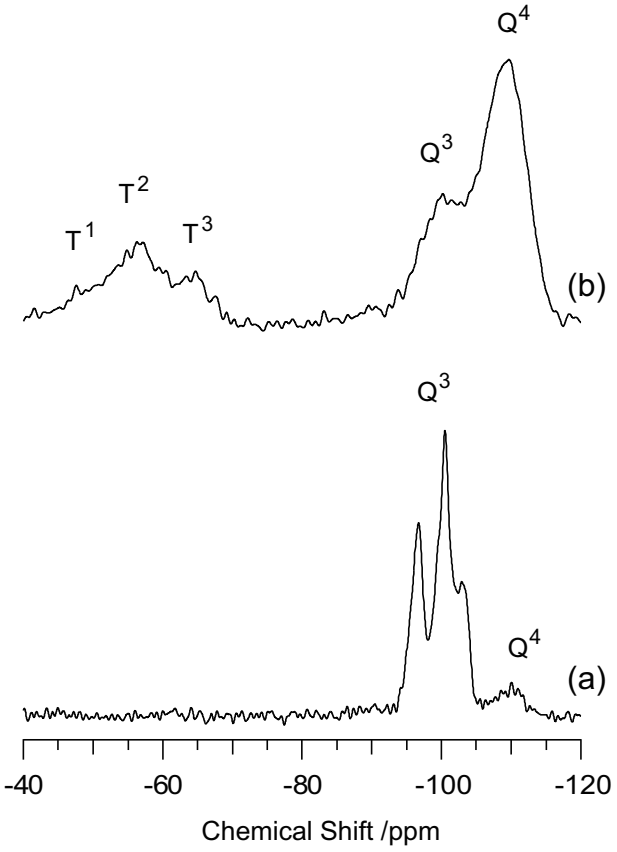

Figure 7. ^{29}Si MAS NMR spectra of (a) C_{16}TMA-kane and (b) Bim-kane.

Table 1. Composition of Bim-kane

Sample	C/mass%	N/mass%	SiO_2/mass%*	C/N	Imidazolium/Silanol group**
Bim-kane	22.2	5.0	54	5.2	0.25

*Residual amount after heating of the sample at 900 °C by TG.
**The ratio of imidazolium group per one SiOH(or SiO^-) group.

silylation ratio (55%) as well as the density of immobilized imidazolium groups (1.4 groups nm^{-2}) of Bim-kane were lower than those of Bim-Oct (83%, 1.8 groups nm^{-2}). Similar phenomena were previously reported for silylation with trichlorosilane groups.[42] In the case of the immobilization of octoxytrichlorosilanes onto octosilicate, more than 90% of the SiOH/SiO^- groups were silylated.[30a] On the other hand, in the case of the immobilization of octyltrichlorosilanes onto kanemite, the ratio of silylated SiOH/SiO^- groups was 65%.[42] The lower degree of silylation of kanemite should come from the excessive number of SiOH/SiO^- groups and their closeness: the full silylation reaction is very difficult because of both the steric hindrance of the silylation reagents and their condensation. Because the confronting SiOH/SiO^- groups on octosilicate are effective for bidentate immobilization, the use of octosilicate is very advantageous for the ordered arrangement of ionic liquids with high density on the crystalline interlayer surfaces.

The C/N molar ratios of Bim-Oct and Oim-Oct (5.3 and 7.3, respectively, Table 2) are less than the calculated ratios (5.8 and 7.8) based on the amount of residual ethoxy groups evaluated from the integral ratio of the peaks of T^1, T^2, and T^3 in the ^{29}Si MAS NMR spectra (see ref [67] for the details of the calculation.). This difference indicates partial hydrolysis of the ethoxy groups. The ratios of imidazolium groups per silylated SiOH/SiO^- groups in Bim-Oct and Oim-Oct were 0.49 and 0.52, respectively, which was calculated from the C/N/Si ratio. Therefore, one silylating reagent reacted with about two

Table 2. Composition of the silylated samples.

Sample	C/mass%	N/mass%	Cl/mass%	SiO_2/mass%*	C/N	Cl/N	Imidazolium/Silanol group**
Bim-Oct	23.8	5.3	6.2	57	5.3	0.46	0.49
Oim-Oct	30.4	4.9	5.8	51	7.3	0.47	0.52

*Residual amount after heating of the sample at 900 °C by TG.
**The ratio of imidazolium group per one SiOH(or SiO^-) group.

SiOH/SiO^- groups. From the elemental analysis and crystal structure of the octosilicate layer, the densities of the immobilized imidazolium groups are 1.8 and 1.9 groups nm^{-2} for Bim-Oct and Oim-Oct, respectively. The Cl/N ratios of Bim-Oct and Oim-Oct were 0.46 and 0.47, respectively (Table 2). This is because one imidazolium salt originally contains two nitrogens (Figure 2), such that the Cl^- anions and imidazolium cations are present with almost a 1:1 ratio in the interlayer region. In addition, on the basis of the results of ^{13}C CP/MAS NMR, the C_{16}TMA cations were completely removed. Taking the charge balance in the interlayer region into account, it is obvious that the unsilylated SiO^- sites are not paired with imidazolium cations, and that probably these are present as not SiO^- anions, but SiOH.

The powder XRD peaks at 2.4, 1.2, and 0.73 nm, assignable to (001), (002), and (003) diffraction peaks, were observed for Bim-Oct (Figure 8b). The basal spacing of 2.4 nm is lower than that of C_{16}TMA-Oct (2.8 nm, Figure 8a). The thickness of the silicate layer of octosilicate is 0.74 nm as estimated from the *d*-spacing of the protonated octosilicate.[46] On the basis of molecular modeling,[68] the full length of the immobilized butylimidazolium group from the alkyl chain terminal group to the silicon is ca. 1.4 nm if the alkyl chain takes an all-trans conformation. The sum of the thickness of the silicate layer and the estimated length of the butylimidazolium group (0.7 nm + 1.4 nm = 2.1 nm) is less than the *d*-value of 2.4 nm. Therefore, the arrangement of the immobilized organic

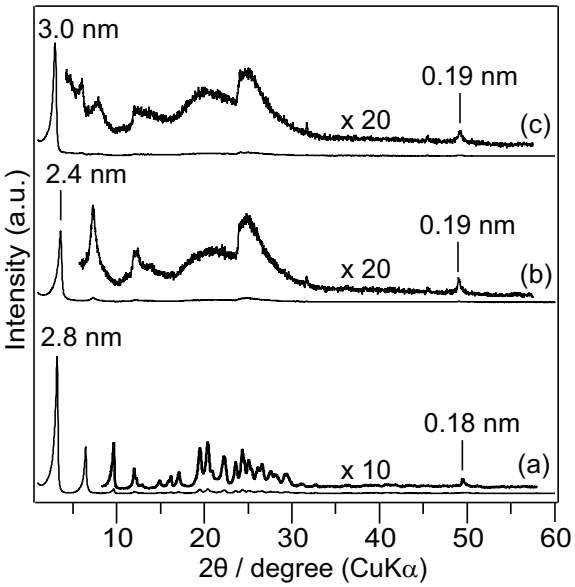

Figure 8. XRD patterns of (a) C_{16}TMA-Oct, (b) Bim-Oct, and (c) Oim-Oct.

groups in the interlayer is estimated to be a bilayer rather than a monolayer. In the case of a monolayer on a Si/SiO_2 substrate, the thickness of the immobilized $BimSi(OEt)_3Cl$ is estimated to be 0.8 nm by ellipsometry.[69] The *d*-spacing of 2.4 nm agrees well with the sum of the thicknesses of the silicate layer and two monolayers of the $BimSi(OEt)_{3-x}$ group (0.7 nm + 0.8 nm × 2 = 2.3 nm). The XRD pattern of Oim-Oct also exhibits similar peaks with *d*-spacings of 3.0, 1.5, and 1.1 nm (Figure 8c), where the larger spacings can be attributed to the longer alkyl chain length compared with the Bim-Oct case.

In the XRD patterns of Bim-Oct and Oim-Oct, the peaks observed at ca. 49°are attributed to the (400) lattice plane of Na-Octosilicate[44-46] as in C_{16}TMA-Oct (Figure 8a). The (400) lattice plane of Na-Octosilicate is perpendicular to the silicate layer. Therefore, the structural regularity of the crystalline silicate layers is retained after silylation. On the other hand, the *d*-values (0.19 nm) of these peaks in Bim-Oct and Oim-Oct are slightly larger than that of C_{16}TMA-Oct (0.18 nm). This difference may be ascribable to the

distortion in the silicate framework by forming new siloxane networks. The same distortion was previously reported for the cases of the silylated samples of C_{16}TMA-Oct with dialkoxydichlorosilanes[44] or alkoxytrichlorosilanes.[45]

SEM images of Na-Octosilicate and C_{16}TMA-Oct showed square, plate-like morphologies of 2−5 μm in lateral size (Figure 9a, b). These square morphologies reflect the crystal structure of Na-Octosilicate ($I4_1/amd$).[50] The morphology of Bim-Oct was a square plate having bending, distortion, and wrinkles on the surface (Figure 9c). In the SEM image of Oim-Oct (Figure 9d), the wrinkles become more apparent compared with that of Bim-Oct. This suggests the progress of a stacking disordering of silicate layers of Oim-Oct during the silylation reaction. These morphological changes have not been observed for the cases of silylated octosilicate with other reagents.[44-47] C_{16}TMA-Oct (Figure 8a) and samples silylated with alkoxytrichlorosilanes[45] or dialkoxydichlorosilanes[44] showed many sharp peaks at the higher 2θ region of the XRD patterns. However, Bim-Oct and Oim-Oct showed only broadened peaks at 25° and a small

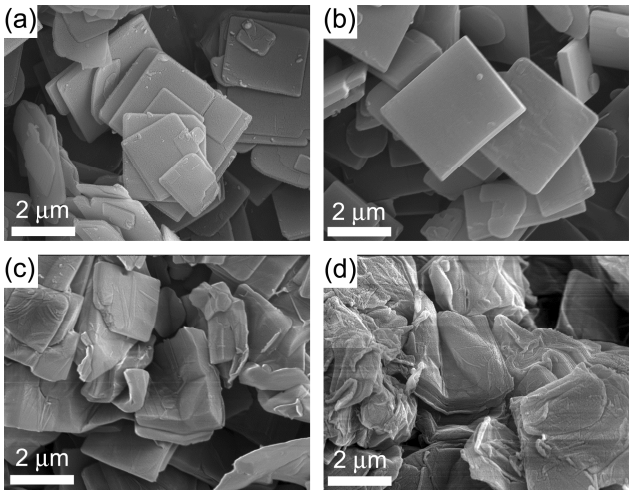

Figure 9. SEM images of (a) Na-Octosilicate, (b) C_{16}TMA-Oct, (c) Bim-Oct, and (d) Oim-Oct.

peak at 49°. The disappearance of the sharp peaks can be attributed to the disordering in the layer structure.

Bim-Oct was analyzed by Raman spectroscopy for the investigation of the state of the immobilized organic groups in the interlayer. The Raman spectrum of Bim-Oct (Figure 10) revealed bands due to the $CH_3CH_2\underline{\boldsymbol{C}}H_2-\underline{\boldsymbol{C}}H_2N$ bond at 692, 597, 487 cm^{-1},[70] which are assignable to a gauche−trans (GT) form. The bands due to this *GT* form are predominantly observed in the spectrum of 1-butyl-3-methyl-imidazolium chloride in the liquid state.[70] Thus I infer that the butyl imidazolium groups in the interlayer are liquid-like. In general, ionic liquids are known as attractive lubricant additives because of the reduction in the friction between the self-assembled monolayers.[71] The bending and distortion of the Bim-Oct and Oim-Oct layers (see Figures 5c and d) can be explained by assuming the liquidlike state of imidazolium groups.

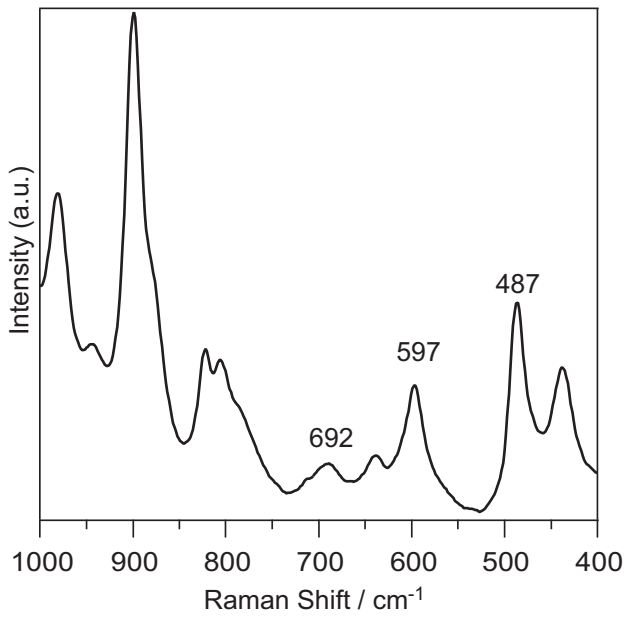

Figure 10. Raman spectrum of Bim-Oct.

3.2. Anion exchange

Because imidazolium cations are successfully immobilized onto the interlayer surface with non-immobilized Cl^- in the ratio of 1 : 1, these imidazolium chloride groups are expected to act as anion exchangeable sites. Anion exchange reactions of Bim-Oct and Oim-Oct with anionic dye of Orange II and inorganic anions (Cl^-, Br^-, I^-, and NO_3^-) were investigated.

After stirring in an aqueous solution of Orange II, the color of the Bim-Oct and Oim-Oct changed from white to red. The XRD patterns of the samples after sorption of Orange II showed peaks with *d*-spacings at 3.5 nm for the samples from Bim-Oct, and 4.1 nm from Oim-Oct (Figure 11), suggesting the successful intercalation of Orange II

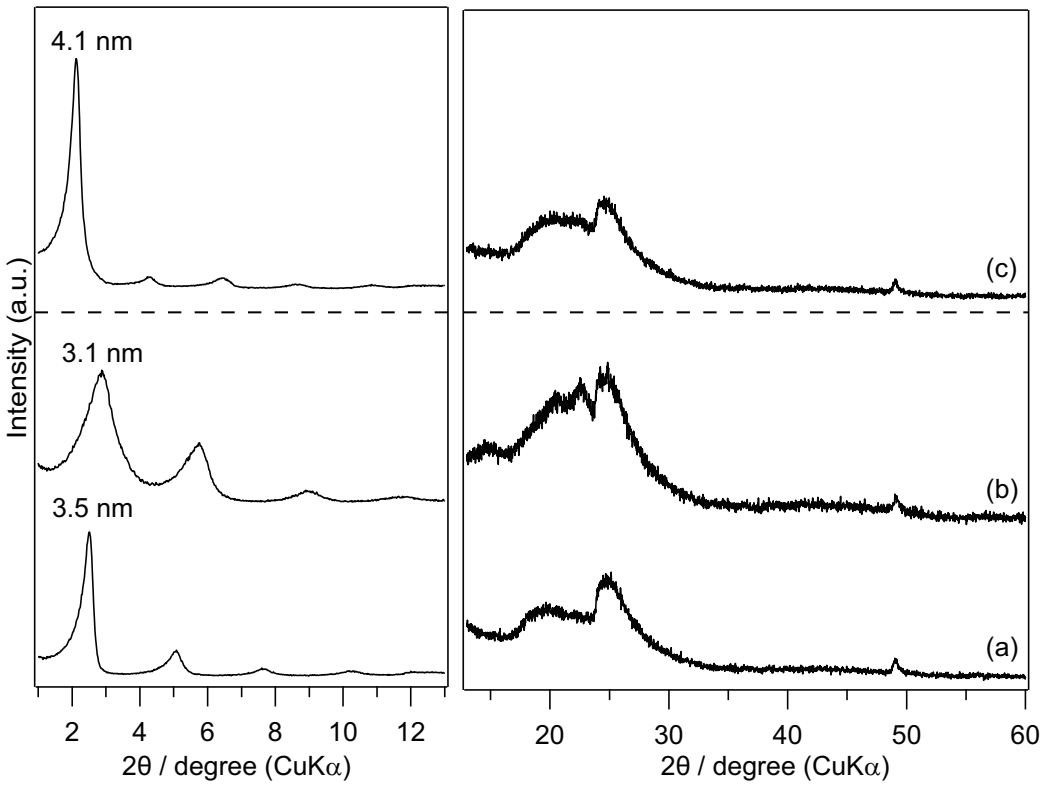

Figure 11. (a) and **(b)**; XRD patterns of Orange II sorbed Bim-Oct. The amounts of accommodated Orange II were (a) 2 mmol/g (equivalent to AEC of Bim-Oct) and (b) 1 mmol/g. Because the XRD pattern of (b) shows only a single phase of lamellar structure, Orange II anions are thought to be intercalated into Bim-Oct homogeneously. **(c)** XRD pattern of Orange II sorbed Oim-Oct

molecules. The amounts of Cl^- in the products were zero for both Bim-Oct and Oim-Oct after the sorption.

The sorption isotherm of Orange II into Bim-Oct (Figure 12) indicates a significant increase at low concentration of up to ca. 1 mM and a plateau at ca. 2 mM. The sorption isotherm of Oim-Oct also indicates a similar curve with a significant increase untill ca. 1 mM, and the following plateau above ca. 2 mM. In the Giles classification of solution sorption isotherms,[72-73] this type of sorption isotherm is classified as an H curve, which is a special case of the L curve (Langmuir type). The origin of the H curve comes from the high affinity between solutes and adsorbents. Therefore, the shape of the isotherm supports the idea that the driving force for the sorption of Orange II into Bim-Oct or

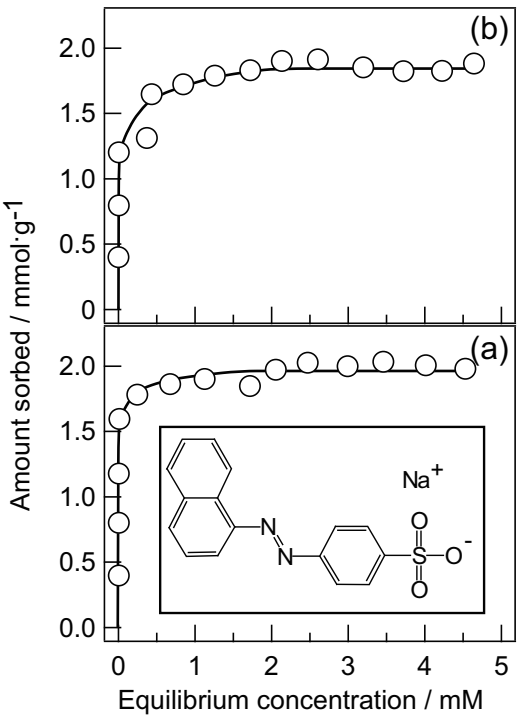

Figure 12. Sorption isotherms of Orange II into (a) Bim-Oct and (b) Oim-Oct. Inset: structural formula of Orange II.

Oim-Oct is an electrostatic one between the cationic imidazolium groups and anionic Orange II. The saturated amounts of sorbed Orange II were 2.0 mmol g^{-1} for Bim-Oct and 1.8 mmol g^{-1} for Oim-Oct, respectively. These values are in good agreement with the amounts of imidazolium groups in Bim-Oct and Oim-Oct (1.9 and 1.7 mmol g^{-1}; CHN analysis and TG data, Table 2). Therefore, almost all of the imidazolium groups can act as anion exchange sites in the interlayer.

In general, pristine octosilicate possesses $SiOH/SiO^-$ groups on the interlayer surface with an ordered arrangement which act as cation exchangeable sites. The maximum cation exchange capacity of octosilicate is equal to the amount of $SiOH/SiO^-$ groups. As described above, two confronting $SiOH/SiO^-$ groups are capped with about one silylating reagent with a bidentate immobilization capability. The silylating reagent is composed of one set of imidazolium cations and Cl^- anions. All Cl^- anions can be exchanged with the anionic dye. As a result, two cation exchangeable sites of the $SiOH/SiO^-$ groups were converted to one anion exchangeable site. The confronting arrangement of $SiOH/SiO^-$ groups must be necessary for this stoichiometric conversion of the exchangeable sites because the bidentate immobilization of silylation reagents is specific for octosilicate. In fact, the $SiOH/SiO^-$ groups of kanemite are not fully silylated, as described above.

The AEC values of Bim-Oct and Oim-Oct were compared with those of other layered inorganic anion exchangeable materials. A hybrid of chitosan intercalated montmorillonite possesses an anion exchange property because of the presence of the excess NH_3^+ sites of chitosan.[12] The maximum AEC is 0.57 meqiv g^{-1} (gram in this case is based on the weight of not the hybrid but the starting clay). Fluoromica accommodating polyelectrolytes in the interlayer by overcompensation also shows anion exchange

reactions. The sorbed amount of anionic dyes into the hybrids is 0.2 meqiv g^{-1} clay at the maximum.[8a] Because these values of AEC are based on the weight of the pristine clays, their AEC values based on the total amount of hybrids are lower than these values. Despite the fact that Bim-Oct and Oim-Oct comprise not only an inorganic framework but also organic species; the exchange capacities of Bim-Oct and Oim-Oct (2.0 mmol g^{-1} and 1.8 mmol g^{-1}) are higher than those of conventional hybrids, and close to those of LDHs (2–4.5 meqiv g^{-1}).[6] Thus, both Bim-Oct and Oim-Oct possess relatively high AEC values, which is attributed to the high density of $SiOH/SiO^-$ groups on the silicate layer of octosilicate.

I also investigated the time course of the sorption of Orange II into Bim-Oct and Oim-Oct in 2.75 mM solutions (Figure 13). The amounts sorbed by Bim-Oct and Oim-Oct reached an equilibrium at 30 and 180 min, respectively. This difference in the sorption

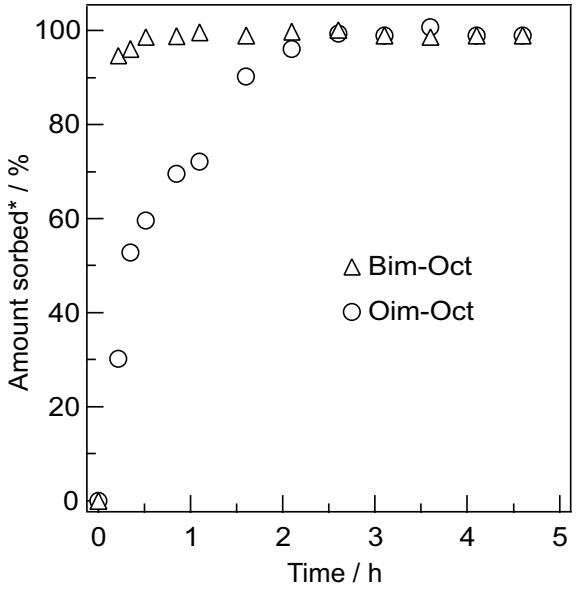

Figure 13. Sorption behavior of Orange II into Bim-Oct and Oim-Oct.

*The amounts sorbed are normalized to 100% at the equilibrium values at 8 h.

behavior may be explained by the low accessibility of Orange II ions into the interlayer of Oim-Oct because of the more hydrophobic longer alkyl chain. Therefore, this result suggests that the sorption of anionic guests into these anion exchangers can be controlled by adjusting the alkyl chain length of the anchored imidazolium cations. In fact, Bim-Oct was dispersed rapidly into water, unlike Oim-Oct, which required stirring to achieve dispersion.

Next, I investigated the sorption behavior of various inorganic anions (Cl^-, Br^-, I^-, and NO_3^-) into Bim-Oct and Oim-Oct. Table 3 shows the molar ratios of each anion sorbed to the imidazolium cations. In the case of Bim-Oct, the order of the amounts of sorbed anions was: $NO_3^- > I^- > Br^- \approx Cl^-$. When Oim-Oct was used as the sorbent, the order was: $I^- > NO_3^- > Br^- \approx Cl^-$. The orders of Bim-Oct and Oim-Oct were quite different from those of LDHs ($Br^- > Cl^- > NO_3^- > I^-$) in the case of sorption of mixed anions.[74] It was reported that the amount of anions sorbed onto imidazolium groups immobilized on silica gel depends on the Hofmeister anion series which is related to the size and degree of hydration: $NO_3^- > I^- > Br^- > Cl^-$.[22] The order of the affinity of Bim-Oct for anions has a good agreement with this order. This trend can be explained by considering that the cationic sites of alkyl imidazolium groups are more hydrophobic and less acceptable for hydrated anions than cationic sites on LDHs. Oim-Oct showed a similar order to that of Bim-Oct. I think that the difference in the order for iodide and nitrate ($I^- > NO_3^-$) may be caused by a lower accessibility for the slightly bulky NO_3^- into the interlayer space with the longer octyl chain.

Table 3. Molar ratios of various sorbed anions to imidazolium cations.

sample	Cl^-/Im	Br^-/Im	I^-/Im	NO_3^-/Im*
Bim-Oct_A	0.05	0.06	0.27	0.51
Oim-Oct_A	0.04	0.08	0.53	0.33

Im: Imidazolium cation immobilized in Bim-Oct or Oim-Oct.
*The ratio of NO_3^-/Im was calculated from the nitrogen contents excluding the contents of imidazolium groups.

3.3. Sorption and controlled release of prodrug depending on pH

Sulfasalazine is metabolized through splitting into mesalamine and sulfapyridine by azo-reduction bacteria in the colon.[59] Therefore, a delivery support for sulfasalazine needs durability in gastric acid. LDH is not usable for this kind of prodrug release because LDH is soluble in acid solution. To prove the usability of Bim-Oct in low-pH solutions, the durability of Bim-Oct in hydrochloric acid at pH 1.0 was investigated. After stirring for 50 h, only 2.9% of silicon was dissolved into the solution, as confirmed by ICP. The XRD pattern of the precipitate showed a peak at 0.19 nm ((400) lattice plane) which is similar to that before the acid treatment (Figure 14), indicating the retention of the structural regularity of the crystalline silicate layers. This durability can be explained by the stability of the silicate frameworks of layered octosilicate.

To investigate the potential of Bim-Oct for application as an intelligent drug carrier, the sorption and release behavior of sulfasalazine into/from the layered solids was studied. After the sorption, the *d*-value of the sample became 2.9 nm (Figure 15) which is larger than that of Bim-Oct (2.4 nm, Figure 8b). It is suggested that the sulfasalazine

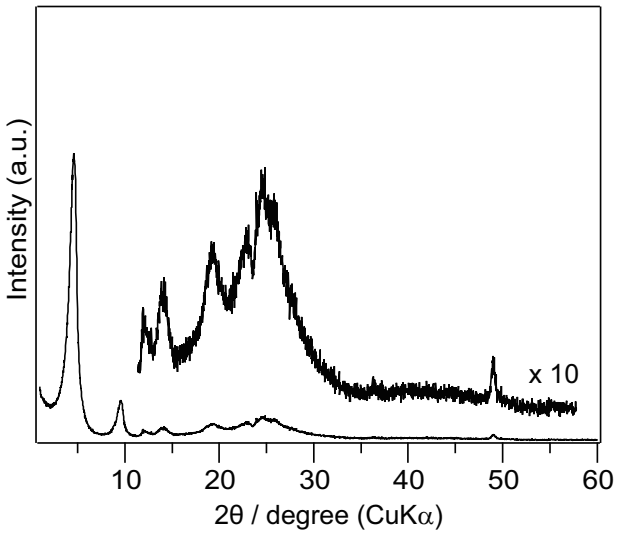

Figure 14. XRD pattern of the precipitate after the acid treatment of Bim-Oct.

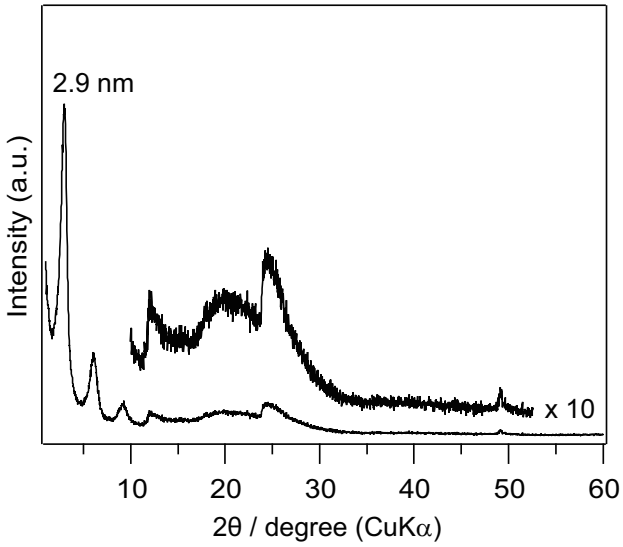

Figure 15. XRD pattern of Bim-Oct containing sulfasalazine

molecules were successfully intercalated into the interlayer of Bim-Oct. No peaks assignable to crystalline sulfasalazine were observed in the pattern of Bim-Oct after the sorption, suggesting that the sulfasalazine molecules are not in a crystal state but well-dispersed in the interlayer.

Typically, a dose of drugs for oral administration needs a high amount. For example, a daily dose of sulfasalazine is usually 2−4 g for adults.[75] Therefore, supports for oral-administration drugs demand high efficiency of sorption.[76] The amount of sulfasalazine sorbed into Bim-Oct was 0.75 mmol g^{-1} (30 wt%) determined by the concentration of residual solution of sulfasalazine. This amount is comparable to the case of certain polymeric supports such as calcium-alginate-chitosan gel (45 wt% at maximum)[77] and polymer microcapsules (72 wt% at maximum) including sulfasalazine crystals on the surface.[76] Lee et al. reported that mesoporous silica nanoparticles functionalized with trimethylammonium groups (MSN-TA) can accommodate sulfasalazine.[64] The amount loaded was 0.0428 mmol g^{-1} at maximum from an aqueous solution in spite of the high surface area of mesoporous silica (ca. 1000 m^2 g^{-1}). It is

remarkable that Bim-Oct can intercalate more than a ten times larger amount of sulfasalazine than MSN-TA. This difference can be explained by the amount of anion exchangeable sites. AEC, determined by sorption of Orange II, of MSN-TA (about 0.17 mmol g^{-1}) is much lower than that of Bim-Oct (2.0 mmol g^{-1}). In addition, bulky guest molecules tend to be stuck around the mesopore entrance.[78] In contrast, all surfaces of the layered structure can be used for the sorption of guest molecules. The interlayer space is flexible for a wide variety of guest molecules with different sizes because of the expansion of the interlayer.

The release of the prodrug was conducted in two simulated fluids of gastric acid at pH 1.2 and intestinal fluid at pH 7.4 (Figure 16). At the strong acidic condition (pH 1.2), only 9% of the sorbed sulfasalazine was released from the Bim-Oct after 50 h. In contrast, at pH 7.4, the rate of released sulfasalazine was increased by up to 83% after stirring for 4 h, 90% after 24 h; and finally, almost all the sulfasalazine (up to 96%) was released from

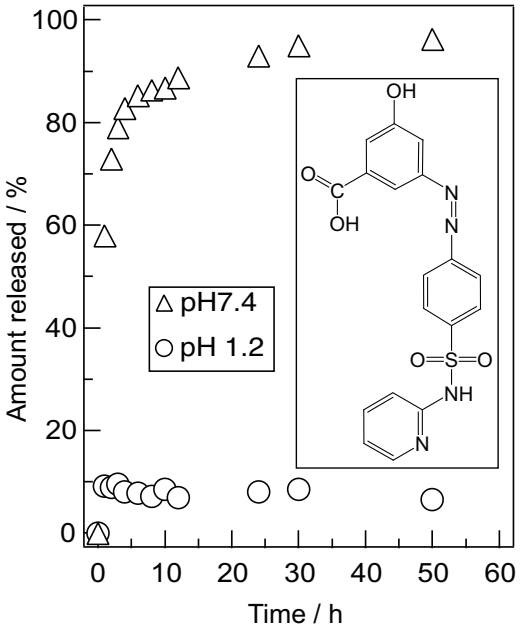

Figure 16. Release behavior of sulfasalazine sorbed on Bim-Oct at pH 7.4 and 1.2. Inset: structural formula of sulfasalazine.

the interlayer after 50 h. This contrast with the pH can be explained by the solubility of sulfasalazine which is almost insoluble into water at low pH and soluble at neutral solution.[77] In the case of MSN-TA,[64] a released amount of sulfasalazine was only ca. 60% at pH 7.4 after 20 h by using the sample with the higher loading of sulfasalazine (0.0428 mmol g^{-1}). In the exceptional case, the released amount reached 90% by using a sample with very low loading (0.0005 mmol g^{-1}). In addition, the amount released was decreased with higher loadings of sulfasalazine in polymer microcapsules.[76] In contrast, Bim-Oct indicated a higher released amount (ca. 90%) at pH 7.4 after 20 h in spite of the very high loading of sulfasalazine. In general, both the size and connectivity of mesopores affect the drug-release rate.[79-80] Larger pores and 3D connected pores are advantageous for high rates of release because of the high accessibility.[79] It is easily inferred that layered structures have high accessibility because guest molecules can be released from all end-facets. Therefore, the larger released amount is probably caused by the higher accessibility of the layered structure. Thus, Bim-Oct shows high durability in acid solutions, high capacity for sulfasalazine, and high accessibility. These properties should be very valuable for their application in drug-delivery systems (DDSs) for prodrugs in oral administration.

4. Conclusion

The functions of layered octosilicate are significantly changed and designed by the creation of two-dimensionally arranged anion exchangeable sites in the interlayer surface. Cation exchangeable sites of the $SiOH/SiO^-$ groups on octosilicate are

stoichiometrically converted to anion exchangeable sites. Octosilicate is very suitable for the creation of highly and closely ordered imidazolium groups because of the presence of ordered SiOH/SiO^- groups on the crystalline silicate layers. The properties of these layered materials can be summarized as follows. (i) The AECs are higher than those of conventional clay-polymer hybrids. In addition, the sorption rate of anionic dye was controllable by changing the alkyl chain length. (ii) The affinity for guest species is completely different from LDH, and it is remarkable that the affinity for inorganic anions was varied by changing the length of the alkyl chain. This controllability may be advantageous for the use as ion-sensing devices with selectivity. (iii) The application of the derivatized silicates in DDS for oral administration should also be focused on because of their high accessibility, capacity, and durability.

Ionic liquids immobilized onto solid supports have also been used for single-site heterogeneous catalysts.[33] Utilizing the crystal structure of the host layered silicates, the density and distance of the immobilized functional groups can be deliberately controlled at the angstrom level in two-dimensionally confined spaces, yielding more intelligent catalytic systems. Therefore, the hybridization of layered silicates and a wide variety of designed ionic liquids will create a new pathway for various practical applications, such as catalysts, green solvents, and ionic conductors, thereby contributing to the expansion of the material science field.

5. References and Footnotes

[1] S. M. Auerbach, K. A. Carrado, P. K. Dutta, *Handbook of Layered Materials*, Marcel Dekker, Inc., New York, **2004**.

[2] V. Ambrogi, G. Fardella, G. Grandolini, L. Perioli, *Int. J. Pharm.* **2001**, *220*, 23-32.

[3] J.-H. Choy, S.-Y. Kwak, J.-S. Park, Y.-J. Jeong, J. Portier, *J. Am. Chem. Soc.* **1999**, *121*, 1399-1400.

[4] J.-H. Choy, S.-Y. Kwak, J.-S. Park, Y.-J. Jeong, *J. Mater. Chem.* **2001**, *11*, 1671-1674.

[5] J. He, M. Wei, B. Li, Y. Kang, D. Evans, X. Duan, in *Layered Double Hydroxides* (Eds.: X. Duan, D. G. Evans), Springer-Verlag, Berlin Heidelberg, **2005**, pp. 89-119.

[6] C. Taviot-Guého, F. Leroux, in *Layered Double Hydroxides* (Eds.: X. Duan, D. G. Evans), Springer-Verlag, Berlin Heidelberg, **2006**, pp. 121-159.

[7] C. Forano, T. Hibino, F. Leroux, C. Taviot-Guého, in *Handbook of Clay Science* (Eds.: F. Bergaya, B. K. G. Theng, G. Lagaly), Elsevier Ltd., Amsterdam, **2006**, pp. 1021-1095.

[8] D. L. Bish, *Bull. Mineral.* **1980**, *103*, 170-175.

[9] S. Miyata, *Clays Clay Miner.* **1983**, *31*, 305-311.

[10] T. Yamaoka, M. Abe, M. Tsuji, *Mater. Res. Bull.* **1989**, *24*, 1183-1199.

[11] T. Kijima, Y. Kato, K. Ohe, M. Machida, Y. Matsushita, T. Matsui, *Bull. Chem. Soc. Jpn.* **1994**, *67*, 2125-2129.

[12] M. Darder, M. Colilla, E. Ruiz-Hitzky, *Chem. Mater.* **2003**, *15*, 3774-3780.

[13] H. Hata, Y. Kobayashi, T. E. Mallouk, *Chem. Mater.* **2007**, *19*, 79-87.

[14] H. Hata, T. E. Mallouk, K. Kuroda, *Chem. Mater.* **2009**, *21*, 985–993.

[15] P. Wasserscheid, T. Welton, *Ionic Liquids in Synthesis*, 2nd ed., WILEY-VCH, Weinheim, **2008**.

[16] H. Ohno, *Bull. Chem. Soc. Jpn.* **2006**, *79*, 1665-1680.

[17] R. A. Sheldon, *Green Chem.* **2005**, *7*, 267-278.

[18] F. Endres, D. MacFarlane, A. Abbott, *Electrodeposition from Ionic Liquids*, WILEY-VCH, Weinheim, **2008**.

[19] M. Yoshio, T. Kagata, K. Hoshino, T. Mukai, H. Ohno, T. Kato, *J. Am. Chem. Soc.* **2006**, *128*, 5570-5577.

[20] T. Welton, *Chem. Rev.* **1999**, *99*, 2071-2084.

[21] C. M. Gordon, *Appl. Catal. A* **2001**, *222*, 101-117.

[22] A. Berthod, M. J. Ruiz-Ángel, S. Carda-Broch, *J. Chromatogr. A* **2008**, *1184*, 6-18.

[23] H. Qiu, Q. Jiang, X. Liu, S. Jiang, *Chromatographia* **2008**, *68*, 167-171.

[24] Y. Wang, M. Tian, W. Bi, K. H. Row, *Int. J. Mol. Sci.* **2009**, *10*, 2591-2610.

[25] M. H. Valkenberg, C. deCastro, W. F. Hölderich, *Top. Catal.* **2001**, *14*, 139-144.

[26] M. H. Valkenberg, C. deCastro, W. F. Hölderich, *Green Chem.* **2002**, *4*, 88-93.

[27] C. P. Mehnert, R. A. Cook, N. C. Dispenziere, M. Afeworki, *J. Am. Chem. Soc.* **2002**, *124*, 12932-12933.

[28] C. P. Mehnert, *Chem. Eur. J.* **2005**, *11*, 50-56.

[29] K. Yamaguchi, C. Yoshida, S. Uchida, N. Mizuno, *J. Am. Chem. Soc.* **2005**, *127*, 530-531.

[30] J. Kasai, Y. Nakagawa, S. Uchida, K. Yamaguchi, N. Mizuno, *Chem. Eur. J.* **2006**, *12*, 4176-4184.

[31] A. Riisager, R. Fehrmann, S. Flicker, R. van Hal, M. Haumann, P. Wasserscheid, *Angew. Chem., Int. Ed.* **2005**, *44*, 815-819.

[32] A. Riisager, R. Fehrmann, M. Haumann, P. Wasserscheid, *Top. Catal.* **2006**, *40*, 91-102.

[33] T. K. Maishal, J. Alauzun, J.-M. Basset, C. Copéret, R. J. P. Corriu, E. Jeanneau, A. Mehdi, C. Reyé, L. Veyre, C. Thieuleux, *Angew. Chem., Int. Ed.* **2008**, *47*, 8654-8656.

[34] D. S. Han, N. Jiang, S. E. Park, in *236th ACS National Meeting, Vol. 53*, Division of Petroleum Chemistry, Inc., Philadelphia, **2008**, pp. 184-186.

[35] A. Berthod, M. J. Ruiz-Angel, S. Huguet, *Anal. Chem.* **2005**, *77*, 4071-4080.

[36] L. Zhu, Y. Liu, J. Chen, *Ind. Eng. Chem. Res.* **2009**, *48*, 3261-3267.

[37] W. Schwieger, G. Lagaly, in *Handbook of Layered Materials* (Eds.: S. M. Auerbach, K. A. Carrado, P. K. Dutta), Marcel Dekker, Inc., New York, **2004**, pp. 541-629.

[38] E. Ruiz-Hitzky, J. M. Rojo, *Nature* **1980**, *287*, 28-30.

[39] E. Ruiz-Hitzky, J. M. Rojo, G. Lagaly, *Colloid Polym. Sci.* **1985**, *263*, 1025-1030.

[40] T. Yanagisawa, K. Kuroda, C. Kato, *React. Solids* **1988**, *5*, 167-175.

[41] M. Ogawa, S. Okutomo, K. Kuroda, *J. Am. Chem. Soc.* **1998**, *120*, 7361-7362.

[42] A. Shimojima, D. Mochizuki, K. Kuroda, *Chem. Mater.* **2001**, *13*, 3603-3609.

[43] D. Mochizuki, K. Kuroda, *New. J. Chem* **2006**, *30*, 277-284.

[44] D. Mochizuki, A. Shimojima, K. Kuroda, *J. Am. Chem. Soc.* **2002**, *124*, 12082-12083.

[45] D. Mochizuki, A. Shimojima, T. Imagawa, K. Kuroda, *J. Am. Chem. Soc.* **2005**, *127*, 7183-7191.

[46] D. Mochizuki, S. Kowata, K. Kuroda, *Chem. Mater.* **2006**, *18*, 5223-5229.

[47] R. Ishii, Y. Shinohara, *J. Mater. Chem.* **2005**, *15*, 551-553.

[48] Y. Ide, G. Ozaki, M. Ogawa, *Langmuir* **2009**, *25*, 5276-5281.

[49] R. K. Iler, *J. Colloid Sci.* **1964**, *19*, 648-657.

[50] S. Vortmann, J. Rius, S. Siegmann, H. Gies, *J. Phys. Chem. B* **1997**, *101*, 1292-1297.

[51] S. Vortmann, J. Rius, B. Marler, H. Gies, *Eur. J. Mineral.* **1999**, *11*, 125-134.

[52] J. W. Gilman, W. H. Awad, R. D. Davis, J. Shields, R. H. Harris, C. Davis, A. B. Morgan, T. E. Sutto, J. Callahan, P. C. Trulove, H. C. DeLong, *Chem. Mater.* **2002**, *14*, 3776-3785.

[53] N. H. Kim, S. V. Malhotra, M. Xanthos, *Microporous Mesoporous Mater.* **2006**, *96*, 29-35.

[54] S. Letaief, C. Detellier, *J. Mater. Chem.* **2007**, *17*, 1476-1484.

[55] S. Letaief, T. Diaco, W. Pell, S. I. Gorelsky, C. Detellier, *Chem. Mater.* **2008**, *20*, 7136-7142.

[56] E. Ruiz-Hitzky, S. Letaïef, V. Prévot, *Adv. Mater.* **2002**, *14*, 439-443.

[57] A. B. Bourlinos, T. Karakostas, D. Petridis, *J. Phys. Chem. B* **2003**, *107*, 920-925.

[58] V. Polshettiwar, P. Hesemann, J. J. E. Moreau, *Tetrahedron Lett.* **2007**, *48*, 5363.

[59] A. I. Qureshi, R. D. Cohen, *Adv. Drug Deliv. Rev.* **2005**, *57*, 281-302.

[60] T. Kimura, D. Itoh, N. Okazaki, M. Kaneda, Y. Sakamoto, O. Terasaki, Y. Sugahara, K. Kuroda, *Langmuir* **2000**, *16*, 7624-7628.

[61] It was confirmed that the sorption and desorption of Orange II reached to equilibrium at 6 h and 2 day, respectively.

[62] M. Ogawa, K. Kuroda, *Bull. Chem. Soc. Jpn.* **1997**, *70*, 2593-2618.

[63] I. Fujita, K. Kuroda, M. Ogawa, *Chem. Mater.* **2003**, *15*, 3134-3141.

[64] C.-H. Lee, L.-W. Lo, C.-Y. Mou, C.-S. Yang, *Adv. Funct. Mater.* **2008**, *18*, 3283-3292.

[65] M. Fang, C. H. Kim, T. E. Mallouk, *Chem. Mater.* **1999**, *11*, 1519-1525.

[66] N. Takahashi, H. Tamura, D. Mochizuki, T. Kimura, K. Kuroda, *Langmuir* **2007**, *23*, 10765-10771.

[67] The immobilized silylating reagents with T^1, T^2 and T^3 have residual two, one, and zero OEt (or OH) group(s), respectively. The T^1 : T^2 : T^3 ratios were 7 : 44 : 20 and 9 : 36 : 21 for Bim-Oct and Oim-Oct, respectively. On the basis of these ratios, the amouts of residual OEt (or OH) groups of Bim-Oct and Oim-Oct are 0.82 and 0.83 per one silylating reagent, respectively. If all the ethoxy groups remained without hydrolysis, one immobilized group has carbon numbers of 11.6 (= 0.82 × 2 + 10) and 15.7 (= 0.83 × 2 + 14) for Bim-Oct and Oim-Oct, and the C/N ratios of 5.8 and 7.8, respectively.

[68] The structurally optimized calculation was performed with Discover Module, MS Modeling Version 4.4; Accelrys Inc.: Sandiego, CA, 2008.

[69] Y. S. Chi, J. K. Lee, S.-g. Lee, I. S. Choi, *Langmuir* **2004**, *20*, 3024-3027.

[70] R. Ozawa, S. Hayashi, S. Saha, A. Kobayashi, H. Hamaguchi, *Chem. Lett.* **2003**, *32*, 948-949.

[71] O. A. Mazyar, G. K. Jennings, C. McCabe, *Langmuir* **2009**, *25*, 5103-5110.

[72] C. H. Giles, D. Smith, A. Huitson, *J. Colloid Interface Sci.* **1974**, *47*, 755-765.

[73] C. H. Giles, A. P. D'Silva, I. A. Easton, *J. Colloid Interface Sci.* **1974**, *47*, 766-778.

[74] R. P. Bontchev, S. Liu, J. L. Krumhansl, J. Voigt, T. M. Nenoff, *Chem. Mater.* **2003**, *15*, 3669-3675.

[75] U.S. Physician Prescribing Information of Azulfidine® from Pharmacia & Upjohn Company.

[76] A. Lamprecht, H. Rodero Torres, U. Schäfer, C.-M. Lehr, *J. Controlled Release* **2000**, *69*, 445-454.

[77] M. Tavakol, E. Vasheghani-Farahani, T. Dolatabadi-Farahani, S. Hashemi-Najafabadi, *Carbohydr. Polym.* **2009**, *77*, 326-330.

[78] H. Hata, S. Saeki, T. Kimura, Y. Sugahara, K. Kuroda, *Chem. Mater.* **1999**, *11*, 1110-1119.

[79] B. G. Trewyn, C. M. Whitman, V. S. Y. Lin, *Nano Lett.* **2004**, *4*, 2139-2143.

[80] M. Vallet-Regí, F. Balas, D. Arcos, *Angew. Chem., Int. Ed.* **2007**, *46*, 7548-7558.

Chapter 6

Exfoliation of Layered Silicates through Immobilization of Imidazolium Groups

1. Introduction

Exfoliation of layered inorganic materials into nanosheets has received considerable attention as a method for significant expansion in applications of layered materials. Crystalline nanosheets are applicable for polymer/nanosheets composites[1-5] and nanobuilding units for various hybrids including modified electrode,[6-9] Langmuir-Blodgett films,[6-7,10-12] layer-by-layer films,[4-5,13-15] hydrogels,[16-17] and self-standing films.[18] Exfoliation of layered inorganic materials into nanosheets has received considerable attention as a method for significant expansion in applications of layered materials[19] such as clay minerals,[20] α-zirconium phosphates and phosphonates,[21-22] layered metal chalcogenides,[23-24] layered metal oxides,[25-27] and layered double hydroxides.[28-29] Exfoliation into nanosheets enhances the pre-existing properties of starting layered materials, such as electrical conductivity,[30] magneto-optical

effect,[31-32] and photocatalystic activity.[33-34] The properties and utilization of nanosheets highly depend on the composition and surface structure of starting layered materials. Thus, the development of exfoliation methods for layered materials, possessing unique properties but not yet exfoliated, is highly demanded for the creation of novel nanosheets and unique nanocomposites.

Layered silicates,[35] whose frameworks are composed of only SiO_4 tetrahedra frameworks, are quite interesting as a host material. The principal feature of layered silicates is the presence of SiOH/SiO^- groups on the interlayer surfaces, unlike layered clay minerals. Various guest species are intercalated by a wide variety of reactions and interactions, such as cation exchange, hydrogen bonding, acid-base reaction, and dipole interaction. In addition, the interlayer surfaces of silicate layers can be designed by the covalent immobilization of various silane coupling reagents.[36-46] Well-ordered SiOH/SiO^- groups should lead the functional groups with two-dimensional well ordering, which is very difficult for other amorphous silica species. Therefore, silicate nanosheets should have high potentials as nanobuilding units with designable surfaces. However, exfoliation of layered silicates into nanosheets has not yet been achieved, although swelling,[47-48] decrease of the stacking number (delamination),[49-50] and dispersion into solvent[51] were reported. The swelling properties of layered clay minerals and layered sodium silicates are very different. At first, layered sodium octosilicate, magadiite, and kanemite do not exhibit any swelling with water. Silanol groups with high density on the interlayer surfaces hinder the swelling because of the hydrogen bond and strong electrostatic interactions between SiO^- and hydrated sodium ions. In addition, organically modified layered silicates are not exfoliated. For example, hexadecyltrimethylammonium-exchanged octosilicate and magadiite do not show swelling and exfoliation in toluene (our unpublished results). The

density of C_{16}TMA cations on the silicate layers of octosilicate is 1.5 C_{16}TMA cations nm^{-2} (calculated from the composition) and is much higher than that of swelling clay minerals, such as saponite[52] (0.8 charge nm^{-2}, cation exchange capacity = 100 mequiv/100 g). It is assumed that interdigitated alkyl chains with all-trans conformation in the interlayer space of octosilicate have high van der Waals interaction and inhibit the intercalation of additional organic molecules. Therefore, both of pristine and organically modified layered silicates are not used for exfoliation in polar and non-polar solvents. Thus, exfoliation of layered silicates is an important challenge for deeper understanding of exfoliation as well as their practical applications. Because the surfaces of layered silicates are designable with silylation reagents, various interlayer surfaces can be used for the investigation of exfoliation. Therefore, layered silicates are the suitable model material for understanding the mechanism of the exfoliation reaction.

One of the methods for decreasing the layer charge is silylation of OH or O^- groups on the interlayer surface of layered materials such as metal oxides and layered silicates. There are a few reports on silylation of niobates and partial exfoliation.[53-54] However, these silylation processes did not focus on the enhancement of exfoliation. In previous study,[46] butyl- or octylimidazolium chloride salts were covalently immobilized onto the interlayer surface of layered octosilicate[55-61] (also known as ilerite or RUB-18) via silylation reaction. The obtained layered composites are anion exchangeable caused by cationic imidazolium groups immobilized covalently. In general, ionic liquids[62] including halide anions, such as dialkylimidazolium halide salts, are hydrophilic and hygroscopic. The layered composite immobilized with butylimidazolium groups was dispersed rapidly into water. Therefore, this layered composite has relatively high hydrophilic surfaces. In this study, butylimidazolium immobilized octosilicate (Bim-Oct) is surprisingly exfoliated

into monolayer nanosheets in water (Figure 1). Using water as a solvent is advantageous from the viewpoint of green chemistry. The obtained nanosheets are cationic because of the imidazolium groups on the surface. Cationic nanosheets are generally obtained from layered double hydroxides (LDHs) by exfoliation in organic solvents.[29,63] To the best of our knowledge, full exfoliation into monolayer sheets of LDH has not been achieved in water, despite a few reports of partial delamination.[64] Regardless of the compositions, this is also the first report of full exfoliation of cationic nanosheets in water. Because of high stability in acid solution (pH 1) of Bim-Oct, the silicate nanosheets are advantageous for hybridization processes and applications in acid solutions. In addition, transparent films were prepared with nanosheets. The transparent films applicable for various optical and photochemical applications[65] which are hardly achieved with powdery samples.

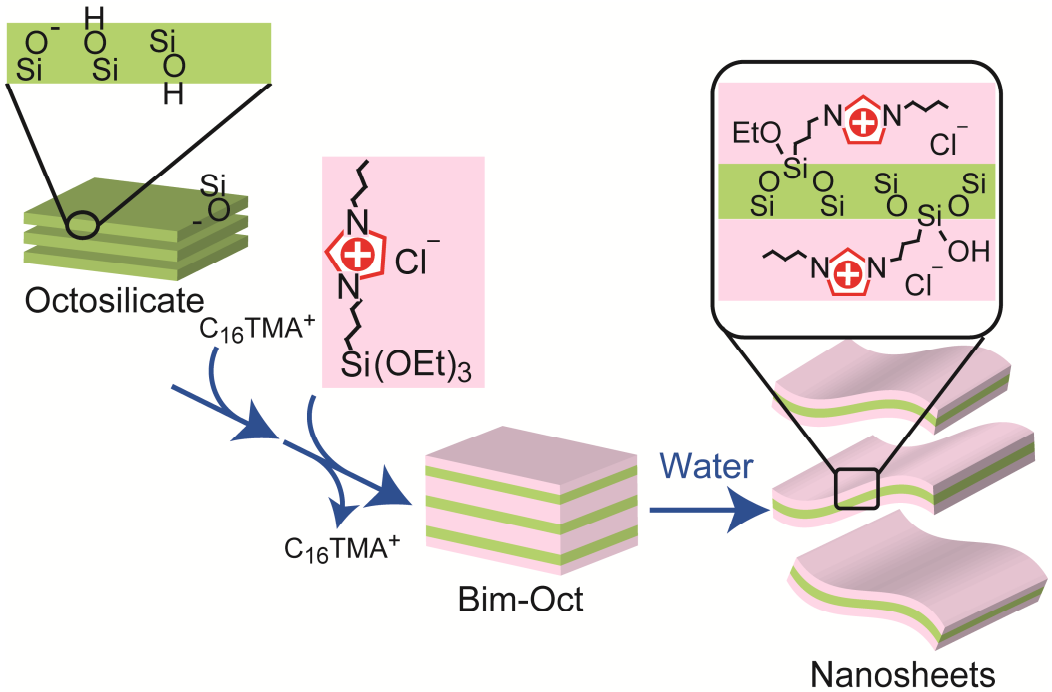

Figure 1. Synthetic pathway of exfoliation of layered octosilicate. The first step is intercalation of hexadecyltrimethylammonium ions for the expansion of the interlayer distance. The second step is immobilization of triethoxysilyl-terminated butylimidazolium salt. The third step is exfoliation of layers in water.

2. Experimental

Materials

Layered Na-octosilicate ($Na_8[Si_{32}O_{64}(OH)_8 \cdot 32H_2O]$, denoted as Na-Oct, theoretical cation exchange capacity is 284 mequiv/100 g calculated from the composition) was synthesized according to previous reports.[42-43] Na-Oct (3.0 g) was reacted with hexadecyltrimethylammonium chloride (C_{16}TMACl, Tokyo Chemical Industry Co.) for cation exchange reaction to form C_{16}TMA-intercalated octosilicate (C_{16}TMA-Oct) as an intermediate for the silylation.[66] The silylation reagent (1-Butyl-3-(3-triethoxysilylpropyl)-4,5-dihydroimidazolium chloride was synthesized according to a procedure reported previously.[46,67-68] Bim-Oct was synthesized by silylation of C_{16}TMA-Oct with the silylating reagent in a similar manner reported previously.[46] No peaks assignable to C_{16}TMA cation were observed in the ^{13}C CP/MAS NMR spectrum of Bim-Oct.[46] The ^{29}Si MAS NMR spectrum shows broad Q^3 (−102 ppm) and Q^4 (−111 ppm) signals with the integral ratio (Q^3 : Q^4) of 18 : 182, suggesting the high degree (82%) of silylation of the SiOH/SiO^- groups in C_{16}TMA-Oct. The square plate morphology of Bim-Oct particles with lateral size of 2−5 μm was observed, as reported previously.[46]

Exfoliation of Bim-Oct

Powdery Bim-Oct (40 mg) was dispersed into de-ionized water (40 mL). After 1 day, the sample was stirred in an ultrasonicator (USS-1, NIHONSEIKI KAISHA LTD., 35W) for 1 h. The obtained transparent solution was denoted as ex-Bim-Oct. The sample for atomic force microscopy (AFM) was prepared by the following method. A silicon

wafer was cleaned beforehand with (i) hydrochloric acid (12 M) + methanol (1:1, volume), (ii) conc. H_2SO_4, and (iii) water, for 20 min, respectively. The ex-Bim-Oct solution was cast out on the silicon wafer and rinsed with ethanol. The samples for X-ray diffraction (XRD) measurements were prepared as follows. The solution of ex-Bim-Oct was ultracentrifuged (45000 × *g*, 20000 rpm) for 20 min. After removing the supernatant, transparent colloidal aggregates were obtained. The colloidal aggregates were put on a sample holder for the XRD measurement. The colloidal aggregates were wet during the measurement (30 min). The sample was dried for 1 day at room temperature in a reduced pressure. The dried sample was peeled off and ground.

Synthesis of various layered silicates composites

All samples were synthesized according to Bim-Oct except some procedures as follows. **(i) Oim-Oct:** The silylation reagent of octyl-3-(3-triethoxysilylpropyl)-4,5-dihydroimidazolium chloride (4.2 g) was used for the silylation reaction. **(ii) d_Bim-Oct**: Added amount of $BimSi(OEt)_3Cl$ was 1.0 equivalents of $SiOH/SiO^-$ groups of C_{16}TMA-Oct. **(iii) TMA-Oct**: An anhydrous acetonitrile (50 mL) was added to a methanol solution of N-trimethoxysilylpropyl-N,N,N-trimethylammonium chloride (50 wt%, 5 mL), and evaporated to remove methanol. This solution and additional anhydrous acetonitrile (50 mL) were added to dried C_{16}TMA-Oct (1.0 g). **(iv) Bim-Mag**: Na-Magadiite was synthesized according to previous reports.[69-70] C_{16}TMA exchanged magadiite (C_{16}TMA-Mag) was used as intermediate for silylation.[38,45] The added amount of $BimSi(OEt)_3Cl$ (1.3 g) was adjusted depends on the $SiOH/SiO^-$ groups of C_{16}TMA-Mag.

Observation of exfoliation

Powdery samples (0.02 g) of Na-Oct, H-Oct, C_{16}TMA-Oct, Bim-Oct, Oim-Oct, TMA-Oct, d_Bim-Oct, and Bim-Mag were dispersed into water, respectively. Ultrasonication was performed with stirring for 1 h. The mixture was separated into the slurry and supernatant by centrifugation at 2200 × *g* (3500 rpm). The supernatant was mixed with ethanol (1:1 volume) and dropped on a grid for observation with HR-SEM (S-5500, HITACHI). The slurry was analyzed with XRD measurement.

Preparation of a spin-coated film and adsorption of an anionic dye

A transparent solution (40 mL) of ex-Bim-Oct was ultracentrifuged at 45000 × *g* (20000 rpm) for 20 min. After removing the supernatant, the colloidal aggregates were obtained. A few drops of de-ionized water were added to the colloidal aggregates and spin-coated (3500 rpm, 15 s) on a glass substrate. After drying under a reduced pressure, a transparent film was obtained. The film was soaked into an aqueous solution (10 mM) of Orange II (4-[(2-hydroxy-1-naphthyl)azo]benzenesulfonic acid, monosodium salt; Tokyo Chemical Industry Co.) for 1 day. The film was rinsed with ethanol. After drying, an orange-colored film was obtained.

Characterization

AFM was performed with a Nanoscope III (Digital Instruments, Inc.) by using a tapping mode. X-ray powder diffraction patterns (XRD) were obtained with a Rigaku Rint-Ultima III powder diffractometer (CuKα, λ = 0.15418 nm) by using a parallel beam geometry equipped with a parabolic multilayer solar slit. Samples were put on a zero-background holder made of silicon single crystal. The amounts of organic constituents

were determined by CHN analysis (Perkin Elmer, 2400 Series II). The halogen contents were measured by ion-chromatography by using an Organic Halogen/Sulfur Analysis System (Yanaco New Science Inc.) which consists of a combustion tube (SQ-10) and an absorption unit (HSU-35). Thermogravimetry (TG) measurements were carried out with a Rigaku Thermo Plus 2 instrument under a dry air flow at a heating rate of 10 °C/min. The in-plane XRD pattern was recorded with an X-ray diffractometer equipped with a four-axes goniometer (Rigaku ATX-G) using CuKα radiation. The incident angle of X-rays in the in-plane geometry was set to 0.2 °. UV-vis absorption spectra were measured with a SHIMADZU UV-vis recording spectrophotometer (UV-2500PC).

3. Results and Discussion

3.1. Exfoliation of Bim-Oct into nanosheets

Powderly Bim-Oct was well dispersed into water, and the solution became turbid (Figure 2 left). After stirring with ultrasonic for 1 h, a transparent and colorless solution was obtained without precipitates (Figure 2 right). Without ultrasonication, precipitates were observed even after stirring for 1 week. The Tyndall effect was clearly observed for the transparent solution (Figure 3). This Tyndall effect was not attributed to C_{16}TMA micelles because C_{16}TMA cations were completely removed, proven by the ^{13}C CP/MAS NMR data as described above. Therefore, the exfoliation of Bim-Oct into thin layers was strongly suggested. The AFM image of ex-Bim-Oct on a Si wafer showed thin nanosheets (Figure 4a). In our previous report,[46] the morphology of Na-Oct, C_{16}TMA-Oct, and Bim-Oct were square plates of 2–5 μm in lateral size. The nanosheets take angular shapes,

Figure 2. Photograph of the aqueous suspensions of Bim-Oct before (left) and after (right) ultrasonication.

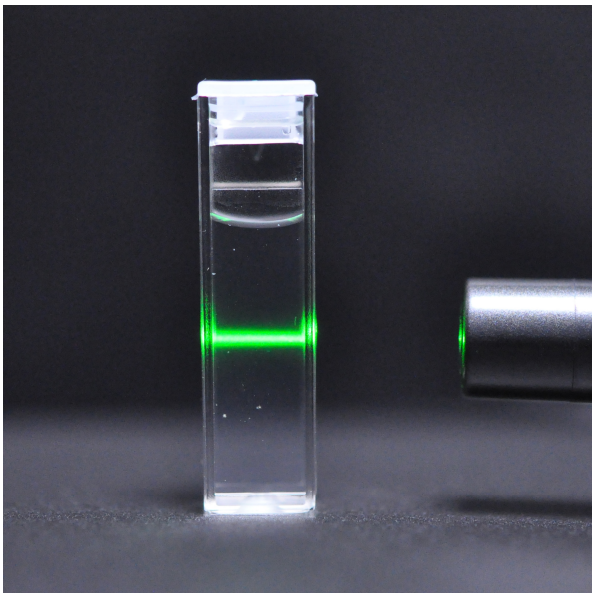

Figure 3. Photograph of ex-Bim-Oct illuminated by a laser light.

reflecting a slight destruction of the original square shape of the Bim-Oct particles. The size of the nanosheets varied from 0.3 to 1 μm in lateral size which was smaller than that of Bim-Oct particles. Probably the ultrasonication in water induces the fragmentation of

Bim-Oct. The height profile of ex-Bim-Oct (Figure 4b) shows the constant thickness of 2 nm along the scanned line. The height of the overlapped section was 4 nm which is two times thicker than those of the other sections. The basal spacing of layered structure of Bim-Oct before exfoliation was 2.4 nm (Figure 5a).[46] The thickness of the nanosheets was less than the basal spacing of Bim-Oct. Therefore, these nanosheets consist of monolayer nanosheets including silicate layer and immobilized butylimidazolium groups on both of the sides. The difference between the thickness of nanosheets and the basal spacing will be discussed below. From the results of the transparency and Tyndall effect of the solution as

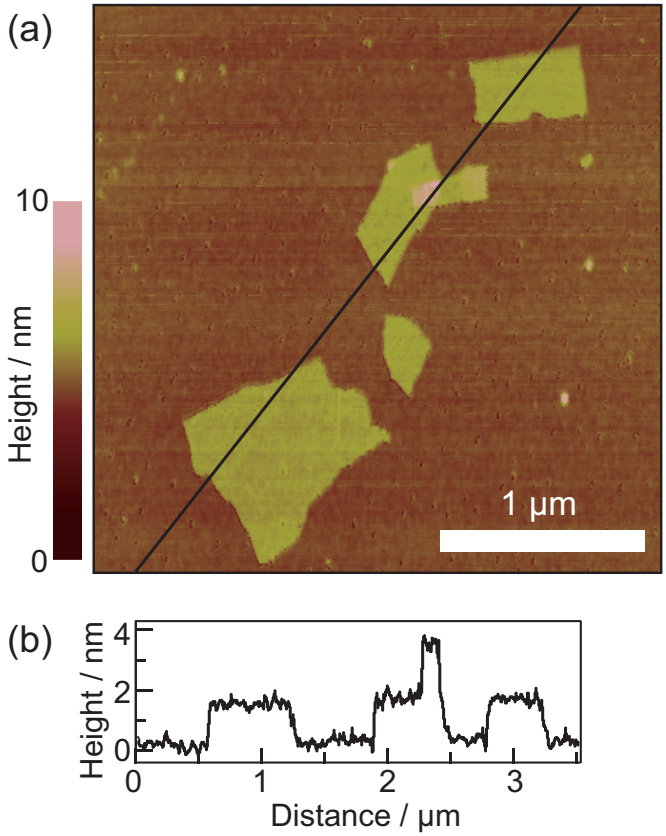

Figure 4. (a) AFM image of ex-Bim-Oct cast on a silicon wafer and **(b)** height profile on the black line of (a).

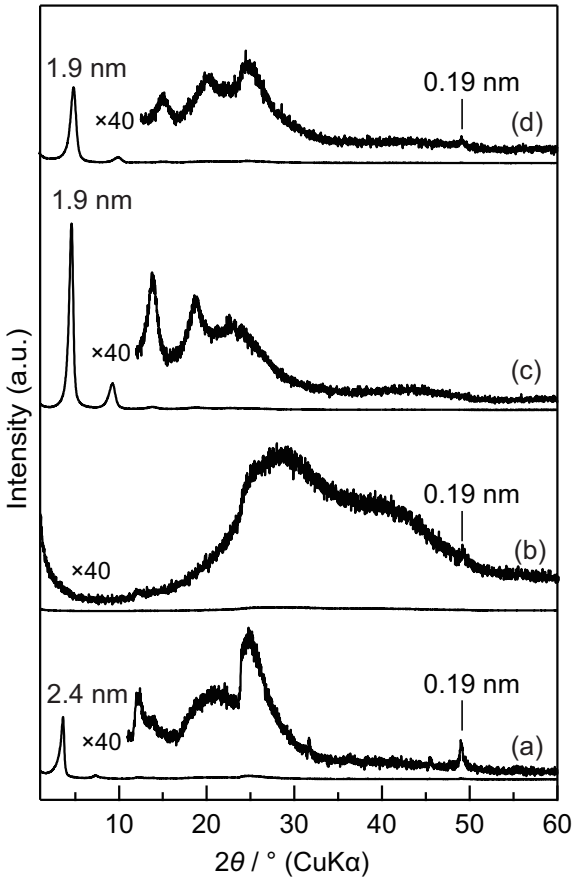

Figure 5. XRD patterns of **(a)** powdery Bim-Oct before exfoliation, **(b)** colloidal aggregates of ex-Bim-Oct obtained after ultracentrifugation, **(c)** dried colloidal aggregates on the sample holder, **(d)** powdery sample after grinding the dried sample.

well as the AFM image of nanosheets, it can be concluded that the silicate layers were successfully exfoliated into monolayer nanosheets.

The colloidal aggregates after ultrasonication and ultracentrifugation show broad XRD peaks around 20–50 ° and a small peak at 0.19 nm. However, no peak was observed at low angle. The broad peaks around 20–50 ° are assignable to diffraction halo of aqueous solutions.[71] Powdery Bim-Oct before exfoliation showed XRD peaks at 2.4, 1.2, and 0.73 nm assignable to a lamellar structure (Figure 5a), as reported previously.[46] In addition, the XRD pattern of colloidal Bim-Oct aggregates showed a peak at 0.19 nm assignable to the

(400) lattice plane in the crystal structure of Na-Oct ($I4_1/amd$)[57]. Because the *a* and *b* axes are parallel to the layer, the crystalline structure of silicate layer of Na-Oct was retained. The disappearance of the peaks in lower angle suggests the lacking in the layer stacking. This is one of the supporting data for the full exfoliation into monolayer nanosheets. After drying the colloidal aggregates on the holder, sharp peaks at 1.9 nm, 0.95 nm, 0.64 nm, and 0.47 nm were observed (Figure 5c) and these peaks are assignable to the diffraction of restacked nanosheets. The *d*-value of 1.9 nm is in good agreement with the thickness of the nanosheets observed by AFM (Figure 4b). The peak assignable to the (400) plane was not observed in the XRD pattern of this dried sample. These results can be explained by the perpendicular directions of both the stacking of the nanosheets and the (400) plane to the surface of the holder. Ground powders of the dried sample showed the peak at 0.19 nm (Figure 5d) because the alignment of the nanosheets changed to random.

The compositions of ex-Bim-Oct (powders of dried colloidal aggregates) and Bim-Oct are summarized in Table 1. The C/Si ratio of ex-Bim-Oct is 1.4, and less than that of Bim-Oct (2.1). The C/N ratio of ex-Bim-Oct (5.2) was almost same as that of Bim-Oct (5.3). The density of the imidazolium groups on the silicate layer of Bim-Oct before exfoliation is 1.8 groups nm^{-2}. The density of imidazolium groups is calculated to decrease to 1.1 groups nm^{-2} on an assumption of that the decrease of carbon content (Table 1) after exfoliation is totally due to the cleavage of siloxane bonds (**Si-O-Si**-CH_2-). Therefore, the

Table 1. Composition of Bim-Oct and ex-Bim-Oct

Sample	C/mass%	N/mass%	Cl/mass%	SiO_2/mass% [a]	C/N	C/Si	Cl/imidazolium [c]
Bim-Oct	23.8	5.3	6.3	57	5.3	2.1	0.95
ex-Bim-Oct [b]	17.0	3.8	2.3	62	5.2	1.4	0.48

[a] Residual amount after heating the samples at 900 °C by TG.
[b] The solution of ex-Bim-Oct was ultracentrifuged and obtained colloidal aggregates were dried.
[c] The amounts of imidazolium group were calculated from the nitrogen contents.

immobilized groups on the surface of silicate layers were partially eliminated during the ultrasonication. The Cl/imidazolium ratio of Bim-Oct is 0.95, indicating the formation of a 1 : 1 pair of imidazolium groups and Cl^-. However, ex-Bim-Oct indicated the decrease of the Cl/imidazolium ratio to 0.48. Therefore, half of Cl^- ions were eliminated. As described above, the thickness of the nanosheets (1.9 nm, Figure 4) was smaller than the *d*-value of the Bim-Oct before exfoliation (2.4 nm, Figure 5a). The elimination of the organic species and Cl^- ions is probably related to the decrease in the *d*-value. Although imidazolium groups and Cl^- ions were partially eliminated, the crystal structure was retained after the exfoliation on the basis of the AFM and XRD results.

3.2. Exfoliation mechanism

Despite the difficulty of exfoliation of layered silicates, Bim-Oct was fully exfoliated to monolayer nanosheets. The effect of the interlayer surface and/or space of layered silicates was investigated. C_{16}TMA-Oct, tetrabutylammonium exchanged octosilicate (TBA-Oct), and octosilicate immobilized with octylimidazolium (Oim-Oct)[46] or trimetylammoniumpropylsilylated group (TMA-Oct) were used. In addition, another sample (d_Bim-Oct) with a reduced amount of immobilized butylimidazolium group (64%) was used. A layered silicate magadiite ($Na_2Si_{14}O_{29}\cdot 11H_2O$)[69-70,72] was also used as a starting material to form butylimidazolium-immobilized silicate (Bim-Mag).

All the samples except ex-Bim-Oct were turbid even after ultrasonication, while the sample from Bim-Oct (ex-Bim-Oct) was transparent (Figure 2). The samples were centrifuged at 2200 × *g* (3500 rpm; not ultracentrifugation) for the separation into supernatant and slurry. The results after the centrifugation are summarized in Table 2. The supernatants were cast on a grid used conventionally for TEM measurement.

Table 2. Results of the exfoliation of the samples by ultrasonication

Used samples	Existence of nanosheets in supernatant [a]	Increase of *d*-value by ultrasonication/nm
C_{16}TMA-Oct	None	0
Bim-Oct	Observed	- [b]
Oim-Oct	Observed	0.1
TMA-Oct	None	0
d_Bim-Oct	None	0
Bim-Mag	Observed	0

[a] Supernatants were cast on carbon-coated Cu grids, and observed by HR-SEM.
[b] Precipitates were not obtained after centrifugation at 2200 × *g* (3500 rpm).

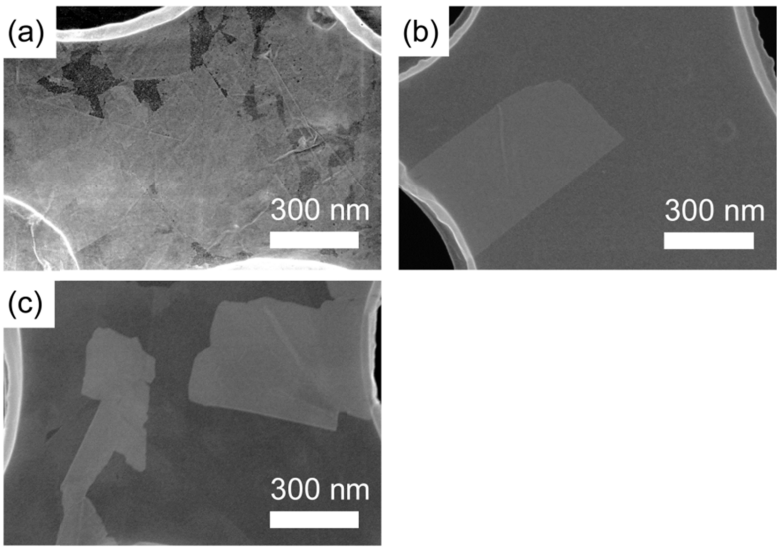

Figure 6. HR-SEM images of (a) Bim-Oct, (b) Oim-Oct, and (c) Bim-Mag after ultrasonication.

High-resolution scanning electron microscopic (HR-SEM) images showed that there were no nanosheets on the grids having the samples obtained from the supernatants of C_{16}TMA-Oct, TMA-Oct, and d_Bim-Oct. In the HR-SEM images of the cast supernatants from Bim-Oct, Oim-Oct, and Bim-Mag, exfoliated nanosheets were observed (Figure 6).

The numbers of the nanosheets from Oim-Oct and Bim-Mag were much fewer than that from Bim-Oct. The AFM image of the supernatant from Bim-Mag shows thin nanosheets (Figure 7a). The thickness of the nanosheets was about 2.4 nm from the height profile (Figure 7b). The XRD peaks at lower angle of Bim-Mag were almost extinct after

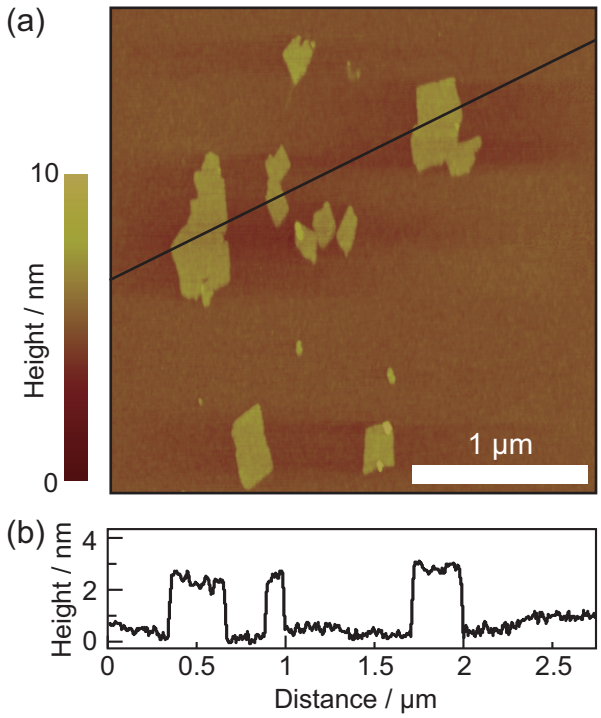

Figure 7. (a) AFM image of Bim-Mag after ultrasonication (supernatant) on a silicon wafer and **(b)** height profile along the black line in the AFM image of (a).

ultrasonication (Figure 8e). Therefore, Bim-Mag exhibits a swelling property with water. The other slurry from C_{16}TMA-Oct, Oim-Oct, TMA-Oct, and d_Bim-Oct showed XRD peaks with *d*-values same as or similar to those of samples before ultrasonication, respectively (Figure 8a-d). Thus, the immobilization of butylimidazolium groups is most effective for exfoliation in water. In addition, this method is potentially applicable for various layered silicates.

The exfoliation property of layered silicates is thought to depend on the three factors of (1) hydrophilicity of interlayer for swelling with water, (2) hydration property of immobilized groups, and (3) degree of silylation for capping SiOH/SiO^- groups for the control of interlayer interactions.

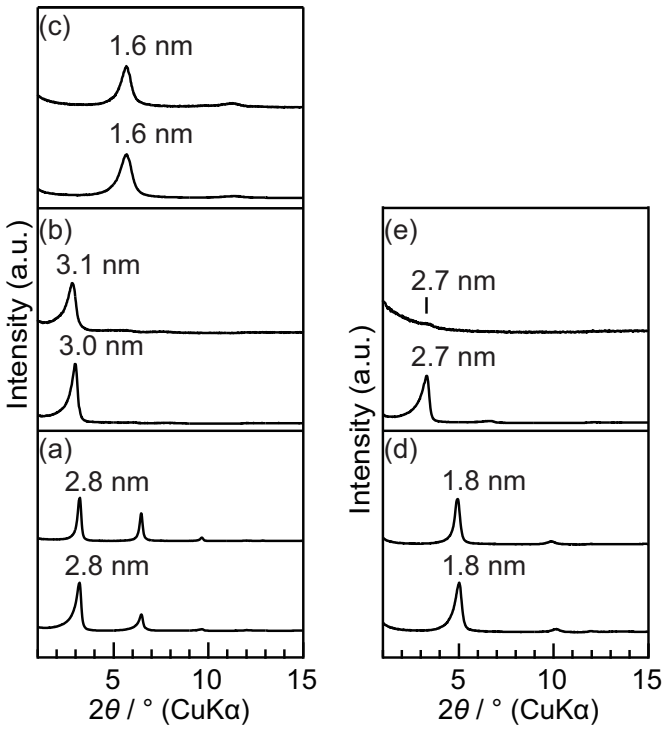

Figure 8. XRD patterns before and after ultrasonication of **(a)** C_{16}TMA-Oct, **(b)** Oim-Oct, **(c)** TMA-Oct, **(d)** d_Bim-Oct, and **(e)** Bim-Mag. The upper and lower patterns show samples before and after ultrasonication, respectively.

The low degree of exfoliation of Oim-Oct can be explained by the lower hydrophilicity of octylimidazolium group than butylimidazolium group. In fact, Bim-Oct was dispersed rapidly into water, while Oim-Oct required stirring to achieve dispersion.[46]

Despite hydrophilic terminal trimethylammonium groups, TMA-Oct does not exhibit a swelling and exfoliation behavior unlike Bim-Oct. The exfoliation behavior can be discussed in relation to the hydration property of immobilized groups. The hydration property of ionic liquids has been investigated by various methods. It is reported that tetramethylammonium (including trimethylammonium group) cation is chaotropic (having weak interaction with water molecules and decrease the structuring of water) rather than kosmotropic (having a strong interaction with water molecules and increases the

structuring of water).[73] In contrast, 1-butyl-3-methylimidazolium cation is kosmotropic.[73] Kosmotropic butylimidazolium groups immobilized on the interlayer surfaces of octosilicate probably induces the hydration and the swelling. The kosmotropic butylimidazolium groups probably stabilized exfoliated nanosheets in water because the imidazolium groups presumably provide the structured water on the surface, and decrease the surface free energy. Thus, kosmotropic imidazolium groups are suitable for exfoliation of layered silicates.

The integral ratio of Q^3:Q^4 of ^{29}Si MAS NMR spectrum (Figure 9) of Bim-Mag was 32:318 (the sum was normalized to 350). The ratio of C_{16}TMA-Mag was 100:250. Therefore, 68% of SiOH/SiO$^-$ groups with Q^3 environment were silylated and changed to Q^4 environmental species. The integral ratio of Q^3:Q^4 in ^{29}Si MAS NMR spectrum of d_Bim-Oct (Figure 10) was 36:164, suggesting that 64% of SiOH/SiO$^-$ groups with Q^3 environment was silylated. Though imidazolium groups were immobilized, Bim-Mag showed a lower degree of exfoliation than Bim-Oct. In addition, d_Bim-Oct showed a non-swelling and non-exfoliation property. Higher degree of silylation is necessary for successful exfoliation. The interlayer hydrogen bonding and electrostatic

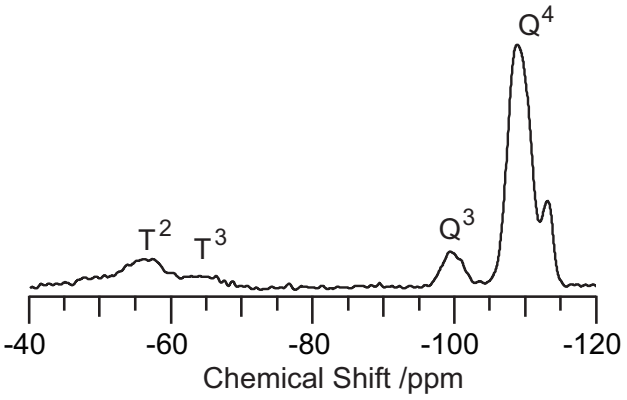

Figure 9. ^{29}Si MAS NMR spectrum of Bim-Mag.

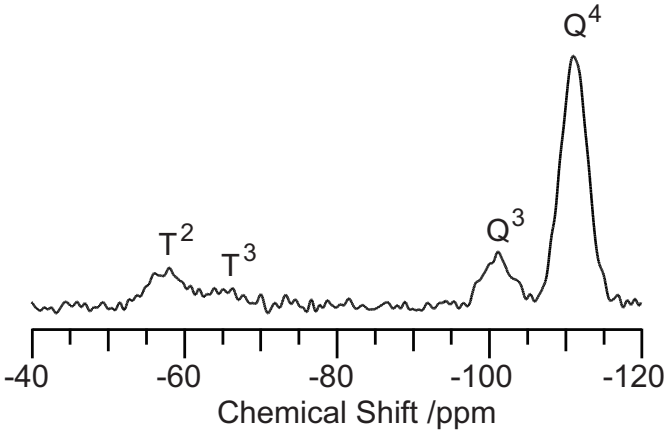

Figure 10. ^{29}Si MAS NMR spectrum of d_Bim-Oct.

interaction of residual SiOH/SiO$^-$ groups probably hinders the exfoliation. Especially, electrostatic interaction between layers should strongly affect the exfoliation property because cohesive free energy of layered material is increased with the charge density.[74] The charge density of pristine layered silicates (e.g. 1.9 charge nm^{-2} for Na-octosilicate, half of SiOH/SiO$^-$ groups) is much higher than that of clay minerals (e.g. 0.8 charge nm^{-2} for saponite[52] with CEC at 100 mequiv/100 g). The high cohesive free energy of pristine octosilicate prevents exfoliation. Silylation reaction, which is a sort of capping of SiOH/SiO$^-$ groups, should reduce the cohesive free energy of the interlayer surfaces. Therefore, high silylation degree of SiOH/SiO$^-$ groups is necessary for successful exfoliation layered silicates.

3.3. Spin-coated films of nanosheets

A transparent and colorless spin-coated film was successfully obtained on a glass substrate from the colloidal aggregates of ex-Bim-Oct (Figure 11 left). Previously,

Figure 11. Photograph of the spin-coated film on a glass substrate (left) and the film after adsorption of Orange II (right). The sizes of the substrates are 28 mm × 48 mm.

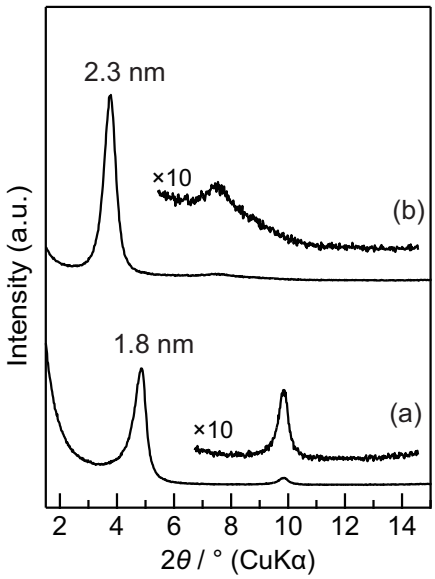

Figure 12. XRD patterns of **(a)** the spin-coated film and **(b)** the film after adsorption of Orange II.

transparent film was prepared with partially delaminated esterified H-magadiite.[51] However, the film was obtained from only a supernatant part of a toluene suspension of the esterified magadiite. In this study, a spin-coated film was obtained from not supernatant but colloidal aggregates consisting of fully exfoliated nanosheets. The film shows the XRD peaks at 1.8, 0.90, and 0.60 nm (Figure 12a), indicating a lamellar structure. The thickness of the film can be estimated to be ca. 0.1 μm from the cross-sectional HR-SEM image of

the film on a silicon substrate (Figure 13). The in-plane XRD pattern of φ-2$\theta\chi$ scanning of the film shows the peaks at 0.73 nm, 0.37 nm, and 0.19 nm (Figure 14), assignable to (100), (200), and (400) lattice plane (a = b = 0.73 nm). Therefore, the crystalline silicate nanosheets are stacked flatly parallel to the substrate. Na-Oct does not show the peak due to (100) lattice plane because of its crystal structure determined as $I4_1/amd$.[57] The appearance of (100) peak from the film can be explained by the decrease of the symmetry along c axis because the direction of the nanosheets is random on the in-plane direction. The *d*-value of the spin-coated film (1.8 nm) was slightly smaller than that of the dried aggregates (1.9 nm). Although the reason for this difference is under investigation, one of

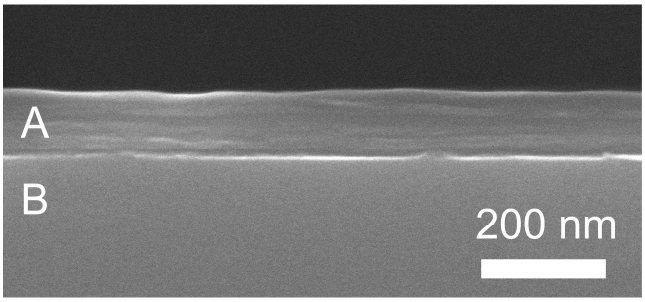

Figure 13. Cross-sectional HR-SEM image of spin-coated film on a silicon substrate (A: film, B: Si substrate).

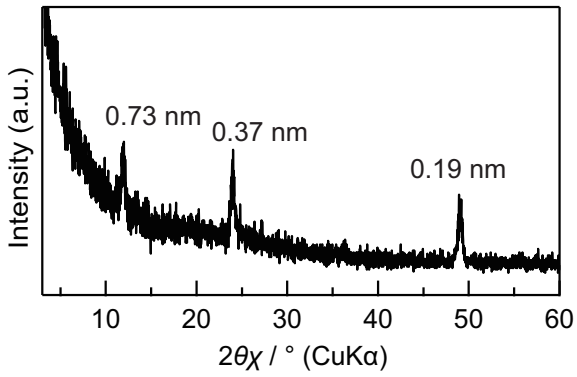

Figure 14. In-plane XRD profile with φ-2$\theta\chi$ scanning of the spin-coated film.

the possibilities is well ordered and closer stacking of nanosheets by spin-coating.

The powdery Bim-Oct is anion-exchangeable with anionic dye and inorganic anions because of the presence of cationic imidazolium groups.[46] The spin-coated film was soaked into an aqueous solution of Orange II, an anionic dye. Then, an orange-colored transparent film was obtained (Figure 11 right). The XRD pattern of the dye-adsorbed film shows peaks at 2.3 nm and 1.2 nm (Figure 12b), and the peak at 1.8 nm before adsorption was not observed. Therefore, Orange II anion was intercalated into the interlayer of the nanosheets stacked on the substrate. The Orange II molecule has a plate-like structure whose size can be estimated to be 1.7 nm × 1.1 nm × 0.5 nm (Figure 15). The increase of *d*-value through the intercalation is 0.5 nm (= 2.3 nm – 1.8 nm). Therefore, Orange II molecules probably lie flat in the interlayer. The UV-vis absorption spectrum of the spin-coated film before adsorption was flat at zero in an overall range from 360 nm to 800 nm (Figure 16a), indicating the high transparency of the film in the visible area. The absorption band of dye-adsorbed film was similar to that of an aqueous solution of Orange II (Figure 16b, c). Therefore, Orange II molecules are well dispersed in the

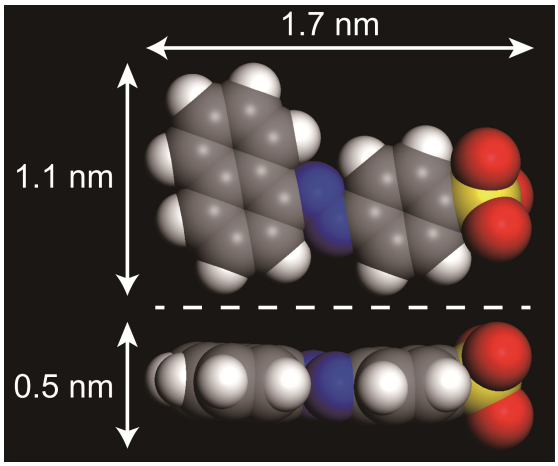

Figure 15. Space filling model of Orange II molecule. Chloride ion is not shown. White: hydrogen, grey: carbon, red: oxygen, blue: nitrogen, yellow: sulfur.

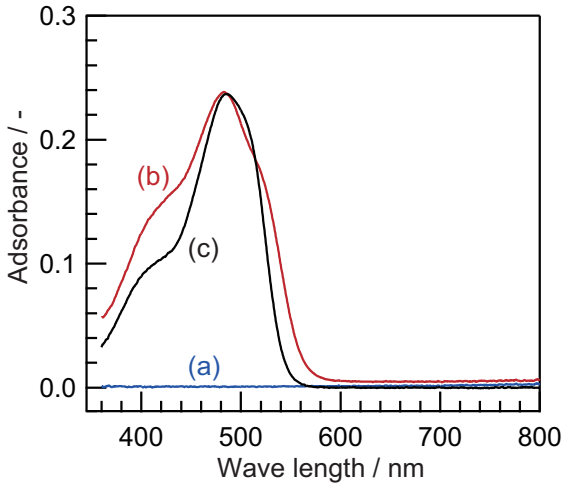

Figure 16. UV-vis absorption spectra of **(a)** the spin-coated film, **(b)** the film after adsorption of Orange II, and **(c)** aqueous solution of Orange II at 12 μM in a cuvette with a pathlength at 1 cm.

interlayer without aggregation. Transparent films containing dyes with high orientation are applicable to photofunctional devises.[18,52,75] Not only the orientation but also the distance of guest molecules highly affects the efficiency of the photofunctions. The density as well as ordering of SiOH/SiO^- groups of layered silicates is varied depending on the crystal structure. Therefore, the position of functional groups, such as imidazolium groups, on the silicate layers, can be controlled. Thus, this films consisting of silicate nanosheets have potential for the precise control of the distance and ordering of guest species in two-dimensionally confined interlayer spaces.

4. Conclusion

The layered octosilicate was fully exfoliated into monolayer nanosheets in water via immobilization of butylimidazolium groups on the surface. This is the first report of exfoliation of layered silicates, whose frameworks are composed of only SiO_4 tetrahedra,

into monolayer nanosheets. Regardless of the layer compositions, this is also the first report of full exfoliation of cationic nanosheets into monolayer in aqueous media. The transparent film of the fully exfoliated nanosheets should be applicable to various optical and photochemical applications. The silylation reagent including butylimidazolium group is more suitable for exfoliation than other silylating reagents, containing octylimidazolium and trimethylammonium groups. From the viewpoint of the science of ionic liquids, the significant change of the silicate surface by the immobilization with butylimidazolium group is novel. Recently, ionic liquids supported on solids have received considerable interests as the supports for heterogeneous catalysts.[67-68,76-79] In general, nanosheet is one of morphology with the highest accessibility and surface area.[80] Therefore, exfoliated nanosheets of Bim-Oct should be applicable for novel and highly efficient catalyst supports. In this study, the property of exfoliation was discussed by using the kosmotropic ability of imidazolium groups. In general, kosmotropicity/chaotropicity can be determined by thermodynamic parameters.[73] In this method, organic groups on the silicate layers can be changed by selection of silylation reagents. Therefore, the ability of exfoliation can be predicted quantitatively with thermodynamic parameters in future. This method is innovative for the design of nanosheets for various applications.

5. References

[1] M. Alexandre, P. Dubois, *Mater. Sci. Eng. R-Rep.* **2000**, *28*, 1-63.

[2] J. Liu, W. J. Boo, A. Clearfield, H. J. Sue, *Mater. Manuf. Processes* **2006**, *21*, 143-151.

[3] H. J. Sue, K. T. Gam, N. Bestaoui, N. Spurr, A. Clearfield, *Chem. Mater.* **2004**, *16*, 242-249.

[4] Z. Tang, N. A. Kotov, S. Magonov, B. Ozturk, *Nat. Mater.* **2003**, *2*, 413-418.

[5] P. Podsiadlo, A. K. Kaushik, E. M. Arruda, A. M. Waas, B. S. Shim, J. Xu, H. Nandivada, B. G. Pumplin, J. Lahann, A. Ramamoorthy, N. A. Kotov, *Science* **2007**, *318*, 80-83.

[6] B. Brahimi, P. Labbe, G. Reverdy, *Langmuir* **1992**, *8*, 1908-1918.

[7] D. Rong, T. E. Mallouk, *Inorg. Chem.* **1993**, *32*, 1454-1459.

[8] A. Fitch, *Clays Clay Miner.* **1990**, *38*, 391-400.

[9] S. M. Macha, A. Fitch, *Microchimica Acta* **1998**, *128*, 1-18.

[10] Y. Umemura, A. Yamagishi, R. Schoonheydt, A. Persoons, F. De Schryver, *J. Am. Chem. Soc.* **2002**, *124*, 992-997.

[11] D. R. Talham, *Chem. Rev.* **2004**, *104*, 5479-5502.

[12] R. H. A. Ras, Y. Umemura, C. T. Johnston, A. Yamagishi, R. A. Schoonheydt, *Phys. Chem. Chem. Phys.* **2007**, *9*, 918-932.

[13] G. Decher, J. Maclennan, U. Sohling, J. Reibel, *Thin Solid Films* **1992**, *210-211*, 504-507.

[14] E. R. Kleinfeld, G. S. Ferguson, *Science* **1994**, *265*, 370-373.

[15] G. Decher, *Science* **1997**, *277*, 1232-1237.

[16] K. Haraguchi, T. Takehisa, *Adv. Mater.* **2002**, *14*, 1120-1124.

[17] Q. Wang, J. L. Mynar, M. Yoshida, E. Lee, M. Lee, K. Okuro, K. Kinbara, T. Aida, *Nature* **2010**, *463*, 339-343.

[18] Y. Suzuki, R. Matsunaga, H. Sato, T. Kogure, A. Yamagishi, J. Kawamata, *Chem. Commun.* **2009**, 6964-6966.

[19] R. Ma, T. Sasaki, *Adv. Mater.* **2010**, *22*, 5082-5104.

[20] F. Bergaya, B. K. G. Theng, G. Lagaly, *Handbook of Clay Science*, Elsevier Ltd., Amsterdam, **2006**.

[21] A. Clearfield, J. A. Stynes, *J. Inorg. Nucl. Chem.* **1964**, *26*, 117-129.

[22] G. Alberti, M. Casciola, U. Costantino, *J. Colloid Interface Sci.* **1985**, *107*, 256-263.

[23] A. Lerf, R. Schoellhorn, *Inorg. Chem.* **1977**, *16*, 2950-2956.

[24] P. Joensen, R. F. Frindt, S. R. Morrison, *Mater. Res. Bull.* **1986**, *21*, 457-461.

[25] M. M. J. Treacy, S. B. Rice, A. J. Jacobson, J. T. Lewandowski, *Chem. Mater.* **1990**, *2*, 279-286.

[26] T. Sasaki, M. Watanabe, H. Hashizume, H. Yamada, H. Nakazawa, *J. Am. Chem. Soc.* **1996**, *118*, 8329-8335.

[27] M. Fang, C. H. Kim, T. E. Mallouk, *Chem. Mater.* **1999**, *11*, 1519-1525.

[28] J. He, M. Wei, B. Li, Y. Kang, D. Evans, X. Duan, in *Layered Double Hydroxides* (Eds.: X. Duan, D. G. Evans), Springer-Verlag, Berlin Heidelberg, **2005**, pp. 89-119.

[29] M. Adachi-Pagano, C. Forano, J.-P. Besse, *Chem. Commun.* **2000**, 91-92.

[30] S. Stankovich, D. A. Dikin, G. H. B. Dommett, K. M. Kohlhaas, E. J. Zimney, E. A. Stach, R. D. Piner, S. T. Nguyen, R. S. Ruoff, *Nature* **2006**, *442*, 282-286.

[31] M. Osada, Y. Ebina, K. Takada, T. Sasaki, *Adv. Mater.* **2006**, *18*, 295-299.

[32] Z. Liu, R. Ma, M. Osada, N. Iyi, Y. Ebina, K. Takada, T. Sasaki, *J. Am. Chem. Soc.* **2006**, *128*, 4872-4880.

[33] Y. Ebina, N. Sakai, T. Sasaki, *J. Phys. Chem. B* **2005**, *109*, 17212-17216.

[34] T. W. Kim, S. G. Hur, S.-J. Hwang, H. Park, W. Choi, J.-H. Choy, *Adv. Funct. Mater.* **2007**, *17*, 307-314.

[35] W. Schwieger, G. Lagaly, in *Handbook of Layered Materials* (Eds.: S. M. Auerbach, K. A. Carrado, P. K. Dutta), Marcel Dekker, Inc., New York, **2004**, pp. 541-629.

[36] E. Ruiz-Hitzky, J. M. Rojo, *Nature* **1980**, *287*, 28-30.

[37] E. Ruiz-Hitzky, J. M. Rojo, G. Lagaly, *Colloid Polym. Sci.* **1985**, *263*, 1025-1030.

[38] T. Yanagisawa, K. Kuroda, C. Kato, *React. Solids* **1988**, *5*, 167-175.

[39] M. Ogawa, S. Okutomo, K. Kuroda, *J. Am. Chem. Soc.* **1998**, *120*, 7361-7362.

[40] A. Shimojima, D. Mochizuki, K. Kuroda, *Chem. Mater.* **2001**, *13*, 3603-3609.

[41] D. Mochizuki, A. Shimojima, K. Kuroda, *J. Am. Chem. Soc.* **2002**, *124*, 12082-12083.

[42] D. Mochizuki, A. Shimojima, T. Imagawa, K. Kuroda, *J. Am. Chem. Soc.* **2005**, *127*, 7183-7191.

[43] D. Mochizuki, S. Kowata, K. Kuroda, *Chem. Mater.* **2006**, *18*, 5223-5229.

[44] R. Ishii, Y. Shinohara, *J. Mater. Chem.* **2005**, *15*, 551-553.

[45] D. Mochizuki, K. Kuroda, *New. J. Chem* **2006**, *30*, 277-284.

[46] N. Takahashi, H. Hata, K. Kuroda, *Chem. Mater.* **2010**, *22*, 3340-3348.

[47] Z. Wang, T. J. Pinnavaia, *Chem. Mater.* **1998**, *10*, 1820-1826.

[48] Y. Ide, G. Ozaki, M. Ogawa, *Langmuir* **2009**, *25*, 5276-5281.

[49] M. Ogawa, M. Miyoshi, K. Kuroda, *Chem. Mater.* **1998**, *10*, 3787-3789.

[50] Y. Matsuo, Y. Yamada, M. Nishikawa, T. Fukutsuka, Y. Sugie, *J. Fluorine Chem.* **2008**, *129*, 1150-1155.

[51] Y. Mitamura, Y. Komori, S. Hayashi, Y. Sugahara, K. Kuroda, *Chem. Mater.* **2001**, *13*, 3747-3753.

[52] S. Takagi, T. Shimada, M. Eguchi, T. Yui, H. Yoshida, D. A. Tryk, H. Inoue, *Langmuir* **2002**, *18*, 2265-2272.

[53] S. Bruzaud, G. Levesque, *Chem. Mater.* **2002**, *14*, 2421-2426.

[54] S. Tahara, Y. Takeda, Y. Sugahara, *Chem. Mater.* **2005**, *17*, 6198-6204.

[55] R. K. Iler, *J. Colloid Sci.* **1964**, *19*, 648-657.

[56] W. Schwieger, D. Heidemann, K. H. Bergk, *Rev. Chim. Minar.* **1985**, *22*, 639-650.

[57] S. Vortmann, J. Rius, S. Siegmann, H. Gies, *J. Phys. Chem. B* **1997**, *101*, 1292-1297.

[58] U. Brenn, H. Ernst, D. Freude, R. Herrmann, R. Jähnig, H. G. Karge, J. Kärger, T. König, B. Mädler, U. T. Pingel, D. Prochnow, W. Schwieger, *Microporous Mesoporous Mater.* **2000**, *40*, 43-52.

[59] I. Wolf, H. Gies, C. A. Fyfe, *J. Phys. Chem. B* **1999**, *103*, 5933-5938.

[60] M. Borowski, I. Wolf, H. Gies, *Chem. Mater.* **2002**, *14*, 38-43.

[61] M. Borowski, O. Kovalev, H. Gies, *Microporous Mesoporous Mater.* **2008**, *107*, 71-80.

[62] P. Wasserscheid, T. Welton, *Ionic Liquids in Synthesis*, 2nd ed., WILEY-VCH, Weinheim, **2008**.

[63] L. Li, R. Ma, Y. Ebina, N. Iyi, T. Sasaki, *Chem. Mater.* **2005**, *17*, 4386-4391.

[64] N. Iyi, Y. Ebina, T. Sasaki, *Langmuir* **2008**, *24*, 5591-5598.

[65] X. Guo, F. Zhang, D. G. Evans, X. Duan, *Chem. Commun.* **2010**, *46*, 5197-5210.

[66] K. Endo, Y. Sugahara, K. Kuroda, *Bull. Chem. Soc. Jpn.* **1994**, *67*, 3352-3355.

[67] K. Yamaguchi, C. Yoshida, S. Uchida, N. Mizuno, *J. Am. Chem. Soc.* **2005**, *127*, 530-531.

[68] J. Kasai, Y. Nakagawa, S. Uchida, K. Yamaguchi, N. Mizuno, *Chem.—Eur. J.* **2006**, *12*, 4176-4184.

[69] A. Y. K. Kosuge, A. Tsunashima, R. Otsuka, *J. Ceram. Soc. Jpn.* **1992**, *100*, 326-331.

[70] O. Y. Kwon, S. Y. Jeong, J. K. Suh, J. M. Lee, *Bull. Korean Chem. Soc.* **1995**, *16*, 737-741.

[71] T. Sasaki, M. Watanabe, *J. Am. Chem. Soc.* **1998**, *120*, 4682-4689.

[72] H. P. Eugster, *Science* **1967**, *157*, 1177-1180.

[73] H. Zhao, *J. Chem. Technol. Biotechnol.* **2006**, *81*, 877-891.

[74] Y.-T. Fu, H. Heinz, *Chem. Mater.* **2010**, *22*, 1595-1605.

[75] R. Sasai, H. Itoh, I. Shindachi, T. Shichi, K. Takagi, *Chem. Mater.* **2001**, *13*, 2012-2016.

[76] C. P. Mehnert, R. A. Cook, N. C. Dispenziere, M. Afeworki, *J. Am. Chem. Soc.* **2002**, *124*, 12932-12933.

[77] C. P. Mehnert, *Chem.—Eur. J.* **2005**, *11*, 50-56.

[78] A. Riisager, R. Fehrmann, S. Flicker, R. van Hal, M. Haumann, P. Wasserscheid, *Angew. Chem., Int. Ed.* **2005**, *44*, 815-819.

[79] A. Riisager, R. Fehrmann, M. Haumann, P. Wasserscheid, *Top. Catal.* **2006**, *40*, 91-102.

[80] M. Choi, K. Na, J. Kim, Y. Sakamoto, O. Terasaki, R. Ryoo, *Nature* **2009**, *461*, 246-249.

Chapter 7

Conclusion of This Thesis and Future Prospects

In this thesis, I summarized the covalent modifications of layered silicates for layer-charge control and their transformations into nanostructured materials. I adopted two ways for their achievements. One is the intralayer condensation of anionic SiO^- groups for intercalation of nonionic surfactants. This method was applied for enlargement of mesopores of 2-D orthorhombic mesoporous silica. The other is capping of anionic SiO^- groups by cationic silylation reagents for the synthesis of an anion exchangeable layered hybrid. The layered hybrid was exfoliated and transformed into single layered nanosheets.

From the viewpoint of each single layer, nanosheets obtained by exfoliation of layered inorganic materials have received considerable attention as a method for significant expansion of applications of layered materials. Various applications have been developed for polymer/nanosheets composites and nanobuilding units for various hybrids including Langmuir-Blodgett films, layer-by-layer films, hydrogels, and photofunctional self-standing films. Exfoliation of layered materials has been reported for layered clay

minerals, α-zirconium phosphates and phosphonates, layered metal chalcogenides, layered metal oxides, and layered double hydroxides etc. However, the exfoliation and delamination of layered silicates, whose frameworks are composed only SiO_4 tetrahedra, has been achieved yet in few reports.[1-4] Exfoliated nanosheets of layered silicates can be regarded as an assembly of functional SiOH groups with a crystalline structure, well ordering of SiOH, high surface area, and high aspect ratio. Thus, exfoliated nanosheets from layered silicates have high potential as building units of hybrid nanomaterials which have covalent bonds between nanosheets and guest species. Especially, methoxylated octosilicate[5] and imidazolium-immobilized silicate nanosheets (Chapter 6) should be applicable as building blocks. Though this thesis clarified the exfoliation of layered silicates, the method into single layer is yet limited to the case of immobilization of imidazolium groups with high density.[4] Future development of the exfoliation process of layered silicates is essential and the studies on this topic will surely become an interesting trend.

Mesoporous silicas and layered silicates have some analogies in terms of siloxane frameworks, silanol groups on the surfaces, confined spaces in a few nanometer size, and high accessibility for guest species. Nowadays, covalent modification of mesoporous silicas has been significantly developed from the viewpoint of applications, such as heterogeneous catalysts and drug delivery system.[6-15] Especially, individual modifications of outer surface and inside of mesopores are quite important for the preparation of carriers by capping mesopores with large nanoparticles.[11] The individual modification will be able to be applied for layered silicates and will provide novel applications unlike mesoporous silicas. Mesoporous silicas can be obtained with various morphologies for example films, nanoparticles, and monolith. From the view point of the versatility of morphology,

mesoporous silicas have advantage over layered silicates. However, layered silicates have advantage for the accessibility and dispersibility of guest species in confined space over mesoporous silicas because mesopores are often stacked with bulky guest species. In addition, frameworks of mesoporous silicas are generally amorphous. Therefore, it is very difficult to obtain highly ordered functional groups immobilized on silanol groups by using mesoporous silicas. Thus, the advantage of the crystalline silicate surfaces with highly ordered silanol groups of layered silicates should be applied for more precise control of ordering and distance of guest species and/or active sites. In addition, each application provided by the functionally-silylated layered silicates should be compared with that of mesoporous silicas.

The development of the covalent modification was totally split into conventional layered silicates (e.g. kanemite, magadiite, and octosilicate) and layered silicates with zeolitic layers (layered zeolite). By using conventional layered silicates, various functional groups, for example alkyl, perfluoroalkyl, amine, and sulfide groups, were immobilized. These hybrids exhibit interesting properties. However, the applications usually depend on immobilized functional groups. In addition, confined interlayer nanospace has not been fully utilized and practical applications have been limited. In contrast, by using layered silicates with zeolitic layers, applications such as catalysts have been achieved because of the presence of active acid sites on the interlayer surfaces. However, the variety of covalent modifications of these layered zeolites is limited to condensation reaction and silylation of singular Si species and some phenylene bridged silylation reagents, so far. I claim that these two separated scientific area must be merged, and this will provide synergistically enhanced applications because of precise control of structure and surface properties corresponding to the applications in future.

In conclusion, the applications of material design based on layered silicates can be categorized to some topics, such as selective adsorbents, catalysts, making building units, and creation of new crystal structures. Covalent modifications by using reaction of SiOH/SiO^- groups make it possible to design layered silicates for all these applications. Thus, important factors for the design of layered silicates for expected applications can be summarized as follows;

(1) Definition of target application which is highly demanded,

(2) Understanding and selection of layered silicates containing SiOH/SiO^- with expected ordering and distribution (layer stacking sequence is also important),

(3) Selection and/or synthesis of immobilization groups such as silylation reagents (selection of SiCl or Si-OMe/-OEt is also important).

In particular, the factor (1) is essential to develop material design of layered silicates. Such a strategic study will surely lead to a breakthrough for novel applications in future. I do hope that the chemical design of layered silicates described here will expand the usefulness of related scientific areas of zeolite science, catalyst, chemistry of nanobuilding units, and mesoporous and mesostructured silicas.

References

[1] M. Ogawa, S. Okutomo, K. Kuroda, *J. Am. Chem. Soc.* **1998**, *120*, 7361-7362.

[2] Y. Matsuo, Y. Yamada, M. Nishikawa, T. Fukutsuka, Y. Sugie, *J. Fluorine Chem.* **2008**, *129*, 1150-1155.

[3] Y. Mitamura, Y. Komori, S. Hayashi, Y. Sugahara, K. Kuroda, *Chem. Mater.* **2001**, *13*,

3747-3753.

[4] N. Takahashi, H. Hata, K. Kuroda, *Chem. Mater.* **2011**, *23*, 266-273.

[5] S. Kiba, T. Itagaki, T. Nakato, K. Kuroda, *J. Mater. Chem.* **2010**, *20*, 3202-3210.

[6] K. Moller, T. Bein, *Chem. Mater.* **1998**, *10*, 2950-2963.

[7] B. J. Scott, G. Wirnsberger, G. D. Stucky, *Chem. Mater.* **2001**, *13*, 3140-3150.

[8] W. H. Zhang, X. B. Lu, J. H. Xiu, Z. L. Hua, L. X. Zhang, M. Robertson, J. L. Shi, D. S. Yan, J. D. Holmes, *Adv. Funct. Mater.* **2004**, *14*, 544-552.

[9] M. Hartmann, *Chem. Mater.* **2005**, *17*, 4577-4593.

[10] F. Hoffmann, M. Cornelius, J. Morell, M. Fröba, *Angew. Chem., Int. Ed.* **2006**, *45*, 3216-3251.

[11] B. G. Trewyn, I. I. Slowing, S. Giri, H.-T. Chen, V. S. Y. Lin, *Acc. Chem. Res.* **2007**, *40*, 846-853.

[12] M. Vallet-Regí, F. Balas, D. Arcos, *Angew. Chem., Int. Ed.* **2007**, *46*, 7548-7558.

[13] E. L. Margelefsky, R. K. Zeidan, M. E. Davis, *Chem. Soc. Rev.* **2008**, *37*, 1118-1126.

[14] I. I. Slowing, J. L. Vivero-Escoto, C.-W. Wu, V. S. Y. Lin, *Adv. Drug Deliv. Rev.* **2008**, *60*, 1278-1288.

[15] J. L. Vivero-Escoto, Slowing, II, B. G. Trewyn, V. S. Y. Lin, *Small* **2010**, *6*, 1952-1967.

LIST OF PUBLICATIONS

Articles*

(1) "Exfoliation of Layered Silicates through Immobilization of Imidazolium Groups"

Chem. *Mater*., **2011**, *23*, 266-273

Nobuyuki Takahashi, Hideo Hata, and Kazuyuki Kuroda

(2) "Enlargement of Mesopores of 2-D Orthorhombic KSW-2 Type Silica by the Addition of Poly(oxyethylene) Alkyl Ether during the Mesostructural Formation"

Solid State Sci., **in press**, DOI:10.1016/j.solidstatesciences.2010.06.023

Nobuyuki Takahashi, Tatsuo Kimura, and Kazuyuki Kuroda

(3) "Anion Exchangeable Layered Silicates Modified with Ionic Liquids on the Interlayer Surface"

Chem. *Mater*., **2011**, *22*, 3340-3348

Nobuyuki Takahashi, Hideo Hata, and Kazuyuki Kuroda

(4) "Intercalation of Poly(oxyethylene) Alkyl Ether into a Layered Silicate Kanemite"

Langmuir, **2007**, *23*, 10765-10771

Nobuyuki Takahashi, Hiroaki Tamura, Dai Mochizuki, Tatsuo Kimura, and Kazuyuki Kuroda

(5) “Synthesis of Layered Silicate-Polyoxyethylene Alkyl Ether Intercalation Compounds from Kanemite”

Proceedings of International Symposium on EcoTopia Science, **2007**, 781-784

Nobuyuki Takahashi, Hiroaki Tamura, Dai Mochizuki, Tatsuo Kimura, Kazuyuki Kuroda

* All publications listed here are related to this thesis.

ACKNOWLEDGEMENT

It is my great pleasure to thank those who made this thesis possible. Firstly, I am heartily thankful to my supervisor, Professor Kazuyuki Kuroda. During six years, I deeply enjoyed student life including experiments, thoughtful discussions, interesting seminars, exiting conferences, and writing papers in this laboratory. It is my proudest moment of my life that I studied as student of Professor Kuroda. I would like to express my gratitude to Professor Tetsuya Osaka, Professor Yoshiyuki Sugahara, and Professor Takayuki Homma for valuable discussion and helpful advices. I owe my deepest gratitude to Professor Eduardo Ruiz-Hitzky. It is very proud that I received his insightful comments and suggestions from the foremost expert on chemical modification of layered silicates. I am also deeply indebted to many advisors for success of my studies. I gratefully acknowledge Dr. Tatsuo Kimura for thoughtful advices and careful review of published papers. I am deeply grateful to Dr. Dai Mochizuki. He has been a professional adviser of my studies, and his advice has been continuously valuable for me for six years. My heartfelt appreciation goes to Dr. Hideo Hata. His practical and intelligent ideas remarkably improved the worth of my studies. Professor Atsushi Shimojima gave valuable comments of my study. I'm really indebted to Mr. Hiroaki Tamura for his kind of advices and encouragements in my first year in this laboratory. Special thanks to all colleagues in this laboratory. Especially, I received generous supports of experiments from Mr. Shimon Osada, Mr. Yusuke Asakura, Ms. Takako Arai, Mr. Ryutaro Wakabayashi, and Mr. Yuki Matsuo. I would like to hope their successful future, sincerely.

I have been received many scholarships from Yoshida Scholarship foundation, The Society of Applied Chemistry of Waseda University, The Nagasawa Kagaku Ikuei Foundation, and Waseda University. Not only this thesis but also my successful student life would not have been possible unless these outstanding scholarships. I am heartily thankful to all who concerned to these foundations and societies. Especially, I have profound respect for Mr. Hiroshi Kawamura because of his great enterprise of scholarship of The Society of Applied Chemistry of Waseda University, and his heartfelt encouragement to me. I also acknowledge Grant-in Aid for JSPS Fellows form Japan Society for the Promotion of Science.

Finally, I wish to express my love and gratitude to my beloved families for their understanding and endless love, through the duration of my studies.

February, 2011

Nobuyuki TAKAHASHI